Spring 2012

Low-complexity soft-decision feedback turbo equalization for multilevel modulations

Huang Lou

Department: Electrical and Computer Engineering

LOW-COMPLEXITY SOFT-DECISION FEEDBACK TURBO EQUALIZATION FOR MULTILEVEL MODULATIONS

by

HUANG LOU

A DISSERTATION

Presented to the Faculty of the Graduate School of the

MISSOURI UNIVERSITY OF SCIENCE AND TECHNOLOGY

In Partial Fulfillment of the Requirements for the Degree

DOCTOR OF PHILOSOPHY

in

ELECTRICAL ENGINEERING

2012

Approved by

Chengshan Xiao, Advisor
Steve Grant
Kurt Kosbar
Sahra Sedigh
Xiaoqing Liu

PUBLICATION DISSERTATION OPTION

This dissertation consists of the following four published or submitted papers, formatted in the style used by the Missouri University of Science and Technology, listed as follows:

Paper I, H. Lou, and C. Xiao, "Soft-decision Feedback Turbo Equalization for Multilevel Modulations," has been published in IEEE Trans. Signal Processing, vol.59, pp.186-195, Jan. 2011. (pages 7-37)

Paper II, H. Lou, and C. Xiao, "Soft Feedback ISI Canceller-based Turbo Equalization for Multilevel modulations," has been submitted to IEEE Trans. Communications, Oct. 2011. (pages 38-50)

Paper III, A. Rafati, H. Lou and C. Xiao, "Low-complexity soft-decision feedback turbo equalization for MIMO systems with multilevel modulations," has been published in IEEE Trans. Veh. Technol., vol.60, No.7, Sept. 2011. (pages 51-79)

Paper IV, A. Rafati, H. Lou, Y. R. Zheng and C. Xiao, "Soft Feedback Turbo Equalization for Underwater Acoustic Communications," has been published in MTS/IEEE OCEANS, Kona, Hawaii, Sep. 19-22, 2011. (pages 80-95)

Paper V, A. Rafati, H. Lou and C. Xiao, "On the Soft-Decision Feedback Turbo Equalization for Underwater Acoustic Communications," has been submitted to Journal of the Acoustical Society of America, Oct. 2011. (pages 96-128)

ABSTRACT

This dissertation proposes two new decision feedback equalization schemes suitable for multilevel modulation systems employing turbo equalization. One is soft-decision feedback equalization (SDFE) that takes into account the reliability of both soft *a priori* information and soft decisions of the data symbols. The proposed SDFE exhibits lower signal to noise ratio (SNR) threshold that is required for "water fall" bit error rate (BER) and much faster convergence than the near-optimal exact minimum mean square error linear equalizer (Exact-MMSE-LE) for high-order constellation modulations. The proposed SDFE also offers a low computational complexity compared to the Exact-MMSE-LE.

The drawback of the SDFE is that its coefficients cannot reach the matched filter bound (MFB) and therefore after a large number of iterations (e.g. 10), its performance becomes inferior to that of the Exact-MMSE-LE. Therefore, soft feedback intersymbol interference (ISI) canceller-based (SIC) structure is investigated. The SIC structure not only exhibits the same low complexity, low SNR threshold and fast convergence as the SDFE but also reaches the MFB after a large number of iterations. Both theoretical analysis and numerical simulations demonstrate why the SIC achieves MFB while the SDFE cannot.

These two turbo equalization structures are also extended from single-input single-output (SISO) systems to multiple-input multiple-output (MIMO) systems and applied in high data-rate underwater acoustic (UWA) communications.

ACKNOWLEDGMENTS

The research work reported in this dissertation was carried out with the Department of Electrical and Computer Engineering at Missouri University of Science and Technology, Rolla, Missouri, USA, from January 2009 to December 2011.

I am most grateful to my supervisor, Dr. Chengshan Xiao. I truly appreciate his valuable encouragement and guidance during the course of the research, his generous support on research funding, his understanding of the special challenges that I have encountered. His diligent working style, zealous scientific attitude, and strict academic requirements have made him an excellent example for me.

I would also like to extend my appreciation to the members of my advisory committee, Drs. Steve L. Grant, Kurt Kosbar, Sahra Sedigh, and Xiaoqing Liu, the specialists of graduate office, Mrs. Sharon Matson, Mrs. Vicki Hudgins, and Regina P. Kohout, for their precious time in examining this dissertation and their valuable advice to my research work.

It is my pleasure to thank all my friends for their company and help during my Ph.D. years and all the colleagues in Missouri S&T for their assistance in my research work, especially, Mr. Amirhossein Rafati, for his efforts on some of the works in this dissertation.

I am indebted to my father Genlang Lou and my mother Huanying Yu, who have set my roots and given me wings, and who have always believed in me and encouraged me. My extraordinary love and gratitude go to my girl friend, Huai Huang, for paying back her true love with all she has.

TABLE OF CONTENTS

LIST OF ILLUSTRATIONS

PAPER III

PAPER IV

PAPER V

LIST OF TABLES

1 INTRODUCTION

1.1 BACKGROUND

In many practical communication systems, data is transmitted over a channel with intersymbol interference (ISI). At the transmitter, the data is often protected by the addition of a controlled amount of redundancy using forward error correction or an error-correction code (ECC). It is then the task of the receiver to exploit both the structure of the transmit symbol constellation and the structure of the code to detect and docode the transmitted data sequence. Methods that exploit the structure of the transmitted symbol constellation are referred to as equalization, whereas those that exploit the structure of the code are termed decoding.

In a typical receiver, the data received from the channel is processed with an equalizer to mitigate the effects of ISI. The equalizer then produces estimates of the data, which are passed onto the decoder for the ECC. For complexity reasons, the equalization task typically consists of linear processing of the received channel output [linear equalizer (LE)] and possibly past symbol estimates [decision feedback equalizer (DFE)] [1], [2]. The parameters of these filters can be designed according to a variety of different optimization criteria, such as the zero foring (ZF) or MMSE criteria [1], [2]. Optimal equalization methods for minimizing the bit error rate (BER) and the sequence error rate are also nonlinear and are based on maximum likelihood (ML) estimation, which turns into maximum *a posterior* probability (MAP) estimation in presence of *a priori* information about the transimtted data. We refer to this estimation method as MAP/ML equalization.

When the data has been protected with a convolutional code, improvements in the BER can be easily obtained through the use of soft-input convolutional decoder.

Most practical communication systems also insert an interleaver after the encoder (in the transmitter) and a deinterleaver before the decoder (in the receiver). The process of interleaving premutes the symbols within a given block of data and, therefore, tends to decorrelate error events introduced by the equalizer between neighboring symbols. Convolutional decoder are often troubled by such error "bursts" if left unpermuted.

A BER-optimal receiver that jointly addresses equalization and decoding is usually impractically complex, in particular, in the presence of an interleaver. However, a number of iterative receiver algorithms have been developed that achieve near-optimal performance by repeating the equalization and decoding tasks on the same set of received data, using feedback information from the decoder in the equalization process. This method, which is called turbo equalization, was first proposed in [3]. By iteratively exchanging soft extrinsic information between a soft-input soft-output (SISO) equalizer and a SISO decoder, turbo equalizer can achieve large performance gains over separated equalizer and decoder structure.

1.2 PROBLEM STATEMENT

In its original form, Douillard *et al.* employed maximum *a posterior* probability (MAP) equalization and decoding methods in an iterative fashion. Unfortunately, the computational complexity of the MAP equalizer depends exponentially on constellation size and the length of the channel impulse response (CIR). Therefore, the design of low-complexity turbo equalizers based on minimum mean square error (MMSE) criterion has attracted considerable interests [4]- [10]. Existing approaches to MMSE-based SISO turbo equalizers can be roughly classified into three categories.

First, MMSE linear equalizers (MMSE-LE) [4, 5] treat each data symbol as a random variable with mean and variance computed from the *a priori* information. The exact solution of MMSE-LE (Exact-MMSE-LE) achieves close to MAP performance, but its all coefficients have to be computed anew for every symbol, resulting in

a time-varying equalizer whose computational complexity is quadratic in the number of equalizer coefficients. The approximate solution of MMSE-LE with "no *a priori* information" (approximate-MMSE-LE), yielding time-invariant coefficients, is also proposed in [5]. However, its performance is not as good as Exact-MMSE-LE.

Second, MMSE decision feedback equalizers under perfect hard decision assumption (MMSE-DFE-HD) are designed in [5]. It feeds back hard decisions and thus suffers error propagation. To alleviate error propagation arising from hard decisions, soft-decision feedback (MMSE-DFE-SD) is employed in [8]- [10]. However, their equalizer coefficients derivation is still under hard decision assumption which could be suboptimal for soft-decision feedback implementation.

Third, soft-feedback equalizer (SFE) proposed in [6, 7] combines soft decisions with the *a priori* information for ISI cancelation. And more importantly, its equalizer coefficients derivation is based on soft-decision feedback, which is different from perfect hard decision assumption. However, SFE is actually an ISI cancelation device with both anti-causal and causal filters rather than a general decision feedback filter. Also, SFE needs an iterative procedure to compute γ_e (probability density function parameter of equalizer extrinsic information output) and restricts itself in BPSK modulation.

Motivated by the respective advantages and limitations of the methods in the literature, two new decision feedback equalizer structures suitable for multilevel modulation systems are proposed for turbo equalization.

1.3 SUMMARY OF CONTRIBUTIONS

This dissertation will consist of a couple of journal publications and conference papers listed in the publication list. The published and expected contributions are:

1. The soft decision feedback turbo equalizer (SDFE) for multilevel modulation. The proposed SDFE took into account the reliability of both soft *a priori* information and soft decisions of the data symbols. For the first iteration, the proposed SDFE starts as MMSE linear equalizer. As iterations progress, the proposed SDFE behaves as soft-decision feedback MMSE DFE. When both soft *a priori* information and soft decisions become more reliable, the feedforward filter of the proposed SDFE approaches matched filter. Both EXIT chart analysis and simulation results have shown that the proposed SDFE performs close to the high-complexity Exact-MMSE-LE in BPSK/QPSK modulation. For high level modulations, the proposed SDFE exhibits lower SNR threshold and converges much faster than the high-complexity Exact-MMSE-LE.

2. The Soft Feedback ISI Canceller-based turbo equalizer (SIC) for multilevel modulation. The drawback of the SDFE is its coefficients couldn't reach matched filter bound and therefore after a large number of iterations (e.g. 10), its performance becomes inferior to that of Exact-MMSE-LE. SIC structure is therefore investigated, which is also a linear complexity equalizer that not only exhibits the same low complexity, low SNR threshold and fast convergence as the SDFE but also reaches matched filter bound after a large number of iterations.

3. Extend SDFE from single-input single-output (SISO) systems to multiple-input multiple-output (MIMO) communication systems. The purpose of this extension is to develop a low-complexity, iterative soft-decision feedback equalization (SDFE) receiver for severe, frequency selective ISI channels in multiple-input multiple-output (MIMO) communication systems. The proposed MIMO-SDFE algorithm offers a novel approach to combat error propagation. Performance of the proposed detection scheme is verified through simulations using different signal constellations. The performance and convergence property of the proposed MIMO-SDFE algorithm

are analyzed using extrinsic information transfer (EXIT) chart and verified by simulations in a severe inter-symbol interference channel. Simulation results show that our proposed algorithm has a significant improvement over the approximate MMSE linear turbo equalizer proposed in [4]. Moreover, we show that the performance of the proposed equalization scheme improves significantly when higher order constellations are used for digital modulation.

4. Apply SDFE and SIC in high data-rate underwater acoustic (UWA) communication systems. Mitigating inter-symbol interference (ISI) is one of the most important challenges in achieving high data rates in underwater acoustic (UWA) communication systems. To alleviate the fast temporal variations and long multi-path delay spreads of the underwater channels, both SDFE and SIC structures are applied for single-carrier underwater acoustic communications. The proposed detection schemes have been tested by undersea trial data collected in the undersea experiment named ACOMM09 and MACE10. The testings have been performed with different transmission ranges, different modulation schemes, and different MIMO system configurations. The results show that the proposed algorithms provided robust detection for MIMO UWA communications.

1.4 REFERENCES

[1] J. Proakis, *Digital Communications*, 4th ed., McGraw-Hill, 2000.

[2] S. Haykin, *Communications Systems*, 3rd ed., New York: Wiley, 1994.

[3] C. Douillard, C. Berrou, A. Picart, and A. Glavieux, "Iterative correction of intersymbol interference: Turbo Equalization," *European Trans. on Telecomm*, vol.6, pp.507-511, Sept.-Oct. 1995.

[4] M. T*ü*chler, A. C. Singer, and R. Koetter, "Minimum mean square error equalization using a priori information," in *IEEE Trans. Signal Processing*, vol.50, pp.673-683, Mar. 2002.

[5] M. T*ü*chler, R. Koetter, and A. C. Singer, "Turbo equalization: Principles and new results," *IEEE Trans. Commun*, vol.50, no.5, pp.754-767, May. 2002.

[6] R. R. Lopes and J. R. Barry, "The soft-feedback equalizer for turbo equalization of highly dispersive channels," *IEEE Trans. Commun*, vol.54, no.5, pp.783-788, May. 2006.

[7] R. R. Lopes, "Iterative estimation, equalization and decoding," *Ph.D. dissertation, Georgia Inst. Technol.*, Atlanta, GA, 2003.

[8] J. Wu and Y. R. Zheng, "Low complexity soft-input soft-output block decision feedback equalization," *IEEE J. Select. Areas Commun.*, vol.26, no.2, pp.281-289, Feb. 2008.

[9] A. Glavieux, C. Laot and J. Labat, "Turbo equalization over a frequency selective channel," in *Proc. Int. Symp. Turbo Codes, Related Topics*, Brest, France, pp.96-102, Sep. 1997.

[10] Z.Wu and J. Cioffi, "Low complexity iterative decoding with Decision-Aided Equalization for magnetic recording channels," *IEEE J. Select. Areas Commun.*, vol.19, no.4, pp.699-708, April. 2001.

PAPER

I. SOFT-DECISION FEEDBACK TURBO EQUALIZATION FOR MULTILEVEL MODULATIONS

Huang Lou and Chengshan Xiao, *Fellow, IEEE*

Abstract—Error propagation phenomena is the major drawback for existing hard-decision feedback turbo equalizers. In this paper, we propose a new soft-decision feedback equalizer (SDFE) suitable for multilevel modulation systems employing turbo equalization. The proposed SDFE offers a low computational complexity growing only linearly with the number of equalizer coefficients, as opposed to the quadratic complexity of MMSE-based linear turbo equalizer with time-varying coefficients (Exact-MMSE-LE). The performance and convergence property of the proposed SDFE are analyzed using extrinsic information transfer (EXIT) chart and verified by simulations in a severe intersymbol interference channel set by Proakis. Results show that our approach performs close to Exact-MMSE-LE for BPSK/QPSK modulation. And for 8PSK/16QAM modulations, the proposed SDFE performs much better. It exhibits lower SNR threshold (SNR required for "water fall" BER) and much faster convergence than Exact-MMSE-LE.

1 Introduction

Turbo equalization is a joint channel equalization and channel decoding scheme used in communication systems with data transmission over intersymbol interference (ISI) channel [1]. By iteratively exchanging soft extrinsic information between a soft-input soft-output (SISO) equalizer and a SISO decoder, turbo equalizer can achieve large performance gains over separated equalizer and decoder structure. In

its original form, Douillard *et al.* employed maximum *a posterior* probability (MAP) equalization and decoding methods in an iterative fashion. Unfortunately, the computational complexity of the MAP equalizer depends exponentially on constellation size and the length of the channel impulse response (CIR). Therefore, the design of low-complexity turbo equalizers based on minimum mean square error (MMSE) criterion has attracted considerable interests [2]- [8]. Existing approaches to MMSE-based SISO turbo equalizers can be roughly classified into three categories.

First, MMSE linear equalizers (MMSE-LE) [2, 3] treat each data symbol as a random variable with mean and variance computed from the *a priori* information. The exact solution of MMSE-LE (Exact-MMSE-LE) achieves close to MAP performance, but its all coefficients have to be computed anew for every symbol, resulting in a time-varying equalizer whose computational complexity is quadratic in the number of equalizer coefficients. The approximate solution of MMSE-LE with "no *a priori* information" (approximate-MMSE-LE), yielding time-invariant coefficients, is also proposed in [3]. However, its performance is not as good as Exact-MMSE-LE.

Second, MMSE decision feedback equalizers under perfect hard decision assumption (MMSE-DFE-HD) are designed in [3]. It feeds back hard decisions and thus suffers error propagation. To alleviate error propagation arising from hard decisions, soft-decision feedback (MMSE-DFE-SD) is employed in [6]- [8]. However, their equalizer coefficients derivation is still under hard decision assumption which could be suboptimal for soft-decision feedback implementation.

Third, soft-feedback equalizer (SFE) proposed in [4, 5] combines soft decisions with the *a priori* information for ISI cancelation. And more importantly, its equalizer coefficients derivation is based on soft-decision feedback, which is different from perfect hard decision assumption. However, SFE is actually an ISI cancelation device with both anti-causal and causal filters rather than a general decision feedback filter. Also, SFE needs an iterative procedure to compute γ_e (probability density

function parameter of equalizer extrinsic information output) and restricts itself in BPSK modulation.

Motivated by the respective advantages and limitations of the methods in the literature, we here propose a low-complexity MMSE-based SISO SDFE, a turbo equalization scheme that shares some similarities with SFE in [4, 5]. However, our approach differs SFE in three aspects:

1) we include time-varying offset d_n (compensating for a possibly nonzero mean of data symbols given *a priori* information) in equalizer coefficients derivation to cancel both anti-causal and causal ISI. Because of d_n, the anti-causal filter is not needed any more. Also, the equalizer structure appears to be a natural generalization of traditional DFE from hard-decision to soft-decision.

2) MMSE-LE is employed in first turbo iteration to replace the iterative procedure for initial γ_e computation. Therefore, the induced convergence delay and computation burden in [4] can be avoided.

3) we extend the modulation from BPSK to MPSK and QAM. For BPSK, the probability density function (pdf) of extrinsic information is easy to obtain. However, for multilevel modulations, proper LLR approximation needs to be made with certain methods for specific symbol alphabets.

Moreover, timing-invariant equalizer coefficients are employed for low-complexity purpose in the proposed SDFE. With the help of both *a priori* information and soft decisions, the proposed SDFE not only successfully mitigates the error propagation phenomena existed in hard-decision feedback turbo equalizers, but also shows better performance than Exact-MMSE-LE for high level modulations.

The remainder of this paper is organized as follows. A brief definition of a coded data transmitter and signals are given in Section II. In section III, we describe the general structure of the proposed SDFE. The performance of the proposed SDFE is analyzed in Section IV with the tool of EXIT chart. Simulation results are verified

and compared to existing turbo equalizations in Section V. Section VI draws the conclusion.

2 Preliminary

We consider the transmitter depicted together with the ISI channel in Figure 1. Length $K_c \times Q$ bit sequences $\mathbf{c} = [\mathbf{c}_1\ \mathbf{c}_2 \cdots \mathbf{c}_{K_c}]$ are subject to transmitting over an ISI channel, where subsequences $\mathbf{c}_n = [c_{n,1}\ c_{n,2} \cdots c_{n,Q}]$ with bits $c_{n,j} \in 0, 1$. The mapper maps each $\mathbf{c}_n$ to a symbol x_n from the 2^Q-ary constellation set $S = \{\alpha_1, \alpha_2, \cdots, \alpha_{2^Q}\}$, where α_i corresponds to the bit pattern $\mathbf{s}_i = [s_{i,1}\ s_{i,2} \cdots s_{i,Q}]$ with $s_{i,j} \in 0, 1$ in Table 1.

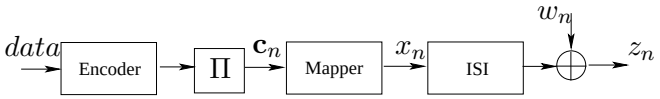

Figure 1. Transmitter section of the data transmission system.

The ISI channel is of length M with impulse response

$$h[n] = \sum_{k=0}^{M-1} h_k \delta[n-k]$$

and the noise samples w_n are independent and identically distributed (i.i.d.) with the variance of $\sigma_w^2/2$ for both real and imaginary part. Thus, the receiver input z_n can be written as

$$z_n = \sum_{k=0}^{M-1} h_k x_{n-k} + w_n \tag{1}$$

Table 1. Symbol alphabets.

BPSK:

i	1	2
$s_{i,1}$	0	1
α_i	$+1$	-1

QPSK:

i	1	2	3	4
$s_{i,1}\ s_{i,2}$	00	01	10	11
α_i	$(+1+i)/\sqrt{2}$	$(+1-i)/\sqrt{2}$	$(-1+i)/\sqrt{2}$	$(-1-i)/\sqrt{2}$

8PSK:

i	1	2	3	4	5	6	7	8
$s_{i,1}\ s_{i,2}\ s_{i,3}$	000	001	010	011	100	101	110	111
α_i	$e^{(\frac{i9\pi}{8})}$	$e^{(\frac{i11\pi}{8})}$	$e^{(\frac{i15\pi}{8})}$	$e^{(\frac{i13\pi}{8})}$	$e^{(\frac{i7\pi}{8})}$	$e^{(\frac{i5\pi}{8})}$	$e^{(\frac{i\pi}{8})}$	$e^{(\frac{i3\pi}{8})}$

16QAM:

i	1	2	3	4	5	6	7	8
$s_{i,1}\ s_{i,2}\ s_{i,3}\ s_{i,4}$	0000	0001	0010	0011	0100	0101	0110	0111
α_i	$\frac{(-1-i)}{\sqrt{10}}$	$\frac{(-1-3i)}{\sqrt{10}}$	$\frac{(-1+i)}{\sqrt{10}}$	$\frac{(-1+3i)}{\sqrt{10}}$	$\frac{(-3-i)}{\sqrt{10}}$	$\frac{(-3-3i)}{\sqrt{10}}$	$\frac{(-3+i)}{\sqrt{10}}$	$\frac{(-3+3i)}{\sqrt{10}}$
i	9	10	11	12	13	14	15	16
$s_{i,1}\ s_{i,2}\ s_{i,3}\ s_{i,4}$	1000	1001	1010	1011	1100	1101	1110	1111
α_i	$\frac{(1-i)}{\sqrt{10}}$	$\frac{(1-3i)}{\sqrt{10}}$	$\frac{(1+i)}{\sqrt{10}}$	$\frac{(1+3i)}{\sqrt{10}}$	$\frac{(3-i)}{\sqrt{10}}$	$\frac{(3-3i)}{\sqrt{10}}$	$\frac{(3+i)}{\sqrt{10}}$	$\frac{(3+3i)}{\sqrt{10}}$

or in matrix form for $N = N_1 + N_2 + 1$ received symbols

$$\mathbf{z}_n = \mathbf{H}\mathbf{x}_n + \mathbf{w}_n \tag{2}$$

$$\mathbf{z}_n = [z_{n-N_2}\ z_{n-N_2+1} \cdots z_{n+N_1}]^T$$

$$\mathbf{x}_n = [x_{n-N_2-M+1}\ x_{n-N_2-M+2} \cdots x_{n+N_1}]^T$$

$$\mathbf{w}_n = [w_{n-N_2}\ w_{n-N_2+1} \cdots w_{n+N_1}]^T$$

$$\mathbf{H} = \begin{bmatrix} h_{M-1} & \cdots & h_0 & \cdots & 0 \\ \vdots & \ddots & \ddots & \ddots & \vdots \\ 0 & \cdots & h_{M-1} & \cdots & h_0 \end{bmatrix}.$$

In the sequel, some frequently used notations are introduced. Vectors are written in bold letters. Matrices are specified in bold capital letters. Time index n is used to denote time-varying quantities. The $i\times j$ matrix $\mathbf{1}_{i\times j}$ and $\mathbf{0}_{i\times j}$ contains all ones and all zeros. I_i is an $i \times i$ identity matrix. $(\cdot)^*$, $(\cdot)^{-1}$, $(\cdot)^T$ and $(\cdot)^H$ are respectively the conjugate, inverse, transpose and hermitian operators. The covariance operator $\mathrm{Cov}(x, y)$ is given by $E(xy^H) - E(x)E(y^H)$, where $E(.)$ is the expectation operator.

3 Soft-Decision Feedback Turbo Equalizer

3.1 SDFE Coefficients

The MMSE estimate $\hat{x}_n$ of the transmitted symbol x_n is given by

$$\begin{aligned} \hat{x}_n &= \mathbf{f}_n\mathbf{z}_n + \mathbf{b}_n\mathbf{x}_n^d + d_n \\ \mathbf{x}_n^d &= [x_{n-N_3}^d \; x_{n-N_3+1}^d \cdots x_{n-1}^d]^T \\ \mathbf{f}_n &= [f_{N_2,n} \; f_{N_2-1,n} \cdots f_{-N_1,n}] \\ \mathbf{b}_n &= [b_{N_3,n} \; b_{N_3-1,n} \cdots b_{1,n}] \end{aligned} \tag{3}$$

where $N_3 = N_2 + M - 1$, x_n^d is the past decided estimate determined by soft *a priori* information λ_n^p and soft extrinsic information λ_n. $\mathbf{f}_n$ and $\mathbf{b}_n$ are feedforward and feedback coefficients, respectively.

Now, we assume that $\mathrm{Cov}(x_n, x_m)$=$\mathrm{Cov}(x_n, x_m^d)$=$\mathrm{Cov}(x_n^d, x_m^d)$=0 for all n, m and $n \neq m$. This is reasonable since x_n^d is approximately equal to x_n. Then, using partial differentiation method, one can show that the minimum MSE values of

$\mathbf{f}_n^H, \mathbf{b}_n^H$(Hermitian of $\mathbf{f}_n, \mathbf{b}_n$) and d_n are obtained as

$$\mathbf{f}_n^H = \left[\sigma_w^2 \mathbf{I}_N + \mathbf{H}\left(\mathbf{C}_n^{ff} - \mathbf{C}_n^{fb}(\mathbf{C}_n^{bb})^{-1}\mathbf{C}_n^{fbH}\right)\mathbf{H}^H\right]^{-1}\mathbf{s}_n \tag{4}$$

$$\mathbf{b}_n^H = -(\mathbf{C}_n^{bb})^{-1}\mathbf{H}\mathbf{C}_n^{fbH}\mathbf{f}_n^H \tag{5}$$

$$d_n = E\{x_n\} - \mathbf{f}_n\mathbf{H}E\{\mathbf{x}_n\} - \mathbf{b}_n E\{\mathbf{x}_n^d\} \tag{6}$$

$$\hat{x}_n = \mathbf{f}_n(\mathbf{z}_n - \mathbf{H}E\{\mathbf{x}_n\}) + \mathbf{b}_n(\mathbf{x}_n^d - E\{\mathbf{x}_n^d\}) + E\{x_n\} \tag{7}$$

where

$$\mathbf{C}_n^{ff} = E\{\mathbf{x}_n\mathbf{x}_n^H\} - E\{\mathbf{x}_n\}E\{\mathbf{x}_n^H\}$$

$$\mathbf{C}_n^{fb} = E\{\mathbf{x}_n\mathbf{x}_n^{dH}\} - E\{\mathbf{x}_n\}E\{\mathbf{x}_n^{dH}\}$$

$$\mathbf{C}_n^{bb} = E\{\mathbf{x}_n^d\mathbf{x}_n^{dH}\} - E\{\mathbf{x}_n^d\}E\{\mathbf{x}_n^{dH}\}$$

$$\mathbf{s}_n = \mathbf{H}(E\{\mathbf{x}_n x_n^*\} - E\{\mathbf{x}_n\}E\{x_n^*\}).$$

Proof: See Appendix.

3.2 SDFE Structure

According to equation (7), we establish the equalizer structure for the proposed SDFE as shown in Figure 2. As we can see, for the first iteration, $\mathbf{H}E\{\mathbf{x}_n\} = \mathbf{0}_{(N_1+N_2+1)\times 1}, E\{x_n\} = 0, E\{\mathbf{x}_n^d\} = \mathbf{0}_{N_3\times 1}$, the proposed SDFE becomes the traditional decision feedback equalizer [14]. As iterations progress, $\mathbf{H}E\{\mathbf{x}_n\}$ in d_n becomes more reliable and is used to cancel both anti-casual and casual ISI from $\mathbf{z}_n$ (the same function as ISI-canceling filters in SFE [4]). Meanwhile, $\mathbf{f}_n$ is approaching matched filter response to $h[n]$.

In order to compute $\mathbf{f}_n, \mathbf{b}_n$ and d_n, covariance matrices $\mathbf{C}_n^{ff}$, $\mathbf{C}_n^{fb}$ and $\mathbf{C}_n^{bb}$ have to be decided first. $\mathbf{C}_n^{ff}$ can be easily computed using the *a priori* information from decoder. For calculating $\mathbf{C}_n^{fb}$ and $\mathbf{C}_n^{bb}$, which are different from perfect hard decision

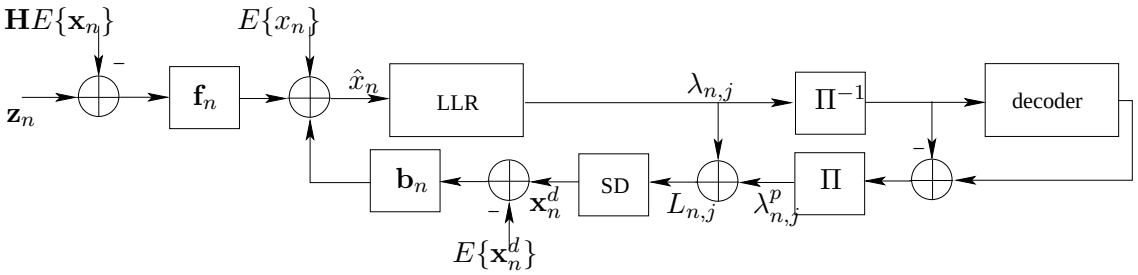

Figure 2. Soft-decision feedback turbo equalizer.

assumption in [3], expectation values ξ=$E\{x_n^d\}$, ζ=$E\{x_n^d x_n^{d*}\}$ and β=$E\{x_n x_n^{d*}\}$ have to be determined according to the quality of both soft *a priori* information and soft decisions of data symbols. Here we have assumed that ξ, β and ζ are time-invariant for all n, since the average symbol error probability is approximately the same for each symbol.

3.3 Expected Value Computation for BPSK

Since the expected values ξ, β and ζ are functions of x_n^d, and x_n^d is a function of LLR values λ_n and λ_n^p, we now have to obtain the pdf of λ_n and λ_n^p. The approach will be similar to the one presented in [4].

At the output of the equalizer, we assume as in [10] that the estimate $\hat{x}_n$ is the output of an equivalent AWGN channel having $x_n \in \{-1, 1\}$ as its input:

$$\hat{x}_n = Ax_n + v_n \tag{8}$$

where $A = E\{\hat{x}_n x_n^*\} = \mathbf{f}_n \mathbf{s}_n$ and v_n is a white Gaussian noise with zero mean and variance $A(1-A)$.

The computation of the extrinsic LLR $\lambda_{n,j}$ of coded bit $c_{n,j}$ ($j = 1$ for BPSK) is obtained as

$$\lambda_{n,1} = \log \frac{P(\hat{x}_n | x_n = 1)}{P(\hat{x}_n | x_n = -1)} = \frac{2\hat{x}_n}{1 - A}. \tag{9}$$

Let $\gamma_e = 2A/(1 - A)$, we have $\lambda_{n,1} \sim \mathcal{N}(x_n \gamma_e, 2\gamma_e)$.

Also, the *a priori* information $\lambda^p_{n,1}$ of $c_{n,1}$ can be computed from another equivalent AWGN channel with output

$$l_n = x_n + u_n \tag{10}$$

where $u_n \sim \mathcal{N}(0, \sigma_u^2)$, let $\gamma_p = 2/\sigma_u^2$, one can get

$$\lambda^p_{n,1} = \log \frac{P(x_n = 1)}{P(x_n = -1)} = \gamma_p l_n \tag{11}$$

and $\lambda^p_{n,1} \sim \mathcal{N}(x_n \gamma_p, 2\gamma_p)$.

After adding $\lambda_{n,1}$ and $\lambda^p_{n,1}$ together, we have the full LLR value $L_{n,1} = \lambda_{n,1} + \lambda^p_{n,1}$ and it follows $L_{n,1} \sim \mathcal{N}(x_n(\gamma_e + \gamma_p), 2(\gamma_e + \gamma_p))$.

The computation of x^d_n is then written as

$$x^d_n = \tanh(L_{n,1}/2) \tag{12}$$

and thus,

$$\begin{aligned} \xi &= E\{x^d_n\} \\ &= E\{\tanh(L_{n,1}/2) | x_n = 1\} P_r(x_n = 1) \\ &\quad + E\{\tanh(L_{n,1}/2) | x_n = -1\} P_r(x_n = -1) = 0 \end{aligned} \tag{13}$$

$$\begin{aligned}\beta &= E\{x_n x_n^{d*}\} \\ &= E\{\tanh(L_{n,1}/2)|x_n = 1\}P_r(x_n = 1) \\ &\quad -E\{\tanh(L_{n,1}/2)|x_n = -1\}P_r(x_n = -1) \\ &= E\{\tanh(L_{n,1}/2)|x_n = 1\} \end{aligned} \tag{14}$$

$$\begin{aligned}\zeta &= E\{x_n^d x_n^{d*}\} \\ &= E\{\tanh^2(L_{n,1}/2)|x_n = 1\}P_r(x_n = 1) \\ &\quad +E\{\tanh^2(L_{n,1}/2)|x_n = -1\}P_r(x_n = -1) \\ &= E\{\tanh^2(L_{n,1}/2)|x_n = 1\}. \end{aligned} \tag{15}$$

Notice here we have made equal probability assumption since ξ, β and ζ are not used for individual x_n. Generally speaking, $E\{x_n^d\}$, $E\{x_n x_n^{d*}\}$ and $E\{x_n^d x_n^{d*}\}$ are time-varying for each x_n according to the *a priori* probability.

Although no closed-form formula exists for β and ζ, they can be computed by numerical methods as long as we know the parameters γ_e and γ_p.

Because $E\{|\lambda_{n,1}^p|^2\} = \gamma_p^2 + 2\gamma_p$, γ_p can be estimated directly from the *a priori* information $\lambda_{n,1}^p$. The maximum-likelihood (ML) estimate of γ_p is then obtained as

$$\gamma_p^{ML} = \sqrt{1 + \frac{1}{K_c}\sum_{n=1}^{K_c} |\lambda_{n,1}^p|^2} - 1. \tag{16}$$

To determine γ_e, we need know $A = \mathbf{f}_n \mathbf{s}_n$, while we need γ_e to calculate β and ζ, and thus $\mathbf{f}_n$. This is problematic. To find both simultaneously, Lopes and Barry propose giving an initial estimate for γ_e, then compute $\mathbf{f}_n$ and γ_e iteratively, until they converge [4]. The disadvantage of this iterative procedure is that it involves a

lot of computations. In our latter subsection, we will introduce a method to avoid this iterative procedure.

3.4 Expected Value Computation for Multilevel Modulations

We rewrite the estimate $\hat{x}_n$ of $x_n \in S$ as:

$$\hat{x}_n = Ax_n + v_n \tag{17}$$

and it follows $\hat{x}_n \sim \mathcal{N}(x_n A, \sigma^2)$, where $\sigma^2 = A(1-A),\ A = \mathbf{f}_n \mathbf{s}_n$ [10].

The symbol extrinsic probability is presented as

$$P(\hat{x}_n | x_n = \alpha_i) = \frac{1}{\sigma^2 \pi} \exp(-\rho_{n,i}) \tag{18}$$

$$\rho_{n,i} = \frac{|\hat{x}_n - A\alpha_i|^2}{\sigma^2}. \tag{19}$$

The extrinsic LLR $\lambda_{n,j}$ of coded bit $c_{n,j}$ is the function of $P(\hat{x}_n | x_n = \alpha_i)$:

$$\begin{aligned} \lambda_{n,j} &= \log \frac{\sum_{\alpha_i : c_{n,j}=0} P(\hat{x}_n|\alpha_i) \prod_{\forall j', j' \neq j} P(c_{n,j'})}{\sum_{\alpha_i : c_{n,j}=1} P(\hat{x}_n|\alpha_i) \prod_{\forall j', j' \neq j} P(c_{n,j'})} \\ &= \log \frac{\sum_{\alpha_i : c_{n,j}=0} \exp(-\rho_{n,i} + \sum_{\forall j', j' \neq j} \tilde{s}_{i,j} L(c_{n,j'})/2)}{\sum_{\alpha_i : c_{n,j}=1} \exp(-\rho_{n,i} + \sum_{\forall j', j' \neq j} \tilde{s}_{i,j} L(c_{n,j'})/2)} \end{aligned} \tag{20}$$

where

$$\tilde{s}_{i,j} = \begin{cases} +1 & \text{if } s_{i,j} = 0 \\ -1 & \text{if } s_{i,j} = 1 \end{cases}$$

Substituting (18) and (19) to (20), one can get $\lambda_{n,j}$ as a function of $\hat{x}_n$. This means that the pdf of $\lambda_{n,j}$ is related to the pdf of $\hat{x}_n$.

For QPSK or QAM modulation, the complexity of the relation between $\lambda_{n,j}$ and $\hat{x}_n$ can be reduced by using minimum-based LLR simplification defined by

$$\log(\exp(-x) + \exp(-y)) = -min(x, y) + \log(1 + \exp(-|x - y|)) \approx -min(x, y) \quad (21)$$

when $|x - y|$ is sufficiently large.

For MPSK ($M > 2$) modulation, the minimum-based LLR simplifications can not be made because several symbols are quite close to each other on the unit circle. Instead, a geometric approach [11] can be applied to estimate LLR $\lambda_{n,j}$. The approximation is listed in Table 2.

Table 2. LLR $\lambda_{n,j}$ approximation for symbol alphabets in Table 1.

QPSK:
- $\lambda_{n,1} \approx 2\sqrt{2}\text{Re}\{\hat{x}_n\}/(1 - A)$.
- $\lambda_{n,2} \approx 2\sqrt{2}\text{Im}\{\hat{x}_n\}/(1 - A)$.

8PSK:
- $\lambda_{n,1} \approx -4\sin(7\pi/8)\text{Im}\{\hat{x}_n\}/(1 - A)$.
- $\lambda_{n,2} \approx -4\sin(7\pi/8)\text{Re}\{\hat{x}_n\}/(1 - A)$.
- $\lambda_{n,3} \approx 1.0824(|\text{Re}\{\hat{x}_n\}| - |\text{Im}\{\hat{x}_n\}|)/(1 - A)$.

16QAM:
- $\lambda_{n,1} \approx -4\text{Re}\{\hat{x}_n\}/(\sqrt{10}(1 - A))$.
- $\lambda_{n,2} \approx (8A - 4\sqrt{10}|\text{Re}\{\hat{x}_n\}|)/(10(1 - A))$.
- $\lambda_{n,3} \approx -4\text{Im}\{\hat{x}_n\}/(\sqrt{10}(1 - A))$.
- $\lambda_{n,4} \approx (8A - 4\sqrt{10}|\text{Im}\{\hat{x}_n\}|)/(10(1 - A))$.

Note: LLR $\lambda_{n,j}$ approximation is only used for computing ξ, β and ζ.

After obtaining $\lambda_{n,j}$, we can calculate full LLR value $L_{n,j}$ of coded bit $c_{n,j}$

$$\lambda_{n,j}^{p} = \log \frac{P(c_{n,j}=0)}{P(c_{n,j}=1)} \tag{22}$$

$$L_{n,j} = \lambda_{n,j} + \lambda_{n,j}^{p} \tag{23}$$

where $\lambda_{n,j}^{p} \sim \mathcal{N}(\gamma_p, 2\gamma_p)$ in condition of $c_{n,j}=0$.

The computation of x_n^d is given by

$$x_n^d = \sum_{\alpha_i \in S} \alpha_i P(\tilde{x_n^d} = \alpha_i) \tag{24}$$

$$P(\tilde{x_n^d} = \alpha_i) = \prod_{j=1}^{Q} \frac{1}{2}(1 + \tilde{s}_{i,j} \tanh(L_{n,j}/2)). \tag{25}$$

By exploiting symmetries and equal probability of $\alpha_i \in S$, we get

$$\xi = 0 \tag{26}$$

$$\beta = \alpha_i E\{x_n^{d*} | x_n = \alpha_i\} \tag{27}$$

$$\zeta = E\{x_n^d x_n^{d*} | x_n = \alpha_i\} \tag{28}$$

where for MPSK, α_i can be any elements in S, while for QAM, β and ζ should be re-scaled when $|\alpha_i| \neq 1$. Since x_n^d is a function of $L_{n,j}$, as long as we know the parameters γ_p of $\lambda_{n,j}^{p}$ and A of $\hat{x}_n$, expected values β and ζ can be calculated through numerical methods.

The ML estimate of γ_p^{ML} can be estimated using

$$\gamma_p^{ML} = \sqrt{1 + \frac{1}{K_c \times Q} \sum_{n=1}^{K_c} \sum_{j=1}^{Q} |\lambda_{n,j}^{p}|^2} - 1. \tag{29}$$

In order to determine A, we need $\mathbf{f}_n$, while we need A to calculate β and ζ, and thus $\mathbf{f}_n$. The same iteration procedure as in BPSK case can be used to find both simultaneously.

3.5 Low-Complexity SDFE

An important aspect of these SISO equalizer algorithms is their computational complexity. Computing $\mathbf{f}_n$, $\mathbf{b}_n$, $\mathbf{C}_n^{fb}$ and $\mathbf{C}_n^{bb}$ for each time step n causes a higher computational load. The complexity can be reduced by using time-invariant $\mathbf{f}_{TI}$, $\mathbf{b}_{TI}$, $\mathbf{C}_{TI}^{fb}$ and $\mathbf{C}_{TI}^{bb}$ in each data block given by

$$\begin{aligned}\mathbf{f}_{TI}^H &= [\sigma_w^2\mathbf{I}_N + \mathbf{H}(\mathbf{I}_{N_1+N_2+M} \\ &\quad -\mathbf{C}_{TI}^{fb}(\mathbf{C}_{TI}^{bb})^{-1}\mathbf{C}_{TI}^{fbH})\mathbf{H}^H]^{-1}\mathbf{s} \qquad (30)\\ \mathbf{b}_{TI}^H &= -(\mathbf{C}_{TI}^{bb})^{-1}\mathbf{H}\mathbf{C}_{TI}^{fbH}\mathbf{f}_{TI}^H \qquad (31)\\ d_n &= E\{x_n\} - \mathbf{f}_{TI}\mathbf{H}E\{\mathbf{x}_n\} - \mathbf{b}_{TI}E\{\mathbf{x}_n^d\} \qquad (32)\\ \hat{x}_n &= \mathbf{f}_{TI}\mathbf{z}_n + \mathbf{b}_{TI}\mathbf{x}_n^d + d_n \qquad (33)\end{aligned}$$

where

$$\begin{aligned}\mathbf{s} &= \mathbf{H}[\mathbf{0}_{1\times(N_2+M-1)}\ 1\ \mathbf{0}_{1\times N_1}]^T\\ \mathbf{C}_{TI}^{bb} &= \zeta\mathbf{I}_{N_3}\\ \mathbf{C}_{TI}^{fb} &= \begin{bmatrix}\beta & 0 & \cdots & 0\\ 0 & \beta & \cdots & 0\\ \vdots & \ddots & \ddots & \vdots\\ 0 & \cdots & 0 & \beta\\ 0 & \cdots & \cdots & 0\\ \vdots & \ddots & \ddots & \vdots\\ 0 & \cdots & \cdots & 0\end{bmatrix}.\end{aligned}$$

When $|\lambda_{n,j}|$ and $|\lambda_{n,j}^{p}|$ go to infinity, $\beta \to 1$ and $\zeta \to 1$, thus $\mathbf{f}_{TI}^{H} \to [\sigma_w^2 \mathbf{I}_N + \mathbf{HCH}^H + \mathbf{ss}^H]^{-1}\mathbf{s}$, which is close to the matched filter response $\mathbf{f}_{MF}^{H} = [\sigma_w^2 \mathbf{I}_N + \mathbf{ss}^H]^{-1}\mathbf{s}$.

$$\mathbf{C}=\begin{bmatrix} \mathbf{I}_{N_1 \times N_1} & \mathbf{0}_{N_1 \times (N_2+M)} \\ \mathbf{0}_{(N_2+M)\times N_1} & \mathbf{0}_{(N_2+M)\times(N_2+M)} \end{bmatrix}.$$

Also we have observed that in [4], in order to reduce computational complexity, they only compute $\mathbf{f}_n$ and γ_e iteratively for first turbo iteration. In later turbo iterations, they calculate $\mathbf{f}_n$ using the γ_e from previous turbo iteration. An updated γ_e is then computed and passed on to the next turbo iteration.

In fact, for the first turbo iteration, soft decisions are usually not reliable. So we suggest replacing the proposed SDFE with MMSE-LE to reduce error propagations and in the meantime, avoid iterative calculation of initial $\mathbf{f}_n$.

The key algorithm for SDFE equalizer is summarized in Table 3, where the index (i) refers to the turbo iteration, $\mathbf{f}_{TI}^{H\,(i)}$, $\mathbf{b}_{TI}^{H\,(i)}$ and ${d_n}^{(i)}$ are equalizer parameters for i–th turbo iteration, ${\gamma_e}^{(i+1)}$ (or $A^{(i+1)}$) is calculated at i–th iteration but passed on to $(i+1)$–th turbo iteration.

Furthermore, for real-time hardware implementation, a mapping table between γ_e (or A) and ξ, ζ and β can be pre-computed and stored in lookup table (LUT) for specific modulations. In this way, lots of computational burdens can be reduced. The total computational complexity will depend only linearly on the number of equalizer coefficients, as opposed to the quadratic complexity of Exact-MMSE-LE.

4 Performance Analysis With EXIT Chart

The performance of the proposed SDFE equalizer is analyzed in this section by using the tool of extrinsic information transfer chart [3, 9, 12, 13], which traces the

Table 3. SDFE equalizer algorithm.

FIRST ITERATION:
- $\mathbf{f}_{TI}^{H\,(1)} = [\sigma_w^2 \mathbf{I}_N + \mathbf{H}\mathbf{H}^H]^{-1}\mathbf{s}$, $\mathbf{b}_{TI}^{H\,(1)} = \mathbf{0}_{N_3 \times 1}$ and ${d_n}^{(1)} = 0$.
- Compute $\hat{x}_n^{(1)}$ using equation (33).

BPSK:
· ${\gamma_e}^{(2)} = 2{\mathbf{f}_{TI}}^{(1)}\mathbf{s}/(1 - {\mathbf{f}_{TI}}^{(1)}\mathbf{s})$.
· Compute ${\lambda_{n,1}}^{(1)}$ and $x_n^{d\,(1)}$ using equations (9) and (12).

MPSK/QAM:
· $A^{(2)} = {\mathbf{f}_{TI}}^{(1)}\mathbf{s}$.
· Compute ${\lambda_{n,j}}^{(1)}$ and $x_n^{d\,(1)}$ using equations (20) and (24).

The i–th **ITERATION** $(i > 1)$**:**
- Compute ${\gamma_p}^{(i)}$ using equation (29).

BPSK:
· Compute $\zeta^{(i)}$ and $\beta^{(i)}$ using equations (14) and (15).

MPSK/QAM:
· Compute $\zeta^{(i)}$ and $\beta^{(i)}$ using equations (27) and (28).
- Compute $\mathbf{f}_{TI}^{H\,(i)}$, $\mathbf{b}_{TI}^{H\,(i)}$ and ${d_n}^{(i)}$ using equations (30), (31) and (32).
- Compute $\hat{x}_n^{(i)}$ using equation (33).

BPSK:
· ${\gamma_e}^{(i+1)} = 2{\mathbf{f}_{TI}}^{(i)}\mathbf{s}/(1 - {\mathbf{f}_{TI}}^{(i)}\mathbf{s})$.
· Compute ${\lambda_{n,1}}^{(i)}$ and $x_n^{d\,(i)}$ using equations (9) and (12)..

MPSK/QAM:
· $A^{(i+1)} = {\mathbf{f}_{TI}}^{(i)}\mathbf{s}$.
· Compute ${\lambda_{n,j}}^{(i)}$ and $x_n^{d\,(i)}$ using equations (20) and (24).

evolution of mutual information between data symbols and its LLR through iterations. It is used to graphically predict the behavior of the iterative algorithm.

The SISO equalizer/decoder can be modeled as a mutual information transfer device, *i.e.*, given *a priori* mutual information at the input, IE_i, ID_i, the equalizer/decoder generates a new mutual information, IE_o, ID_o, at the output by exploiting the channel/code structure. This concept is illustrated in Figure 3.

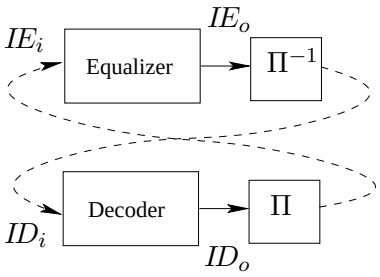

Figure 3. Model for analysis of the iterative receiver.

4.1 EXIT Chart of a MAX-LOG-MAP Decoder

Figure 4 shows the EXIT chart of a MAX-LOG-MAP decoder using rate $R = 1/2$ convolutional code with generator polynomial in octal notation $G = [7, 5]$. To obtain this EXIT chart, 10^6 coded bits generated from randomly chosen equiprobable information bits and 10^6 corresponding Gaussian distributed *a priori* LLRs given a preset σ_i are used. For the chosen σ_i, the mutual information ID_i is computed numerically using

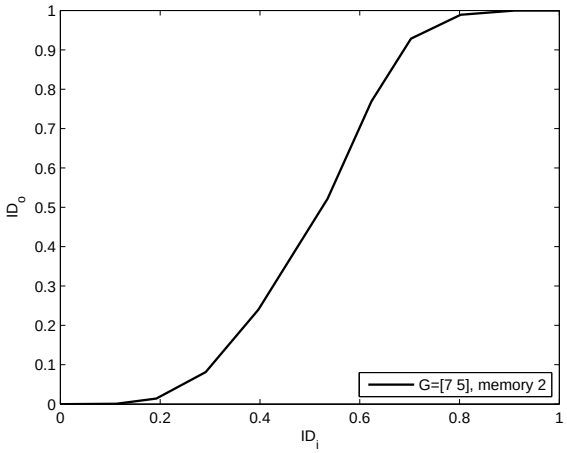

Figure 4. EXIT charts of a MAX-Log-MAP decoder.

$$ID_i = \frac{1}{2} \sum_{x \in \{+1,-1\}} \int_{-\infty}^{+\infty} f_L(l|x) \cdot \log_2 \frac{2 f_L(l|x)}{f_L(l|+1) + f_L(l|-1)} dl \quad (34)$$

$$f_L(l|x) = \phi((l - x\sigma_i^2/2)/\sigma_i)/\sigma_i \quad (35)$$

where $\phi(x) = e^{-x^2/2}/\sqrt{2\pi}$. The pdfs of the output LLRs are estimated using histogram method, which is then used to obtain ID_o using the same equation in (34). The EXIT chart is depicted by repeating the procedure above for several values of σ_i yielding pairs (ID_i, ID_o).

4.2 BER Estimation

The EXIT analysis is also used to estimate the BER of MAX-LOG-MAP decoder output after an arbitrary number of iterations [9]. This estimation is based on the Gaussian assumption (35) yielding a unique BER corresponding to decoder input ID_i.

Figure 5 displays the BER as a function of ID_i on logarithmic scales for rate $R = 1/2$ convolutional code with generator polynomial in octal notation $G = [7, 5]$. As we can see, when input mutual information $ID_i = 0.5$ or less, the corresponding decoder BER will be 0.07 or higher. when ID_i is greater than 0.8, the decoder achieves BER lower than 10^{-4}.

4.3 EXIT Chart of Turbo Equalizer

We now study EXIT charts of several Turbo equalizers for BPSK, QPSK, 8PSK and 16QAM modulations with different SNR values. We consider the length-5 ISI channel $h = [0.227, 0.46, 0.6880.460.227]$. This channel causes severe ISI, enabling turbo equalization to yield large performance gains. The estimator filter parameters are set up as follows: $N_1 = 9, N_2 = 5, N_3 = N_2 + M - 1$. The iteration process

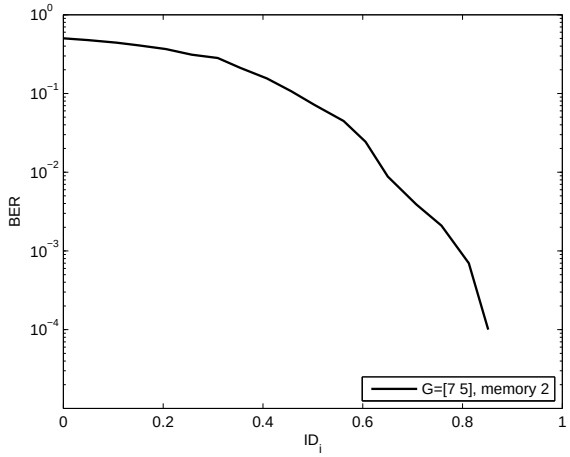

Figure 5. BER of a MAX-Log-MAP decoder as a function of ID_i.

between equalizer and decoder can be visualized by using a trajectory trace following $IE_i/ID_o \rightarrow IE_o/ID_i$ and $IE_o/ID_i \rightarrow IE_i/ID_o$.

For BPSK case in Figure 6, the proposed SDFE has the same slope as Exact-MMSE-LE for small value of IE_i. However, it shows a poorer performance than Exact-MMSE-LE for large value of IE_i. The maximum IE_o for the proposed SDFE is only 0.7 while Exact-MMSE-LE could achieve 0.87. The reason is Exact-MMSE-LE approaches matched filter $\mathbf{f}_{MF}^H$ closer than the proposed SDFE in case of large IE_i input. Approximate-MMSE-LE is the worst. For example, it stops improving the performance after around three iterations and remains in the fixed point $IE_o = 0.4$.

Figure 7 depicts the EXIT charts for QPSK modulation. As we can see, in small and medium IE_i input region, the proposed SDFE has a wider tunnel than Exact-MMSE-LE, which means the proposed SDFE has a faster convergence rate. For example, the proposed SDFE could reach $IE_o = 0.83$ after 3 iterations while Exact-MMSE-LE only gets $IE_o = 0.68$. In large IE_i input region, Exact-MMSE-LE starts to output larger IE_o and outperforms the proposed SDFE. For example, after

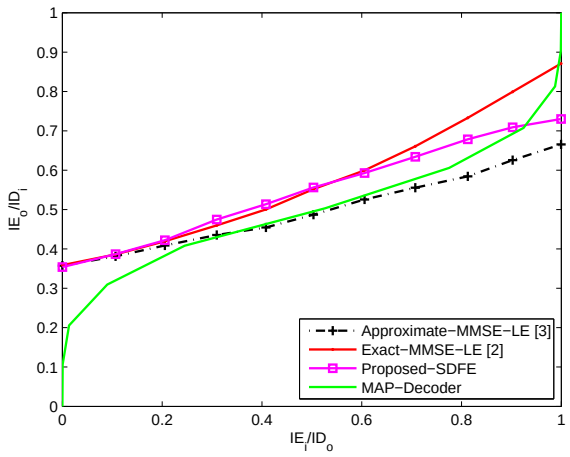

Figure 6. EXIT chart of turbo equalizer at 5 dB SNR for BPSK.

5 iterations, Exact-MMSE-LE reaches $IE_o = 0.96$, which is greater than $IE_o = 0.9$ for the proposed SDFE.

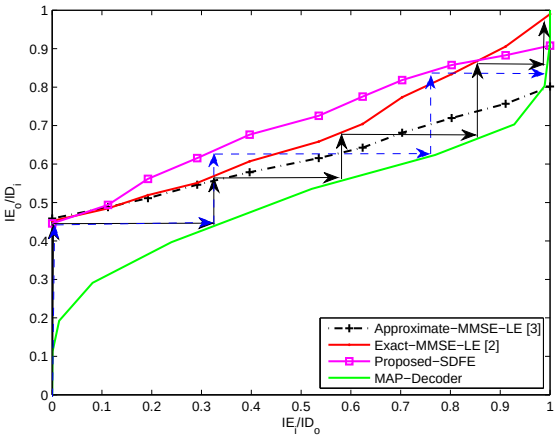

Figure 7. EXIT chart at 9 dB SNR for QPSK in Channel B.

For 8PSK case in Figure 8, it can be seen from the trajectory trace that the convergence rate, which is determined by the width of the tunnel between the

transfer curves of the equalizer and the decoder, of the proposed SDFE is faster than Exact-MMSE-LE. The proposed SDFE could reach $IE_o = 0.67$ ($IE_o = 0.87$) after 3 (5) iterations while Exact-MMSE-LE only gets $IE_o = 0.54$ ($IE_o = 0.78$). Although Exact-MMSE-LE is capable of achieving the mutual information $IE_o = 1$ as the iterations progress, which is better than $IE_o = 0.88$ for the proposed SDFE, $IE_o = 0.88$ is actually high enough for decoder to get near error free performance as we can see from Figure 5. Approximate-MMSE-LE is still the worst, it touches the flipped decoder transfer curve at $IE_o = 0.57$ and stops improvement.

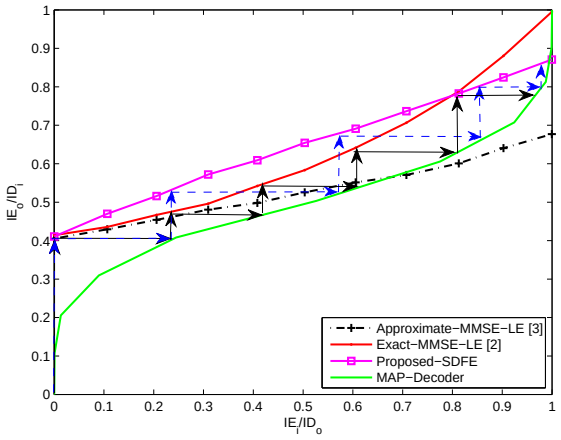

Figure 8. EXIT chart of turbo equalizer at 15 dB SNR for 8PSK.

The similar convergence property occurs for 16QAM case in Figure 9. The proposed SDFE could reach $IE_o = 0.67$ ($IE_o = 0.9$) after 3 (5) iterations while Exact-MMSE-LE only gets $IE_o = 0.53$ ($IE_o = 0.77$). And also, the output mutual information $IE_o = 0.92$ for large value of IE_i for the proposed SDFE is indeed high enough to get low BER.

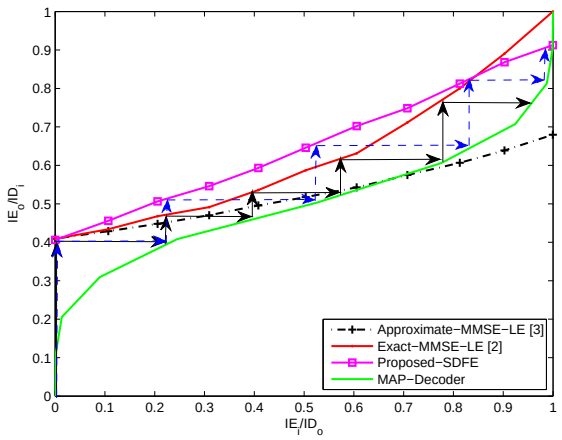

Figure 9. EXIT chart of turbo equalizer at 20 dB SNR for 16QAM.

Following the traces of all SISO equalizers in Figure 7, 8 and 9 yields values for ID_i after each iteration. Using Figure 5, we can compute estimates of the BER given in Table 4.

4.4 SNR Threshold

The EXIT chart can be used to determine the threshold SNR for a turbo equalizer defined as the SNR above which the turbo equalizer converges to a small BER, and below which the turbo equalizer does not converge to a small BER. The thresholds were obtained by generating equalizer EXIT charts at varying SNRs until the transfer curve touched or intersected the flipped decoder transfer curve at $ID_o = 0.5$ or less, which corresponds to a fixed point of the system with a BER of 0.07 or more. Since the equalizer and the flipped decoder transfer curve have a similar slope, increasing the SNR will nearly result in a parallel upshift of the equalizer transfer curve, yielding a quickly moving fixed point in the area around $ID_o = 0.5$. The corresponding BER changes quickly too, which is usually observed water fall region in the BER plot.

Table 4. Expected BER for various SISO equalizers and a MAP decoder.

Mod (SNR)	SISO Equalizer	1st iteration	3rd iteration	5th iteration
QPSK (9 dB)	Exact-MMSE-LE	0.1069	5e-3	0
	Approximate-MMSE-LE	0.1069	0.015	2.3e-3
	Proposed-SDFE	0.1069	2e-4	0
8PSK (15 dB)	Exact-MMSE-LE	0.1553	0.055	1.2e-3
	Approximate-MMSE-LE	0.1553	0.0717	0.05
	Proposed-SDFE	0.1553	6e-3	5e-4
16QAM (20 dB)	Exact-MMSE-LE	0.1553	0.06	1.5e-3
	Approximate-MMSE-LE	0.1553	0.0717	0.05
	Proposed-SDFE	0.1553	6e-3	0

Figure 10 shows EXIT transfer curves for QPSK case. As we can see, when $SNR = 5dB$, Exact-MMSE-LE stop improvements at a small value of $ID_i = 0.45$. While for the proposed SDFE, a narrow tunnel guides the convergence point to approach $ID_i = 0.73$. This tells us that SNR threshold for the proposed SDFE is lower than that of Exact-MMSE-LE.

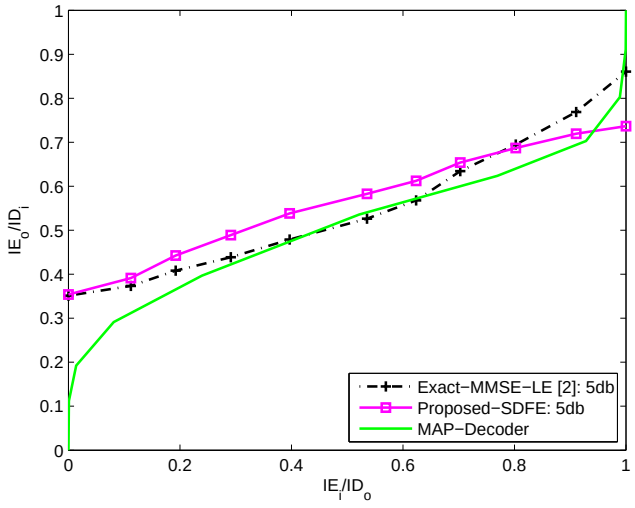

Figure 10. EXIT chart at 5 dB SNR for QPSK.

Figure 11 shows EXIT transfer curves for 8PSK case. When $SNR = 12dB$, Exact-MMSE-LE stop improvements at a small value of $ID_i = 0.43$. While for the proposed SDFE, a narrow tunnel guides the convergence point to approach $ID_i = 0.78$.

Figure 12 shows SNR thresholds for 16QAM case. Similar results were obtained from EXIT chart. SNR thresholds for Exact-MMSE-LE is more than $17dB$, while for the proposed SDFE, SNR thresholds is less than $17dB$.

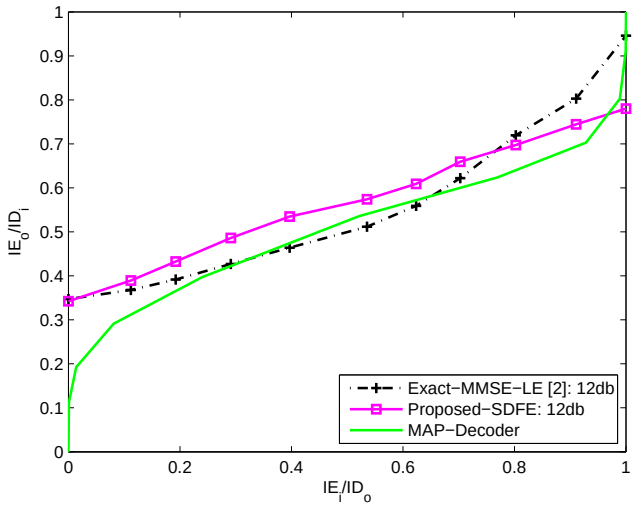

Figure 11. EXIT chart at 12 dB SNR for 8PSK.

Therefore, for both 8PSK and 16QAM, the proposed SDFE exhibits a lower SNR threshold than Exact-MMSE-LE. We also conclude that the proposed SDFE would performance better than Exact-MMSE-LE in low SNR region, because the proposed SDFE has a longer and wider tunnel in the EXIT chart.

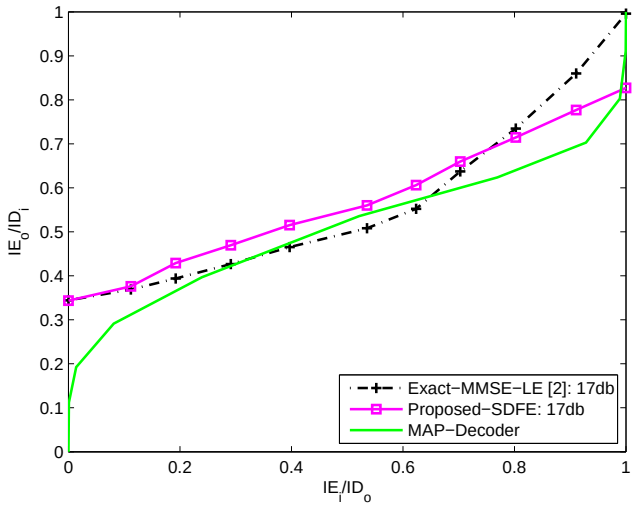

Figure 12. EXIT chart at 17 dB SNR for 16QAM.

5 Simulation Results

We compare the performance of different turbo equalizers, including Exact-MMSE-LE [2], approximate-MMSE-LE [3], SFE [4], MMSE-DFE-SD, and the proposed SDFE with time-invariant coefficients $\mathbf{f}_{TI}$ and $\mathbf{b}_{TI}$. The performance of MMSE-DFE-HD can be found in [3] and is not included here. It suffers severe error propagation and doesn't improve as iteration goes. In all cases, the transmitted binary bits are encoded by a rate $R = 1/2$ convolutional code with generator polynomial in octal notation $G = [7, 5]$, followed by a size 10560 random interleaver. We consider the same ISI channel as in [2]- [4] with the impulse responses $h = [0.227, 0.46, 0.688, 0.46, 0.227]$ causing severe ISI. The filter parameters for Exact-MMSE-LE and approximate-MMSE-LE are set to ($N_1 = 9$, $N_2 = 5$) and for the proposed SDFE to ($N_1 = 9$, $N_2 = 5$, $N_3 = N_2 + M - 1$). MAX-LOG-MAP algorithm is employed for channel decoder.

We begin with the performance for BPSK modulation depicted in Figure 13. After 3 or 10 iterations, the BER curves exhibit that the system using Exact-MMSE-LE is the best, followed by the proposed SDFE, MMSE-DFE-SD and the approximate-MMSE-LE. The gain improvement between 3 and 10 iterations is significant in this channel because of the larger slope in exit chart. It is also interesting to note that the proposed SDFE achieves a performance similar to that of SFE after 10 iterations. This result makes sense since both the proposed SDFE and SFE combine soft decisions with the *a priori* information for equalization.

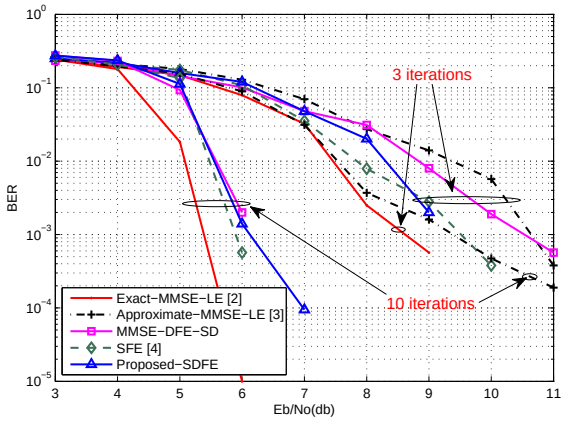

Figure 13. BPSK BER performance.

Figure 14 shows the BER results for QPSK modulation. SFE is not included since it only considers BPSK in [4]. As we can see, the BER curves exhibit the expected behavior as indicated in EXIT chart. For 3 iterations, the proposed SDFE has a lower BER than Exact-MMSE-LE. After 5 iterations, Exact-MMSE-LE outperforms the proposed SDFE. Also, we notice that the performance gap between the proposed SDFE and MMSE-DFE-SD starts to increase.

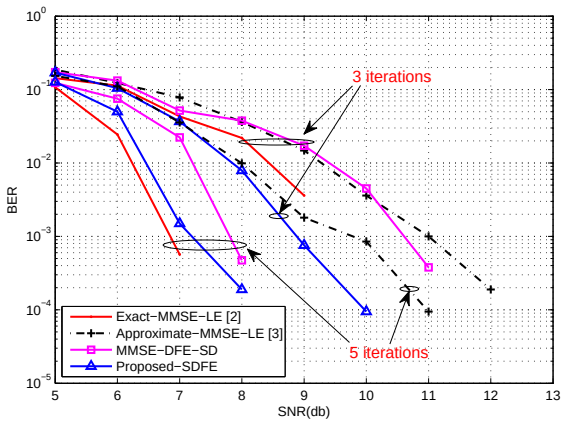

Figure 14. QPSK BER performance.

For 8PSK modulation, all BER performance curves are plotted in Figure 15 (MMSE-DFE-SD starts to suffer error propagation for 8PSK modulation and its BER performance is not included). From this figure, the system using the proposed SDFE performs the best, followed by Exact-MMSE-LE and the approximate-MMSE-LE. After 5 iterations, the proposed SDFE provides nearly 1.3 dB (5.6 dB) gain at 10^{-3} BER compared to Exact-MMSE-LE (the approximate-MMSE-LE). This result agrees with the analysis from EXIT chart in Figure 8 and BER predictions in Table 4.

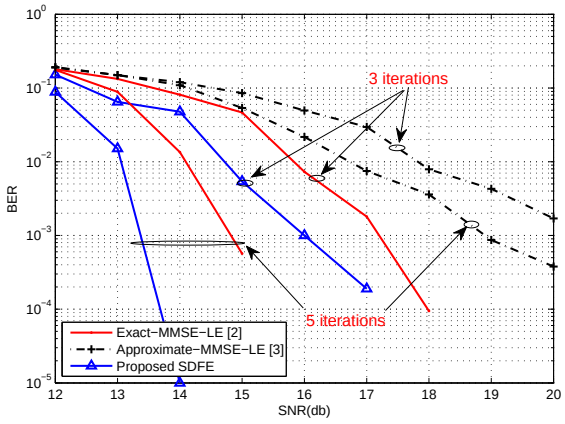

Figure 15. 8PSK BER performance.

Similar performance results are observed for 16QAM case shown in Figure 16 (MMSE-DFE-SD suffers error propagation for 16QAM modulation and its BER performance is not included). The proposed SDFE exhibits lowest SNR threshold and fastest convergence. After 5 iterations, the proposed SDFE provides nearly 1.5 dB (6 dB) gain at 10^{-3} BER compared to Exact-MMSE-LE (the approximate-MMSE-LE). These BER curves also matches well with the EXIT chart in Figure 9 and BER predictions in Table 4.

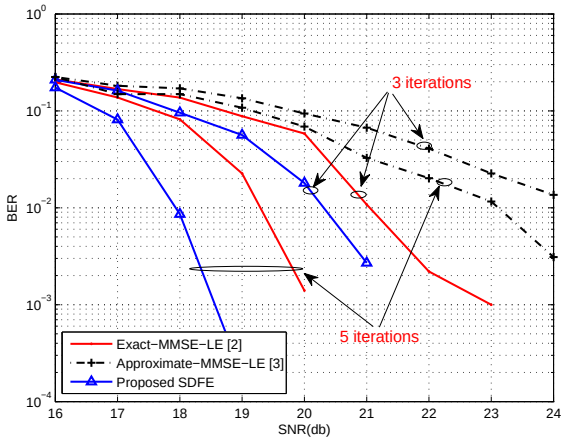

Figure 16. 16QAM BER performance.

It is noted that the proposed SDFE is also working well for 64QAM. Details are omitted for brevity.

6 Conclusions

A low-complexity MMSE-based soft-decision feedback turbo equalizer has been proposed for both BPSK and multilevel modulations. The proposed SDFE took into

account the reliability of both soft *a priori* information and soft decisions of the data symbols. For the first iteration, the proposed SDFE starts as MMSE linear equalizer. As iterations progress, the proposed SDFE behaves as soft-decision feedback MMSE DFE. When both soft *a priori* information and soft decisions become more reliable, the feedforward filter of the proposed SDFE approaches matched filter. Both EXIT chart analysis and simulation results have shown that the proposed SDFE performs close to the high-complexity Exact-MMSE-LE in BPSK/QPSK modulation. For high level modulations, the proposed SDFE exhibits lower SNR threshold and converges much faster than the high-complexity Exact-MMSE-LE.

7 Appendix

We solve the set $(\mathbf{f}_n, \mathbf{b}_n, d_n)$ that minimize $E\{|x_n - \hat{x}_n|^2\}$ using partial differentiation.

$$\frac{\partial E\{|x_n - \hat{x}_n|^2\}}{\partial d_n^*} = -2E\{x_n - \mathbf{f}_n\mathbf{z}_n - \mathbf{b}_n\mathbf{x}_n^d - d_n\} \tag{36}$$

$$\frac{\partial E\{|x_n - \hat{x}_n|^2\}}{\partial \mathbf{f}_n^H} = -2E\{(x_n - \mathbf{f}_n\mathbf{z}_n - \mathbf{b}_n\mathbf{x}_n^d - d_n)\mathbf{z}_n^H\} \tag{37}$$

$$\frac{\partial E\{|x_n - \hat{x}_n|^2\}}{\partial \mathbf{b}_n^H} = -2E\{(x_n - \mathbf{f}_n\mathbf{z}_n - \mathbf{b}_n\mathbf{x}_n^d - d_n)\mathbf{x}_n^{dH}\} \tag{38}$$

By replacing $\mathbf{z}_n$ with equation (2) and setting equation (36) to zero, we get

$$d_n = E\{x_n\} - \mathbf{f}_n\mathbf{H}E\{\mathbf{x}_n\} - \mathbf{b}_n E\{\mathbf{x}_n^d\}.$$

We then insert d_n into equations (37) and (38) and set both to zero. After combining elements using the quantities $\mathbf{C}_n^{ff}$, $\mathbf{C}_n^{fb}$, $\mathbf{C}_n^{bb}$ and $\mathbf{s}_n$, we have

$$\mathbf{f}_n\mathbf{H}\mathbf{C}_n^{fb} + \mathbf{b}_n\mathbf{C}_n^{bb} = 0 \tag{39}$$

$$(\sigma_w^2\mathbf{I}_N + \mathbf{H}\mathbf{C}_n^{ff}\mathbf{H}^H)\mathbf{f}_n^H + \mathbf{H}\mathbf{C}_n^{fb}\mathbf{b}_n^H = \mathbf{s}_n. \tag{40}$$

Solving equations (39) and (40) for $(\mathbf{f}_n, \mathbf{b}_n)$ yields

$$\mathbf{f}_n^H = \left[\sigma_w^2\mathbf{I}_N + \mathbf{H}\left(\mathbf{C}_n^{ff} - \mathbf{C}_n^{fb}(\mathbf{C}_n^{bb})^{-1}\mathbf{C}_n^{fbH}\right)\mathbf{H}^H\right]^{-1}\mathbf{s}_n$$

$$\mathbf{b}_n^H = -(\mathbf{C}_n^{bb})^{-1}\mathbf{H}\mathbf{C}_n^{fbH}\mathbf{f}_n^H.$$

8 References

[1] C. Douillard, C. Berrou, A. Picart, and A. Glavieux, "Iterative correction of intersymbol interference: Turbo Equalization," *European Trans. on Telecomm*, vol.6, pp.507-511, Sept.-Oct. 1995.

[2] M. T*ü*chler, A. C. Singer, and R. Koetter, "Minimum mean square error equalization using a priori information," in *IEEE Trans. Signal Processing*, vol.50, pp.673-683, Mar. 2002.

[3] M. T*ü*chler, R. Koetter, and A. C. Singer, "Turbo equalization: Principles and new results," *IEEE Trans. Commun*, vol.50, no.5, pp.754-767, May. 2002.

[4] R. R. Lopes and J. R. Barry, "The soft-feedback equalizer for turbo equalization of highly dispersive channels," *IEEE Trans. Commun*, vol.54, no.5, pp.783-788, May. 2006.

[5] R. R. Lopes, "Iterative estimation, equalization and decoding," *Ph.D. dissertation, Georgia Inst. Technol.*, Atlanta, GA, 2003.

[6] J. Wu and Y. R. Zheng, "Low complexity soft-input soft-output block decision feedback equalization," *IEEE J. Select. Areas Commun.*, vol.26, no.2, pp.281-289, Feb. 2008.

[7] A. Glavieux, C. Laot and J. Labat, "Turbo equalization over a frequency selective channel," in *Proc. Int. Symp. Turbo Codes, Related Topics*, Brest, France, pp.96-102, Sep. 1997.

[8] Z. Wu and J. Cioffi, "Low complexity iterative decoding with Decision-Aided Equalization for magnetic recording channels," *IEEE J. Select. Areas Commun.*, vol.19, no.4, pp.699-708, April. 2001.

[9] S. Ten Brink, "Convergence behavior of iteratively decoded parallel concatenated codes," *IEEE Trans.Commun*, vol.40, no.10, pp.1727-1737, Oct. 2001.

[10] A. Dejonghe and L. Vanderdorpe, "Turbo equalization for multilevel modulation: An efficient low-complexity scheme," in *Proc. IEEE Int. Conf. Commun*, vol.3, pp.1863-1867, 2002.

[11] P. Vila, I. Fijalkow, C. Laot, D. Leroux, D. Pirez, S. Ronger, and C. Langlais, "Reduced-complexity M-ary decoders for turbo-equalization," in *2nd Int. Symp. Turbo Codes and Related Topics*, Brest, France, Sept.4-7 2000.

[12] J. Hagenauer, "The EXIT chart - introduction to the extrinsic information transfer in iterative processing," EUSIPCO, 2004.

[13] Seok-Jun Lee, A. C. Singer, and N. R. Shanbhag, "Linear Turbo Equalization Analysis via BER Transfer and EXIT Charts," in *IEEE Trans. Signal Processing*, vol.53, pp.2883-2897, August. 2005.

[14] J. Proakis, *Digital Communications*, 4th ed., McGraw-Hill, 2000.

II. SOFT FEEDBACK ISI CANCELLER-BASED TURBO EQUALIZATION FOR MULTILEVEL MODULATIONS

Huang Lou and Chengshan Xiao, *Fellow, IEEE*

Abstract—A low-complexity soft-decision feedback turbo equalizer (SDFE) for multilevel modulations was proposed by Lou *et al.*. It was shown that the SDFE exhibits lower complexity, lower SNR threshold and much faster convergence than MMSE-based linear turbo equalizer with time-varying coefficients (Exact-MMSE-LE). The drawback of the SDFE is its coefficients couldn't reach matched filter bound and therefore after large number of iterations (*e.g.* 10), its performance becomes inferior to that of Exact-MMSE-LE. In this letter, we investigate the low-complexity soft feedback intersymbol interference (ISI) canceller (SIC) structure proposed by Lopes *et al.* for multilevel modulation cases. Interesting results reveal that the SIC structure not only exhibits lower comlexity, lower SNR threshold and faster convergence as SDFE but also reaches matched filter bound after large number of iterations.

1 Introduction

Turbo equalization is a powerful approach to perform joint equalization and decoding over intersymbol interference (ISI) channel [1]. In its original form, Douillard *et al.* employed maximum *a posterior* probability (MAP) equalization and decoding methods in an iterative fashion. One drawback of the MAP equalizer is that its computational complexity depends exponentially on constellation size and the length of the channel impulse response (CIR). This has motivated the development of complexity-reduced alternatives to MAP equalizer, such as minimum mean square error (MMSE) linear equalizers (MMSE-LE), MMSE decision feedback equalizers (DFE) and MMSE interference cancellers (MMSE-IC) in [2]- [8].

The exact solution of MMSE-LE (Exact-MMSE-LE) in [2, 3] achieves close to MAP performance, but its all coefficients have to be computed anew for every symbol, resulting in a time-varying equalizer with quadratic computational complexity. The approximate solution of MMSE-LE with "no *a priori* information" (approximate-MMSE-LE), yielding time-invariant coefficients, is also proposed in [3]. However, its performance is not as good as Exact-MMSE-LE.

MMSE-DFE under perfect hard decision assumption is designed in [3]. Error propagation phenomena is the major drawback of this kind of equalizers. To alleviate error propagation arising from hard decisions, soft-decision DFE (SDFE) is employed in [4]. It was shown that SDFE exhibits lower complexity (update per iteration), lower SNR threshold and much faster convergence than Exact-MMSE-LE (update per symbol). The drawback of SDFE is its coefficients couldn't reach matched filter response to CIR and therefore it becomes inferior to Exact-MMSE-LE after large number of iterations.

In this letter, we investigate the low-complexity SIC structure in [7, 8] for multilevel modulation cases. Interesting results are found through EXIT chart analysis and BER simulations. It shows that the SIC structure not only exhibits lower complexity, lower SNR threshold and faster convergence as SDFE but also reaches matched filter response to CIR after large number of iterations.

The remainder of this letter is organized as follows. A brief definition of signals are given in Section II. In Section III, we describe the structure and coefficients of SIC. The performance of SIC is analyzed in Section IV with the tool of EXIT chart. Simulation results are verified and compared to both SDFE and Exact-MMSE-LE in Section V. Section VI draws the conclusion.

2 Preliminary

We consider the transmission of length $K_c \times Q$ bit sequences $\mathbf{c} = [\mathbf{c}_1\ \mathbf{c}_2 \cdots \mathbf{c}_{K_c}]$, where subsequences $\mathbf{c}_n = [c_{n,1}\ c_{n,2} \cdots c_{n,Q}]$ with bits $c_{n,j} \in 0, 1$. The mapper maps each $\mathbf{c}_n$ to a symbol x_n from the 2^Q-ary constellation set $S = \{\alpha_1, \alpha_2, \cdots, \alpha_{2^Q}\}$, where α_i corresponds to the bit pattern $\mathbf{s}_i = [s_{i,1}\ s_{i,2} \cdots s_{i,Q}]$ with $s_{i,j} \in 0, 1$ in Table 1.

The receiver input can be written as $z_n = \sum_{k=0}^{M-1} h_k x_{n-k} + w_n$ or in matrix form for $N = N_1 + N_2 + 1$ received symbols

$$\mathbf{z}_n = \mathbf{H}\mathbf{x}_n + \mathbf{w}_n \tag{1}$$

$$\mathbf{z}_n = [z_{n-N_2}\ z_{n-N_2+1} \cdots z_{n+N_1}]^T$$

$$\mathbf{x}_n = [x_{n-N_2-M+1}\ x_{n-N_2-M+2} \cdots x_{n+N_1}]^T$$

$$\mathbf{w}_n = [w_{n-N_2}\ w_{n-N_2+1} \cdots w_{n+N_1}]^T$$

$$\mathbf{H} = \begin{bmatrix} h_{M-1} & \cdots & h_0 & \cdots & 0 \\ \vdots & \ddots & \ddots & \ddots & \vdots \\ 0 & \cdots & h_{M-1} & \cdots & h_0 \end{bmatrix}$$

where h_k is the channel impulse response with length M and w_n is the independent and identically distributed (i.i.d.) noise with variance of $\sigma_w^2/2$ for both real and imaginary part.

In the sequel, some frequently used notations are introduced. Vectors are written in bold letters. Matrices are specified in bold capital letters. Time index n is used to denote time-varying quantities. The $i \times j$ matrix $\mathbf{1}_{i\times j}$ and $\mathbf{0}_{i\times j}$ contains all ones and all zeros. I_i is an $i \times i$ identity matrix. $(\cdot)^*$, $(\cdot)^{-1}$, $(\cdot)^T$ and $(\cdot)^H$ are respectively the conjugate, inverse, transpose and hermitian operators. $E(.)$ is the expectation operator.

Table 1. Symbol alphabets.

BPSK:

i	1	2
$s_{i,1}$	0	1
α_i	$+1$	-1

QPSK:

i	1	2	3	4
$s_{i,1}\ s_{i,2}$	00	01	10	11
α_i	$(+1+i)/\sqrt{2}$	$(+1-i)/\sqrt{2}$	$(-1+i)/\sqrt{2}$	$(-1-i)/\sqrt{2}$

8PSK:

i	1	2	3	4	5	6	7	8
$s_{i,1}\ s_{i,2}\ s_{i,3}$	000	001	010	011	100	101	110	111
α_i	$e^{(\frac{i9\pi}{8})}$	$e^{(\frac{i11\pi}{8})}$	$e^{(\frac{i15\pi}{8})}$	$e^{(\frac{i13\pi}{8})}$	$e^{(\frac{i7\pi}{8})}$	$e^{(\frac{i5\pi}{8})}$	$e^{(\frac{i\pi}{8})}$	$e^{(\frac{i3\pi}{8})}$

16QAM:

i	1	2	3	4	5	6	7	8
$s_{i,1}\ s_{i,2}\ s_{i,3}\ s_{i,4}$	0000	0001	0010	0011	0100	0101	0110	0111
α_i	$\frac{(-1-i)}{\sqrt{10}}$	$\frac{(-1-3i)}{\sqrt{10}}$	$\frac{(-1+i)}{\sqrt{10}}$	$\frac{(-1+3i)}{\sqrt{10}}$	$\frac{(-3-i)}{\sqrt{10}}$	$\frac{(-3-3i)}{\sqrt{10}}$	$\frac{(-3+i)}{\sqrt{10}}$	$\frac{(-3+3i)}{\sqrt{10}}$
i	9	10	11	12	13	14	15	16
$s_{i,1}\ s_{i,2}\ s_{i,3}\ s_{i,4}$	1000	1001	1010	1011	1100	1101	1110	1111
α_i	$\frac{(1-i)}{\sqrt{10}}$	$\frac{(1-3i)}{\sqrt{10}}$	$\frac{(1+i)}{\sqrt{10}}$	$\frac{(1+3i)}{\sqrt{10}}$	$\frac{(3-i)}{\sqrt{10}}$	$\frac{(3-3i)}{\sqrt{10}}$	$\frac{(3+i)}{\sqrt{10}}$	$\frac{(3+3i)}{\sqrt{10}}$

3 Soft Intersymbol Interference Canceller

3.1 SIC Structure And Coefficients

Figure 1 shows the block diagram of SIC in the context of a turbo equalizer [7, 8]. Both causal and anti-causal soft-decided symbols x_n^d and x_n^p are estimated and fed back for ISI cancellation. $\mathbf{f}_n$, $\mathbf{b}_n$ and $\mathbf{p}_n$ are filter coefficients. $\lambda_{n,j}$ and $\lambda_{n,j}^p$ are log likelihood ratio (LLR) values.

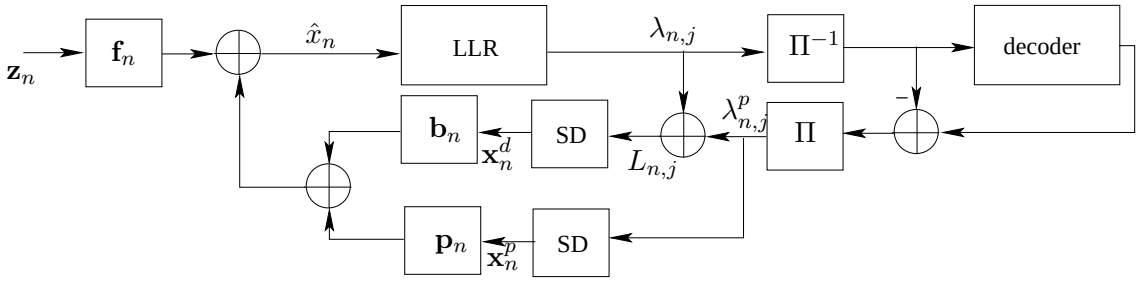

Figure 1. Soft feedback ISI canceler.

The MMSE estimate $\hat{x}_n$ of the transmitted symbol x_n is given by

$$\hat{x}_n = \mathbf{f}_n \mathbf{z}_n + \mathbf{b}_n \mathbf{x}_n^d + \mathbf{p}_n \mathbf{x}_n^p \tag{2}$$

$$\mathbf{x}_n^d = [x_{n-N_3}^d \; x_{n-N_3+1}^d \cdots x_{n-1}^d]^T$$

$$\mathbf{x}_n^p = [x_{n+1}^p \; x_{n+2}^p \cdots x_{n+N_1}^p]^T$$

$$\mathbf{f}_n = [f_{N_2,n} \; f_{N_2-1,n} \cdots f_{-N_1,n}]$$

$$\mathbf{b}_n = [b_{N_3,n} \; b_{N_3-1,n} \cdots b_{1,n}]$$

$$\mathbf{p}_n = [p_{-1,n} \; p_{-2,n} \cdots p_{-N_1,n}]$$

where $N_3 = N_2 + M - 1$.

According to [7, 8], the time-invariant (without time index n) minimum MSE values of $\mathbf{f}_n^H, \mathbf{b}_n^H$ and $\mathbf{p}_n^H$ are obtained as

$$\mathbf{f}^H = \left(\sigma_w^2 \mathbf{I}_N + \mathbf{H}\mathbf{H}^H - \frac{\beta_p^2}{\zeta_p} \mathbf{H}_\mathbf{p} \mathbf{H}_\mathbf{p}^H - \frac{\beta_b^2}{\zeta_b} \mathbf{H}_\mathbf{b} \mathbf{H}_\mathbf{b}^H \right)^{-1} \mathbf{s} \tag{3}$$

$$\mathbf{b}^H = -\frac{\beta_b}{\zeta_b} \mathbf{H}_\mathbf{b}^H \mathbf{f}^H \tag{4}$$

$$\mathbf{p}^H = -\frac{\beta_p}{\zeta_p} \mathbf{H}_\mathbf{p}^H \mathbf{f}^H \tag{5}$$

where $\mathbf{s} = \mathbf{H}[\mathbf{0}_{1\times(N_2+M-1)}\ 1\ \mathbf{0}_{1\times N_1}]^T$, β_b=$E\{x_n x_n^{d*}\}$, β_p=$E\{x_n x_n^{p*}\}$, ζ_b=$E\{x_n^d x_n^{d*}\}$ and ζ_p=$E\{x_n^p x_n^{p*}\}$. Also, $\mathbf{H_p}$ is the most right N_1 columns of $\mathbf{H}$ and $\mathbf{H_b}$ is the most left N_3 columns of $\mathbf{H}$.

When LLR $|\lambda_{n,j}|$ and $|\lambda_{n,j}^p|$ go to infinity, $\beta_b \to 1, \beta_p \to 1, \zeta_b \to 1$ and $\zeta_p \to 1$, thus $\mathbf{f}^H \to [\sigma_w^2\mathbf{I}_N + \mathbf{s}\mathbf{s}^H]^{-1}\mathbf{s}$, which is the matched filter response $\mathbf{f}_{MF}^H$ to $h[n]$.

3.2 Expected Value Computation for Multilevel Modulations

In order to compute $\mathbf{f}, \mathbf{b}$ and $\mathbf{p}$, $\beta_b, \beta_p, \zeta_b$ and ζ_p have to be decided first.

Since the *a priori* information can be modeled as an equivalent AWGN channel, we have $\lambda_{n,j}^p \sim \mathcal{N}(\gamma_p, 2\gamma_p)$ when $c_{n,j} = 0$ ($\lambda_{n,j}^p \sim \mathcal{N}(-\gamma_p, 2\gamma_p)$ when $c_{n,j} = 1$). And the computation of x_n^p can be given by

$$x_n^p = \sum_{\alpha_i \in S} \alpha_i P(\tilde{x}_n^p = \alpha_i) \tag{6}$$

$$P(\tilde{x}_n^p = \alpha_i) = \prod_{j=1}^{Q} \frac{1}{2}(1 + \tilde{s}_{i,j} \tanh(\lambda_{n,j}^p/2)). \tag{7}$$

By exploiting symmetries and equal probability of $\alpha_i \in S$, we get

$$\beta_p = \alpha_i E\{x_n^{p*} | x_n = \alpha_i\} \tag{8}$$

$$\zeta_p = E\{x_n^p x_n^{p*} | x_n = \alpha_i\} \tag{9}$$

where for MPSK, α_i can be any elements in S, while for QAM, β_p and ζ_p should be re-scaled when $|\alpha_i| \neq 1$.

Notice that the value of γ_p is needed. Fortunately, the ML estimate of γ_p^{ML} can be obtained using

$$\gamma_p^{ML} = \sqrt{1 + \frac{1}{K_c \times Q} \sum_{n=1}^{K_c} \sum_{j=1}^{Q} |\lambda_{n,j}^p|^2} - 1. \tag{10}$$

Similarly, we assume that the estimate $\hat{x}_n$ is the output of another equivalent AWGN channel having x_n as its input:

$$\hat{x}_n = Ax_n + v_n \tag{11}$$

and it follows $\hat{x}_n \sim \mathcal{N}(x_n A, \sigma^2)$, where $\sigma^2 = A(1-A),\ A = \mathbf{fs}$ [9].

The symbol extrinsic probability is presented as

$$P(\hat{x}_n | x_n = \alpha_i) = \frac{1}{\sigma^2 \pi} \exp(-\rho_{n,i}) \tag{12}$$

$$\rho_{n,i} = \frac{|\hat{x}_n - A\alpha_i|^2}{\sigma^2}. \tag{13}$$

The extrinsic LLR $\lambda_{n,j}$ of coded bit $c_{n,j}$ is the function of $P(\hat{x}_n | x_n = \alpha_i)$:

$$\lambda_{n,j} = \log \frac{\sum_{\alpha_i : c_{n,j}=0} P(\hat{x}_n|\alpha_i) \prod_{\forall j', j' \neq j} P(c_{n,j'})}{\sum_{\alpha_i : c_{n,j}=1} P(\hat{x}_n|\alpha_i) \prod_{\forall j', j' \neq j} P(c_{n,j'})} = \log \frac{\sum_{\alpha_i : c_{n,j}=0} \exp(-\rho_{n,i} + \sum_{\forall j', j' \neq j} \tilde{s}_{i,j} L(c_{n,j'})/2)}{\sum_{\alpha_i : c_{n,j}=1} \exp(-\rho_{n,i} + \sum_{\forall j', j' \neq j} \tilde{s}_{i,j} L(c_{n,j'})/2)} \tag{14}$$

where

$$\tilde{s}_{i,j} = \begin{cases} +1 & \text{if } s_{i,j} = 0 \\ -1 & \text{if } s_{i,j} = 1 \end{cases}$$

Substituting (12) and (13) into (14), one can get $\lambda_{n,j}$ as a function of $\hat{x}_n$. This means that the pdf of $\lambda_{n,j}$ is related to the pdf of $\hat{x}_n$. We adopt the following LLR approximation in Table 2.

Once we know $\lambda_{n,j}$, we can calculate full LLR value $L_{n,j}$ of coded bit $c_{n,j}$

$$\lambda^p_{n,j} = \log \frac{P(c_{n,j} = 0)}{P(c_{n,j} = 1)} \tag{15}$$

$$L_{n,j} = \lambda_{n,j} + \lambda^p_{n,j}. \tag{16}$$

Table 2. LLR $\lambda_{n,j}$ approximation for symbol alphabets.

8PSK:
- $\lambda_{n,1} \approx -4\sin(7\pi/8)\mathrm{Im}\{\hat{x}_n\}/(1-A)$.
- $\lambda_{n,2} \approx -4\sin(7\pi/8)\mathrm{Re}\{\hat{x}_n\}/(1-A)$.
- $\lambda_{n,3} \approx 1.0824(|\mathrm{Re}\{\hat{x}_n\}| - |\mathrm{Im}\{\hat{x}_n\}|)/(1-A)$.

16QAM:
- $\lambda_{n,1} \approx -4\mathrm{Re}\{\hat{x}_n\}/(\sqrt{10}(1-A))$.
- $\lambda_{n,2} \approx (8A - 4\sqrt{10}|\mathrm{Re}\{\hat{x}_n\}|)/(10(1-A))$.
- $\lambda_{n,3} \approx -4\mathrm{Im}\{\hat{x}_n\}/(\sqrt{10}(1-A))$.
- $\lambda_{n,4} \approx (8A - 4\sqrt{10}|\mathrm{Im}\{\hat{x}_n\}|)/(10(1-A))$.

Using the same computation as x_n^p, we get

$$x_n^d = \sum_{\alpha_i \in S} \alpha_i P(\tilde{x}_n^d = \alpha_i) \tag{17}$$

$$P(\tilde{x}_n^d = \alpha_i) = \prod_{j=1}^{Q} \frac{1}{2}(1 + \tilde{s}_{i,j} \tanh(L_{n,j}/2)) \tag{18}$$

$$\beta_b = \alpha_i E\{x_n^{d*} | x_n = \alpha_i\} \tag{19}$$

$$\zeta_b = E\{x_n^d x_n^{d*} | x_n = \alpha_i\} \tag{20}$$

Since x_n^d is a function of $L_{n,j}$, as long as we know the pdf parameters γ_p of $\lambda_{n,j}^p$ and A of $\hat{x}_n$, expected values β_b and ζ_b can be calculated numerically.

In order to determine A, we need $\mathbf{f}$, while we need A to calculate β_b and ζ_b, and thus $\mathbf{f}$. This is problematic. To find both A and $\mathbf{f}$ simultaneously, Lopes *et al.* proposed an iterative procedure for initial A and $\mathbf{f}$ computation [7]. However, it still involves a lot of computations and induces convergence delay. In this letter, MMSE-LE is employed in first turbo iteration to replace this iterative procedure for initial A and $\mathbf{f}$ computation as in [4].

4 Performance Analysis With EXIT Chart

The performance of SIC turbo equalizer is analyzed by using the tool of EXIT chart [3, 11, 12], which traces the evolution of mutual information between data symbols and its LLR through iterations. It is used to graphically predict the behavior of the iterative algorithm.

We study the EXIT charts of three turbo equalizers for 8PSK and 16QAM modulations in Figure 2 and 3. We consider the length-3 ISI channel $h = [0.407, 0.8150.407]$ [13]. The estimator filter parameters are set up as follows: $N_1 = 9, N_2 = 5, N_3 = N_2 + M - 1$.

As we can see, for both 8PSK and 16QAM cases, SDFE and SIC have wider tunnels than Exact-MMSE-LE, which indicates lower SNR threshold and faster convergence rate [4]. For example, SDFE and SIC could reach higher IE_os than Exact-MMSE-LE after 3 iterations. However, for large value of IE_i, SIC and Exact-MMSE-LE achieve matched filter bound and therefore converge to a higher end point than that of SDFE.

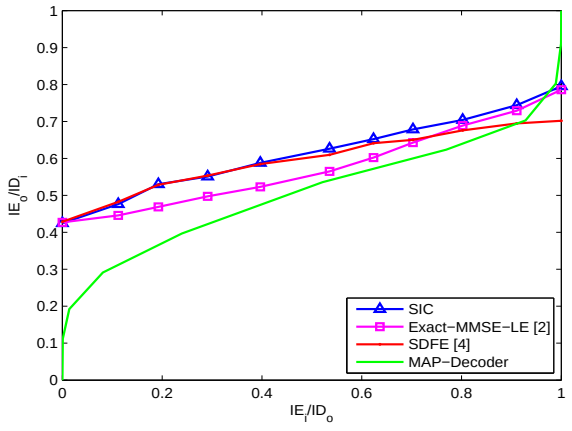

Figure 2. EXIT chart of turbo equalizer at 8dB SNR for 8PSK.

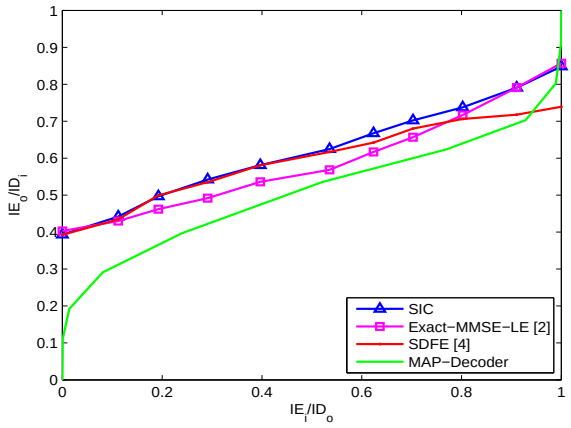

Figure 3. EXIT chart of turbo equalizer at 12dB SNR for 16QAM.

We also like to mention here that, these properties stay true for other channels as well.

5 Simulation Results

We compare the performance of Exact-MMSE-LE [2], SDFE [4] and SIC. In both 8PSK and 16QAM cases, the transmitted bits are encoded by a rate $R = 1/2$ convolutional code with generator polynomial $G = [7, 5]$, followed by a size 10560 random interleaver. We use the length-3 ISI channel in Section IV. Same filter parameters as in [8] are set for Exact-MMSE-LE ($N_1 = 9$, $N_2 = 5$), SDFE and SIC ($N_1 = 9$, $N_2 = 5$, $N_3 = N_2 + M - 1$). MAX-LOG-MAP algorithm is employed for channel decoder.

We begin with the performance for 8PSK modulation depicted in Figure 4. As we can see, the BER curves exhibit the expected behavior as indicated in EXIT chart. For 3 iterations, both SIC and SDFE exhibit faster convergence and provide nearly 0.3 dB gain at 10^{-3} compared to Exact-MMSE-LE. However, after 10 iterations,

both SIC and Exact-MMSE-LE approach matched filter bound and exhibit better BER performance than SDFE. We also notice that at 6dB SNR, SIC and SDFE have lower BERs. This is because both of them have lower SNR thresholds than Exact-MMSE-LE [4].

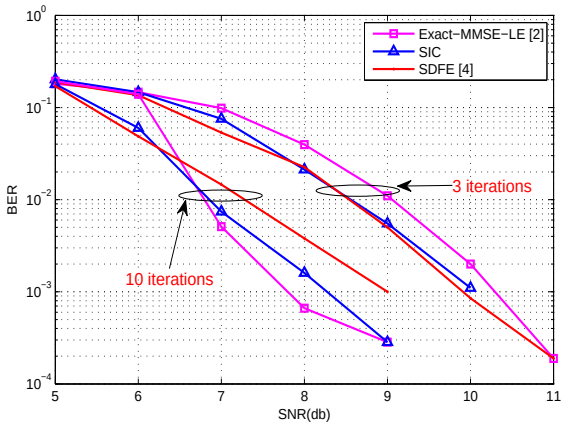

Figure 4. 8PSK BER performance.

Similar performance results are observed for 16QAM case shown in Figure 5. After 3 iterations, SIC and SDFE exhibit similar BER performance and provide nearly 1 dB gain at 10^{-3} BER compared to Exact-MMSE-LE. However, after 10 iterations, SIC and Exact-MMSE-LE exhibit better BER performance than SDFE. These BER curves also matches well with the EXIT chart in Figure 3.

6 Conclusions

We have investigated SIC structure for multilevel modulations. For the first iteration, SIC starts as MMSE linear equalzier. In following iterations, it took into

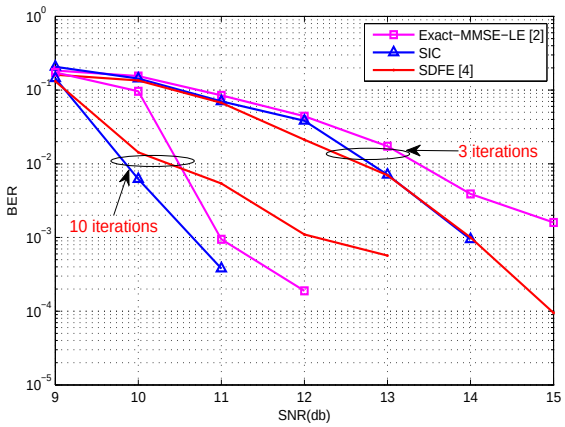

Figure 5. 16QAM BER performance.

account the reliability of both soft *a priori* information and soft decisions of the data symbols as SDFE. Both EXIT chart and BER simulations showed that SIC exhibits lower complexity, lower SNR threshold and much faster convergence than Exact-MMSE-LE for multilevel cases. SIC also outperforms SDFE after large number of iterations.

7 References

[1] C. Douillard, C. Berrou, A. Picart, and A. Glavieux, "Iterative correction of intersymbol interference: Turbo Equalization," *European Trans. on Telecomm*, vol.6, pp.507-511, Sept.-Oct. 1995.

[2] M. T*ü*chler, A. C. Singer, and R. Koetter, "Minimum mean square error equalization using a priori information," *IEEE Trans. Signal Processing*, vol.50, pp.673-683, Mar. 2002.

[3] M. T*ü*chler, R. Koetter, and A. C. Singer, "Turbo equalization: Principles and new results," *IEEE Trans. Commun*, vol.50, no.5, pp.754-767, May. 2002.

[4] H. Lou and C. Xiao, "Soft-decision feedback turbo equalization for multilevel modulations," *IEEE Trans. Signal Processing*, vol.59, pp.186-195, Jan. 2011.

[5] A. Glavieux, C. Laot and J. Labat, "Turbo equalization over a frequency selective channel," in *Proc. Int. Symp. Turbo Codes, Related Topics*, Brest, France, pp.96-102, Sep. 1997.

[6] Z. Wu and J. Cioffi, "Low complexity iterative decoding with Decision-Aided Equalization for magnetic recording channels," *IEEE J. Select. Areas Commun.*, vol.19, no.4, pp.699-708, April. 2001.

[7] R. R. Lopes and J. R. Barry, "The soft-feedback equalizer for turbo equalization of highly dispersive channels," *IEEE Trans. Commun*, vol.54, no.5, pp.783-788, May. 2006.

[8] R. R. Lopes, "Iterative estimation, equalization and decoding," *Ph.D. dissertation, Georgia Inst. Technol.*, Atlanta, GA, 2003.

[9] A. Dejonghe and L. Vanderdorpe, "Turbo equalization for multilevel modulation: An efficient low-complexity scheme," in *Proc. IEEE Int. Conf. Commun*, vol.3, pp.1863-1867, 2002.

[10] P. Vila, I. Fijalkow, C. Laot, D. Leroux, D. Pirez, S. Ronger, and C. Langlais, "Reduced-complexity M-ary decoders for turbo-equalization," in *2nd Int. Symp. Turbo Codes and Related Topics*, Brest, France, Sept.4-7 2000.

[11] S. Ten Brink, "Convergence behavior of iteratively decoded parallel concatenated codes," *IEEE Trans.Commun*, vol.40, no.10, pp.1727-1737, Oct. 2001.

[12] J. Hagenauer, "The EXIT chart - introduction to the extrinsic information transfer in iterative processing," EUSIPCO, 2004.

[13] J. Proakis, *Digital Communications*, 4th ed., McGraw-Hill, 2000.

III. LOW COMPLEXITY SOFT-DECISION FEEDBACK TURBO EQUALIZATION FOR MIMO SYSTEMS WITH MULTILEVEL MODULATIONS

Amirhossein Rafati, Huang Lou and Chengshan Xiao, *Fellow IEEE*

Abstract—Many communication systems today encounter the problem of data transmission over a channel with inter-symbol interference (ISI). The purpose of this paper is to develop a low-complexity, iterative soft-decision feedback equalization (SDFE) receiver for severe, frequency selective ISI channels in multiple-input multiple-output (MIMO) communication systems. The proposed SDFE algorithm offers a novel approach to combat error propagation . In addition, its computational complexity grows only linearly with the number of equalizer coefficients, compared to the quadratic complexity of minimum mean square error (MMSE)-based linear turbo equalizer with time-varying coefficients. Performance of the proposed detection scheme is verified through simulations using different signal constellations.The performance and convergence property of the proposed SDFE algorithm are analyzed using extrinsic information transfer (EXIT) chart and verified by simulations in a severe inter-symbol interference channel. Simulation results show that our proposed algorithm has a significant improvement over the approximate MMSE linear turbo equalizer proposed in [1]. Moreover, we show that the performance of the proposed equalization scheme improves significantly when higher order constellations are used for digital modulation.

1 Introduction

Multiple-input multiple-output (MIMO) wireless communication systems have attracted a lot of interest in the past decade due to their capability in delivering high

spectral efficiency as well as their robust performance against fading. In MIMO inter-symbol interference (ISI) channels, a severe interference problem occurs due to the ISI, spatial and co-channel interference. Thus, the error propagation problem becomes more serious, and its mitigation has to be considered when designing the receiver. In this regard, a turbo equalizer which exchanges soft information between the equalizer and the decoder has been shown to be an effective method to combat the ISI caused by frequency-selective channels. By iteratively exchanging soft extrinsic information between a soft-input soft-output equalizer and a decoder, turbo equalizer can achieve large performance gains over a separated equalizer and decoder structure. In its original form, Douillard *et al.* employed maximum *a posterior* probability (MAP) equalization and decoding methods in an iterative fashion [2]. However, the computational complexity required to derive the *a posteriori* log likelihood ratio (LLR) for the MAP decoder is prohibitive. This is because the number of states in the trellis diagram for the frequency-selective MIMO channels increases exponentially with the product of the number of users and their channel memory length. Therefore, the design of low-complexity turbo equalizers based on minimum mean square error (MMSE) criterion has attracted considerable attention in the past few years. The existing approaches to MMSE-based turbo equalizers can be roughly classified into three categories.

First, MMSE linear equalizers (MMSE-LE) treat each data symbol as a random variable with mean and variance computed from the *a priori* information. Exact and approximate solutions for MMSE linear turbo equalization were introduced in [1] and [3] for SISO and MIMO systems, respectively. While the exact solution of MMSE-LE (Exact-MMSE-LE) achieves a performance which is close to that of MAP algorithm, its computational complexity is quadratic with the number of equalizer coefficients since all coefficients have to be computed anew for every symbol. As a result, its practical implementation becomes very costy when the channel length is

large. On the other hand, the approximate solution of MMSE-LE without any *a priori* information (approximate-MMSE-LE), yields time-invariant coefficients which need not be computed for each symbol. However, this approximation causes the overall performance to degrade considerably with respect to the Exact-MMSE-LE algorithm.

Second, MMSE decision feedback equalizers under perfect hard decision assumption utilize the idea of using past decisions to mitigate inter-symbol interference [1]. However, the decision errors from the equalizer may result in erroneous cancelation of the ISI through the feedback filter and, consequently, degrade the overall performance. Solutions have been provided in [5]- [7] to alleviate this problem by employing soft decisions in the feedback structure of equalizer. However, their equalizer coefficients derivation is under hard decision assumption which might be suboptimal for soft-decision feedback implementation.

Finally, soft-feedback equalizer (SFE) proposed in [8, 9] combines soft decisions with the *a priori* information for ISI cancelation and their equalizer coefficients derivation is based on soft-decision feedback, which is different from perfect hard decision assumption. However, SFE is actually an ISI cancelation device with both anti-causal and causal filters rather than a general decision feedback filter. Also, SFE needs an iterative procedure to compute γ_e (probability density function parameter of equalizer extrinsic information output) and restricts itself in BPSK modulation.

Recently, a new soft-decision feedback equalizer for SISO systems was proposed in [10] for multilevel constellations that is more computationally efficient compared to the above equalizers. Motivated by [10], in this paper we propose a new low-complexity MMSE-based MIMO SDFE scheme for multiple antenna systems. In addition, we provide approximate solutions for higher order modulation schemes and show by means of computer simulations that our proposed algorithm outperforms the conventional solutions for linear turbo equalization.

Throughout this paper, upper case boldface letters are used to indicate matrices, lower case boldface letters are used to show vectors, kth row and kth diagonal element of matrix $\mathbf{A}$ are denoted by $\langle \mathbf{A} \rangle_k$ and $[\mathbf{A}]_k$, respectively and $E\{\cdot\}$ denotes the expectation operator.

2 System Model

Structure of the transmitter and receiver is shown in Figure 1. We consider a MIMO communication system with t transmit and r receive antennas that employs a digital modulation with constellation size 2^q. Here, the binary information sequence $\{a_n^k\}$ represents the input bits to kth channel encoder at time instant n which is followed by an interleaver Π and a constellation mapper and then transmitted through the k transmit antenna. Let $\mathbf{b}_n^k = \left[b_{n,(k-1)q+1} \ \cdots b_{n,kq}\right]^T$ denote the block of q encoded bits at the output of the kth encoder at time instant n. After interleaving, the output of the kth interleaver can be stated as $\mathbf{c}^k = \left[\mathbf{c}_1^k \ \ \mathbf{c}_2^k \cdots \mathbf{c}_{K_c}^k\right]$ where $\mathbf{c}_n^k$ represents $\left[c_{n,1}^k \ \ c_{n,1}^k \cdots c_{n,q}^k\right]$ with bits $c_{n,j}^k \in \{0,1\}$ and $\prod(.)$ denotes the interleaving operation.

The mapper maps each random vector $\mathbf{c}_n^k$ to a symbol x_n^k from the 2^q-ary constellation set $S = \{\alpha_1, \alpha_2, \cdots, \alpha_{2^q}\}$, where α_i corresponds to the deterministic bit pattern $\mathbf{s}_i = [s_{i,1} \ s_{i,2} \cdots s_{i,q}]$ with $s_{i,j} \in 0, 1$ in Table 1 which specifies the mapping

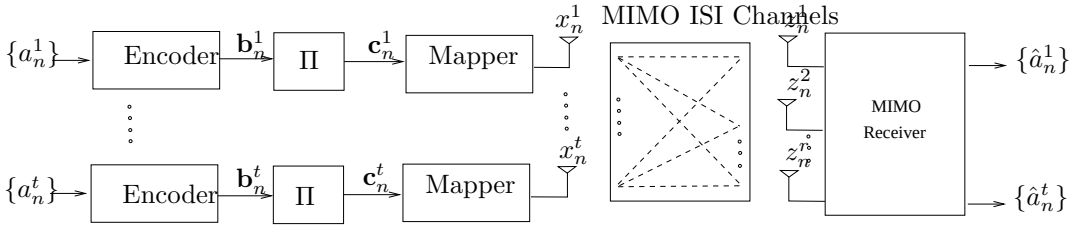

Figure 1. Block diagram of the SDFE transmitter and receiver.

Table 1. Symbol alphabets.

BPSK:

i	1	2
$s_{i,1}$	0	1
α_i	$+1$	-1

QPSK:

i	1	2	3	4
$s_{i,1}\ s_{i,2}$	00	01	10	11
α_i	$(+1+i)/\sqrt{2}$	$(+1-i)/\sqrt{2}$	$(-1+i)/\sqrt{2}$	$(-1-i)/\sqrt{2}$

8PSK:

i	1	2	3	4	5	6	7	8
$s_{i,1}\ s_{i,2}\ s_{i,3}$	000	001	010	011	100	101	110	111
α_i	$e^{(\frac{i9\pi}{8})}$	$e^{(\frac{i11\pi}{8})}$	$e^{(\frac{i15\pi}{8})}$	$e^{(\frac{i13\pi}{8})}$	$e^{(\frac{i7\pi}{8})}$	$e^{(\frac{i5\pi}{8})}$	$e^{(\frac{i\pi}{8})}$	$e^{(\frac{i3\pi}{8})}$

16QAM:

i	1	2	3	4	5	6	7	8
$s_{i,1}\ s_{i,2}\ s_{i,3}\ s_{i,4}$	0000	0001	0010	0011	0100	0101	0110	0111
α_i	$\frac{(-1-i)}{\sqrt{10}}$	$\frac{(-1-3i)}{\sqrt{10}}$	$\frac{(-1+i)}{\sqrt{10}}$	$\frac{(-1+3i)}{\sqrt{10}}$	$\frac{(-3-i)}{\sqrt{10}}$	$\frac{(-3-3i)}{\sqrt{10}}$	$\frac{(-3+i)}{\sqrt{10}}$	$\frac{(-3+3i)}{\sqrt{10}}$
i	9	10	11	12	13	14	15	16
$s_{i,1}\ s_{i,2}\ s_{i,3}\ s_{i,4}$	1000	1001	1010	1011	1100	1101	1110	1111
α_i	$\frac{(1-i)}{\sqrt{10}}$	$\frac{(1-3i)}{\sqrt{10}}$	$\frac{(1+i)}{\sqrt{10}}$	$\frac{(1+3i)}{\sqrt{10}}$	$\frac{(3-i)}{\sqrt{10}}$	$\frac{(3-3i)}{\sqrt{10}}$	$\frac{(3+i)}{\sqrt{10}}$	$\frac{(3+3i)}{\sqrt{10}}$

between the encoded bits and the elements of the constellation. Here, the explicit dependencies on transmitter index and time instant in $\mathbf{s}_i$ have been dropped for the sake of brevity. Finally, x_n^k is the nth symbol to be transmitted by the kth antenna.

Then, a discrete-time representation of the received signal at the mth received antenna at time instant n is given by

$$z_n^{(m)} = \sum_{l=0}^{L-1} \sum_{k=1}^{t} h_l^{(m,k)} x_{n-l}^k + w_n^{(m)} \tag{1}$$

where $h_l^{(m,k)}$ is the lth tap of the channel between the kth transmitter and mth receiver and L is the number of channel taps. In addition, the noise samples $w_n^{(m)}$ are

independent and identically distributed (i.i.d.) with the variance of $\sigma_w^2/2$ for both real and imaginary parts. Under the block-fading assumption, we can assume that the channel is constant over the block of transmitted symbols. Stacking up all the received symbols on r receiver antennas as $\mathbf{z}_n = [z_n^{(1)}, z_n^{(2)}, \ldots, z_n^{(r)}]^T$, we can write,

$$\mathbf{z}_n = \sum_{l=0}^{L-1} \mathbf{h}_l \mathbf{x}_{n-l} + \mathbf{w}_n \tag{2}$$

where

$$\mathbf{x}_n = [x_n^1, x_n^2, \ldots, x_n^t]^T \tag{3}$$

$$\mathbf{w}_n = [w_n^1, w_n^2, \ldots, w_n^r]^T \tag{4}$$

and

$$\mathbf{h}_l = \begin{bmatrix} h_l^{(1,1)} & h_l^{(1,2)} & \cdots & h_l^{(1,t)} \\ h_l^{(2,1)} & h_l^{(2,2)} & \cdots & h_l^{(2,t)} \\ \vdots & \vdots & \ddots & \vdots \\ h_l^{(r,1)} & h_l^{(r,2)} & \cdots & h_l^{(r,t)} \end{bmatrix}. \tag{5}$$

Finally, temporal sampling to capture the multi-path signals for diversity combining yields the following space-time representation for $rN = r(N_1+N_2+1)$ received symbols,

$$\mathbf{Z}_n = \mathbf{H}\mathbf{X}_n + \mathbf{W}_n \tag{6}$$

where $\mathbf{Z}_n$, $\mathbf{H}$, $\mathbf{X}_n$ and $\mathbf{W}_n$ are defined in (7) and N_1 and N_2 are the number of anti-causal and causal elements of the received vector $\mathbf{Z}_n$. N_1 and N_2 should be chosen as to include all the received symbols that are correlated with the transmitted symbol at time n. In general, N_1 and N_2 should be chosen according to the channel

$$\underbrace{\begin{bmatrix} \mathbf{z}_{n-N_2} \\ \vdots \\ \mathbf{z}_n \\ \vdots \\ \mathbf{z}_{n+N_1} \end{bmatrix}}_{\mathbf{Z}_n} = \underbrace{\begin{bmatrix} \mathbf{h}_{L-1} & \cdots & \mathbf{h}_0 & \cdots & \cdots & 0 \\ \vdots & \ddots & \ddots & \ddots & & \vdots \\ & & \ddots & \ddots & \ddots & \vdots \\ 0 & \cdots & & \mathbf{h}_{L-1} & \cdots & \mathbf{h}_0 \end{bmatrix}}_{\mathbf{H}} \underbrace{\begin{bmatrix} \mathbf{x}_{n-N_2-L} \\ \vdots \\ \mathbf{x}_n \\ \vdots \\ \mathbf{x}_{n+N_1} \end{bmatrix}}_{\mathbf{X}_n} + \underbrace{\begin{bmatrix} \mathbf{w}_{n-N_2} \\ \vdots \\ \mathbf{w}_n \\ \vdots \\ \mathbf{w}_{n+N_1} \end{bmatrix}}_{\mathbf{W}_n} \tag{7}$$

characteristics and specifically, location of the major channel tap with respect to other taps.

To detect $\mathbf{x}_n$, equalizing matrices $\mathbf{F}_n$, $\mathbf{B}_n$ and $\mathbf{d}_n$ can be applied as,

$$\hat{\mathbf{x}}_n = \mathbf{F}_n \mathbf{Z}_n + \mathbf{B}_n \mathbf{X}_n^d + \mathbf{d}_n \tag{8}$$

where

$$\mathbf{X}_n^d = \left[\mathbf{x}_{n-N_3}^d \mathbf{x}_{n-N_3+1}^d \cdots \mathbf{x}_{n-1}^d\right]^T \tag{9}$$

$$\mathbf{x}_n^d = \left[\left(x_n^1\right)^d \left(x_n^2\right)^d \cdots \left(x_n^t\right)^d\right] \tag{10}$$

$N_3 = N_2 + L - 1$, $\left(x_n^k\right)^d$ is the soft estimate of the nth symbol transmitted by the kth antenna which is a function of *a priori* information $(\lambda_n^k)^p$ and extrinsic information λ_n^k to be specified later. Here, the superscripts $(.)^p$ and $(.)^d$ denote quantities obtained from the previous iteration and past time instances, respectively.

Here, we propose to obtain $\mathbf{F}_n$, $\mathbf{B}_n$ and $\mathbf{d}_n$ in order to minimize the mean square error. That is, these parameters have to be obtained from the following minimization problem,

$$\text{MMSE} = \min_{\mathbf{F}_n, \mathbf{B}_n, \mathbf{d}_n} E\left\{\left|\left|\mathbf{F}_n \mathbf{Z}_n + \mathbf{B}_n \mathbf{X}_n^d + \mathbf{d}_n - \mathbf{x}_n\right|\right|^2\right\}. \tag{11}$$

We assume that $\mathrm{Cov}\left(x_n^p x_m^q\right) = \mathrm{Cov}\left(\left(x_n^p\right)\left(x_m^q\right)^d\right) = \mathrm{Cov}\left(\left(x_n^p\right)^d\left(x_m^q\right)^d\right) = 0$ for all combinations of p, q and n, m given that if $p = q$ then $n \neq m$ and vice versa.

By taking the gradient with respect to $\mathbf{F}_n$, $\mathbf{B}_n$ and $\mathbf{d}_n$ and setting the result to zero, it can be shown that the MMSE estimate $\hat{\mathbf{x}}_n$ of the transmitted symbol $\mathbf{x}_n$ is given by,

$$\hat{\mathbf{x}}_n = \mathbf{F}_n(\mathbf{Z}_n - \mathbf{H}E\left\{\mathbf{X}_n\right\}) + \mathbf{B}_n\left(\mathbf{X}_n^d - E\left\{\mathbf{X}_n^d\right\}\right) + E\left\{\mathbf{x}_n\right\} \tag{12}$$

where

$$\mathbf{F}_n^H = \left[\sigma_w^2\mathbf{I}_N + \mathbf{H}\left(\mathbf{C}_n^{ff} - \mathbf{C}_n^{fb}(\mathbf{C}_n^{bb})^{-1}\left(\mathbf{C}_n^{fb}\right)^H\right)\mathbf{H}^H\right]^{-1}\mathbf{s}_n \tag{13}$$

$$\mathbf{B}_n^H = -\left(\mathbf{C}_n^{bb}\right)^{-1}\left(\mathbf{H}\mathbf{C}_n^{fb}\right)^H\mathbf{F}_n^H \tag{14}$$

$$\mathbf{d}_n = E\left\{\mathbf{x}_n\right\} - \mathbf{F}_n\mathbf{H}E\left\{\mathbf{X}_n\right\} - \mathbf{B}_n E\left\{\mathbf{X}_n^d\right\} \tag{15}$$

and

$$\mathbf{C}_n^{ff} = E\left\{\mathbf{X}_n\mathbf{X}_n^H\right\} - E\left\{\mathbf{X}_n\right\}E\left\{\mathbf{X}_n^H\right\} \tag{16}$$

$$\mathbf{C}_n^{fb} = E\left\{\mathbf{X}_n\left(\mathbf{X}_n^d\right)^H\right\} - E\left\{\mathbf{X}_n\right\}E\left\{\left(\mathbf{X}_n^d\right)^H\right\} \tag{17}$$

$$\mathbf{C}_n^{bb} = E\left\{\mathbf{X}_n^d\left(\mathbf{X}_n^d\right)^H\right\} - E\left\{\mathbf{X}_n^d\right\}E\left\{\left(\mathbf{X}_n^d\right)^H\right\} \tag{18}$$

$$\mathbf{s}_n = \mathbf{H}(E\left\{\mathbf{X}_n\mathbf{x}_n^H\right\} - E\left\{\mathbf{X}_n\right\}E\left\{\mathbf{x}_n^H\right\}). \tag{19}$$

3 SDFE Structure

The equalizer structure for the proposed SDFE can be understood from equation (12). The block diagram of the SDFE receiver is shown in Figure 2. As we can see, for the first iteration, $\mathbf{H}E\{\mathbf{X}_n\} = \mathbf{0}_{t(N_1+N_2+1)\times 1}$, $E\{\mathbf{x}\}_n = \mathbf{0}_{t\times 1}$, $E\{\mathbf{X}_n^d\} = \mathbf{0}_{tN_3\times 1}$,

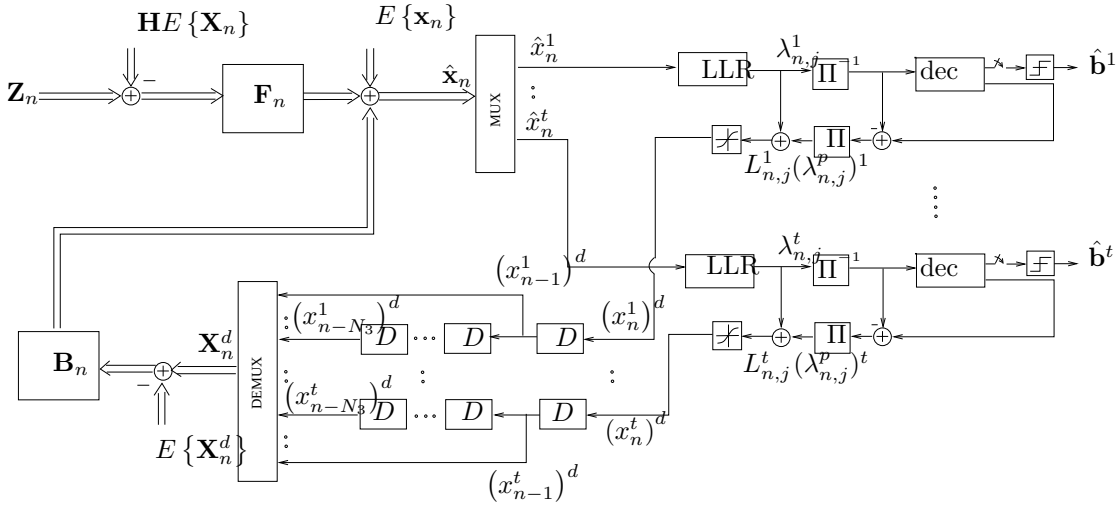

Figure 2. Block diagram of the proposed SDFE receiver.

the proposed SDFE becomes a conventional decision feedback equalizer. With the subsequent iterations, $\mathbf{H}E\{\mathbf{X}_n\}$ becomes more reliable and is used to cancel both anti-casual and casual ISI from $\mathbf{Z}_n$. Moreover, $\mathbf{F}_n$ is approaching matched filter response to $\mathbf{h}_n$.

As it can be seen, knowledge of the covariance matrices $\mathbf{C}_n^{ff}$, $\mathbf{C}_n^{fb}$ and $\mathbf{C}_n^{bb}$ is a key step in finding $\hat{\mathbf{x}}_n$. While $\mathbf{C}_n^{ff}$ can be computed from the *a priori* information, computation of $\mathbf{C}_n^{fb}$ and $\mathbf{C}_n^{bb}$ requires the knowledge of $\Xi = E\left\{\mathbf{X}_n^d\right\}$, $\Phi = E\left\{\mathbf{X}_n^d\left(\mathbf{X}_n^d\right)^H\right\}$ and $\Psi = E\left\{\mathbf{X}_n\left(\mathbf{X}_n^d\right)^H\right\}$. Based on the assumption that the transmitted symbols are mutually independent, we can argue that $E\left\{\left(x_n^k\right)^{d^*}\left(x_m^l\right)^{d^*}\right\} = E\left\{x_n^k\left(x_m^l\right)^{d^*}\right\} = 0$ except when $n = m$ and $k = l$. Hence, using (3) and (10), it is easy to see that the problem of finding Ξ, Φ and Ψ boils down to the computation of $\xi^k = E\left\{\left(x_n^k\right)^d\right\}$, $\psi^k = E\left\{x_n^k\left(x_n^k\right)^{d^*}\right\}$ and $\phi^k = E\left\{\left(x_n^k\right)^d\left(x_n^k\right)^{d^*}\right\}$, which are in turn functions of LLR values λ_n^k and $(\lambda_n^k)^p$. While the above expected values are generally

time-varying for each x_n^k due to the *a priori* probability, here we can assume that they are time invariant since the statistics do not change for individual x_n^k.

3.1 Expected Value Computation for BPSK Modulation

As explained in the previous section, ξ^k, ψ^k and ϕ^k have to be determined according to the quality of both soft *a priori* information and soft decisions of data symbols. As a result, the knowledge of probability density function (pdf) of λ_n^k and $(\lambda_n^k)^p$ is needed to find the equalization matrix. In this section, we use the same approach as introduced in [9].

Here, as in [11] we can assume that the estimate $\hat{x}_n^k$ at the output of the equalizer is the output of an equivalent AWGN channel having $x_n^k \in \{-1, 1\}$ as its input:

$$\hat{x}_n^k = A_k x_n^k + v_n^k \tag{20}$$

where $A_k = E\{\hat{x}_n^k x_n^{k*}\} = [\mathbf{A}]_k$ where $\mathbf{A} = \mathbf{F}_n \mathbf{s}_n$ and v_n^k is a white Gaussian noise with zero mean and variance $A_k(1 - A_k)$ that includes the effect of channel noise and cross transmitter ISI. Let us define the extrinsic LLR $\lambda_{n,j}^k$ of coded bit $c_{n,j}^k$ ($j = 1$ for the BPSK constellation) as $\lambda_{n,1}^k$ where,

$$\lambda_{n,1}^k = \log \frac{P(\hat{x}_n^k | x_n^k = 1)}{P(\hat{x}_n^k | x_n^k = -1)} = \frac{2\hat{x}_n^k}{(1 - A_k)}. \tag{21}$$

Now, it can be shown that $\lambda_{n,1}^k \sim \mathcal{N}(x_n^k \gamma_e^k, 2\gamma_e^k)$ where $\gamma_e^k = \dfrac{2A_k}{(1 - A_k)}$.

Moreover, the *a priori* information $\lambda_{n,1}^p$ of $c_{n,1}$ can be computed in the same fashion from another equivalent AWGN channel with output

$$l_n^k = x_n^k + u_n^k \tag{22}$$

where $u_n^k \sim \mathcal{N}(0, \sigma_u^2)$. If we let $\gamma_p = 2/\sigma_u^2$, we may write,

$$\left(\lambda_{n,1}^k\right)^p = \log \frac{P(x_n^k = 1)}{P(x_n^k = -1)} = \gamma_p l_n^k \tag{23}$$

and it can be shown that $\lambda_{n,1}^k \sim \mathcal{N}(x_n^k \gamma_p, 2\gamma_p)$.

After adding $\lambda_{n,1}^k$ and $\left(\lambda_{n,1}^k\right)^p$ together, we have the full LLR value $L_{n,1}^k = \lambda_{n,1}^k + \left(\lambda_{n,1}^k\right)^p$ and it follows $L_{n,1}^k \sim \mathcal{N}(x_n^k(\gamma_e^k + \gamma_p^k), 2(\gamma_e^k + \gamma_p^k))$.

Then, $\left(x_n^k\right)^d$ can be computed as

$$\left(x_n^k\right)^d = \tanh(L_{n,1}^k/2). \tag{24}$$

After some mathematical manipulations we have,

$$\xi^k = 0 \tag{25}$$

$$\psi^k = E\{x_n^k \left(x_n^k\right)^{d^*}\} = E\{\tanh(L_{n,1}^k/2) | x_n^k = 1\} \tag{26}$$

$$\phi^k = E\{\left(x_n^k\right)^d \left(x_n^k\right)^{d^*}\} = E\{\tanh^2(L_{n,1}^k/2) | x_n^k = 1\}. \tag{27}$$

Although no closed-form formula exists for ψ^k and ϕ^k, they can be computed by numerical methods as long as we know the parameters γ_e^k and γ_p^k.

Because $E\{|\left(\lambda_{n,1}^k\right)^p|^2\} = \gamma_p^{2k} + 2\gamma_p^k$, γ_p^k can be estimated directly from the *a priori* information $\left(\lambda_{n,1}^k\right)^p$. The maximum-likelihood (ML) estimate of γ_p is then obtained as

$$\gamma_p^k = \sqrt{1 + \frac{1}{K_c} \sum_{n=1}^{K_c} \left|\left(\lambda_{n,1}^k\right)^p\right|^2} - 1. \tag{28}$$

To determine γ_e^k, we need to know $\mathbf{A} = \mathbf{F}_n \mathbf{s}_n$, while we need γ_e^k to calculate ψ^k and ϕ^k, and thus $\mathbf{F}_n$. To find both simultaneously, Lopes and Barry proposed giving an initial estimate for γ_e^k, then compute $\mathbf{F}_n$ and γ_e^k iteratively, until they

converge [9]. This procedure is generally not computationally efficient and requires a lot of operations . In the sequel, we introduce a method to alleviate this problem.

3.2 Expected Value Computation for Multilevel Modulations

Similar to the BPSK case, we can express the estimate $\hat{x}_n^k$ of $x_n^k \in S$ as an output of an equivalent AWGN channel as,

$$\hat{x}_n^k = A_k x_n^k + v_n^k \tag{29}$$

and it follows that $\hat{x}_n^k \sim \mathcal{N}(x_n^k A_k, \sigma_k^2)$, where $\sigma_k^2 = A_k(1 - A_k)$.

We define the symbol extrinsic probability as

$$P(\hat{x}_n^k | x_n^k = \alpha_i) = \frac{1}{\sigma^2 \pi} \exp(-\rho_{n,i}^k) \tag{30}$$

$$\rho_{n,i}^k = \frac{|\hat{x}_n^k - A_k \alpha_i|^2}{\sigma_k^2} \tag{31}$$

where α_i is defined in table 1. The extrinsic LLR $\lambda_{n,j}^k$ of coded bit $c_{n,j}^k$ is the function of $P(\hat{x}_n^k | x_n^k = \alpha_i)$:

$$\begin{aligned} \lambda_{n,j}^k &= \log \frac{\sum_{\alpha_i : c_{n,j}^k = 0} P(\hat{x}_n^k | \alpha_i) \prod_{\forall j', j' \neq j} P(c_{n,j'}^k)}{\sum_{\alpha_i : c_{n,j}^k = 1} P(\hat{x}_n^k | \alpha_i) \prod_{\forall j', j' \neq j} P(c_{n,j'})} \\ &= \log \frac{\sum_{\alpha_i : c_{n,j}^k = 0} \exp(-\rho_{n,i}^k + \sum_{\forall j', j' \neq j} \tilde{s}_{i,j} L(c_{n,j'}^k)/2)}{\sum_{\alpha_i : c_{n,j}^k = 1} \exp(-\rho_{n,i}^k + \sum_{\forall j', j' \neq j} \tilde{s}_{i,j} L(c_{n,j'}^k)/2)} \end{aligned} \tag{32}$$

where

$$\tilde{s}_{i,j} = \begin{cases} +1 & \text{if } s_{i,j} = 0 \\ -1 & \text{if } s_{i,j} = 1. \end{cases}$$

Using (30), (31) and (32), it can be seen that $\lambda_{n,j}^k$ can be computed as a function of $\hat{x}_n^k$ which implies that the pdf of $\lambda_{n,j}^k$ is related to the pdf of $\hat{x}_n^k$.

For QPSK or QAM modulation, the computational complexity in (32) can be reduced by using minimum-based LLR simplification defined by

$$\log(\exp(-x) + \exp(-y)) \approx -min(x, y) \tag{33}$$

when $|x - y|$ is sufficiently large.

For MPSK ($M > 2$) modulation, the minimum-based LLR simplifications can not be made because several symbols are quite close to each other on the unit circle. Instead, a geometric approach [12] can be applied to estimate LLR $\lambda_{n,j}$. The approximation is listed in Table 2.

Using $\lambda_{n,j}^k$, we can calculate full LLR value $L_{n,j}^k$ of coded bit $c_{n,j}^k$ as,

$$\left(\lambda_{n,j}^k\right)^p = \log \frac{P(c_{n,j}^k = 0)}{P(c_{n,j}^k = 1)} \tag{34}$$

$$L_{n,j}^k = \lambda_{n,j}^k + \left(\lambda_{n,j}^k\right)^p. \tag{35}$$

Note that if $c_{n,j}^k = 0$, the distribution of $\left(\lambda_{n,j}^k\right)^p$ can be expressed as, $\sim \mathcal{N}(\gamma_p, 2\gamma_p)$. Finally, the computation of $\left(x_n^k\right)^d$ is given by

$$\left(x_n^k\right)^d = \sum_{\alpha_i \in S} \alpha_i P((\tilde{x_n^k})^d = \alpha_i) \tag{36}$$

$$P((\tilde{x_n^k})^d = \alpha_i) = \prod_{j=1}^{q} \frac{1}{2}(1 + \tilde{s}_{i,j} \tanh(L_{n,j}^k/2)). \tag{37}$$

By exploiting symmetries and equal probability of $\alpha_i \in S$, we get

$$\xi^k = 0 \tag{38}$$

$$\psi^k = \alpha_i E\{\left(x_n^k\right)^{d^*} | x_n^k = \alpha_i\} \tag{39}$$

$$\phi^k = E\{\left(x_n^k\right)^d \left(x_n^k\right)^{d^*} | x_n^k = \alpha_i\} \tag{40}$$

Table 2. LLR simplifications for different constellations.

QPSK:
- $\lambda_{n,1}^k \approx 2\sqrt{2}\mathrm{Re}\{\hat{x}_n^k\}/\left(1-A_k\right)$.
- $\lambda_{n,2}^k \approx 2\sqrt{2}\mathrm{Im}\{\hat{x}_n^k\}/\left(1-A_k\right)$.

8PSK:
- $\lambda_{n,1}^k \approx -4\sin(7\pi/8)\mathrm{Im}\{\hat{x}_n^k\}/\left(1-A_k\right)$.
- $\lambda_{n,2}^k \approx -4\sin(7\pi/8)\mathrm{Re}\{\hat{x}_n^k\}/\left(1-A_k\right)$.
- $\lambda_{n,3}^k \approx 1.0824(|\mathrm{Re}\{\hat{x}_n^k\}|-|\mathrm{Im}\{\hat{x}_n^k\}|)/\left(1-A_k\right)$.

16QAM:
- $\lambda_{n,1}^k \approx -4\mathrm{Re}\{\hat{x}_n^k\}/(\sqrt{10}\left(1-A_k\right))$.
- $\lambda_{n,2}^k \approx (8A_k-4\sqrt{10}|\mathrm{Re}\{\hat{x}_n^k\}|)/(10\left(1-A_k\right))$.
- $\lambda_{n,3}^k \approx -4\mathrm{Im}\{\hat{x}_n^k\}/(\sqrt{10}((1-A_k))$.
- $\lambda_{n,4}^k \approx (8A_k-4\sqrt{10}|\mathrm{Im}\{\hat{x}_n^k\}|)/(10\left(1-A_k\right))$.

where for MPSK, α_i can be any elements in S, while for QAM, ψ^k and ϕ^k should be re-scaled when $|\alpha_i| \neq 1$. Since $\left(x_n^k\right)^d$ is a function of $L_{n,j}^k$, as long as we know the parameters γ_p^k of $\left(\lambda_{n,j}^k\right)^p$ and A_k of $\hat{x}_n^k$, expected values ψ^k and ϕ^k can be calculated through numerical methods.

The ML estimate of γ_p^k can also be estimated using

$$\gamma_p^k = \sqrt{1+\frac{1}{K_c \times q}\sum_{n=1}^{K_c}\sum_{j=1}^{q}\left|\left(\left(\lambda_{n,j}^k\right)^p\right)^2\right|}-1. \tag{41}$$

In order to determine A_k, we need $\mathbf{F}_n$, while we need A_k to calculate ψ^k and ϕ^k, and thus $\mathbf{F}_n$. These steps are summarized in Table 3.

4 Low-Complexity Implementation

Computational complexity is an important aspect of MIMO equalization algorithms. The computational burden is mostly due to the fact that the equalization

Table 3. SDFE equalizer algorithm.

FIRST ITERATION:
- Set $\mathbf{F}_{TI}^{H\,(1)} = [\sigma_w^2 \mathbf{I}_N + \mathbf{H}\mathbf{H}^H]^{-1}\mathbf{s}$, $\mathbf{B}_{TI}^{H\,(1)} = \mathbf{0}_{tN_3 \times 1}$, $\mathbf{d}^{(1)} = \mathbf{0}_{tN_3 \times 1}$ and $(\lambda_{n,j}^k)^p = L_{n,j}^k = 0$ $(j = 1, 2, \cdots, q)$
- Compute $\hat{\mathbf{x}}_n^{(1)}$ using equation (12)
- Compute $\mathbf{A}^{(2)} = \mathbf{F}_{TI}{}^{(1)}\mathbf{s}$.
- For $k = 1 : t$
- Compute $A_k = \left[\mathbf{A}^{(2)}\right]_k$
- Compute $\lambda_{n,j}^{k\;(1)}$ and $(x_n^k)^{d^{(1)}}$ using equations (32) and (36).
- End
- Compute $\mathbf{x}_n^{d\,(1)}$ using (10).

i–th **ITERATION** $(i > 1)$**:**
- For $k = 1 : t$
- Compute$A_k = \left[\mathbf{A}^{(i)}\right]_k$
- Compute $\gamma_p^{k(i)}$ using equation (41).
- Compute $\psi^{k(i)}$ and$\phi^{k(i)}$ using equations (39) and (40).
- End
- Compute $\mathbf{F}_{TI}^{H\,(i)}$, $\mathbf{B}_{TI}^{H\,(i)}$ and $\mathbf{d}_n{}^{(i)}$using equations (42), (43) and (44).
- Compute $\hat{\mathbf{x}}_n^{(i)}$ using equation (12).
- Set $\mathbf{A}^{(i+1)} = \mathbf{F}_{TI}{}^{(i)}\mathbf{s}$.
- For $k = 1 : t$
- Compute $\lambda_{n,j}^{k\;(i)}$ and $(x_n^k)^{d^{(i)}}$ using equations (32) and (36).
- End

matrices $\mathbf{F}_n$ and $\mathbf{B}_n$ have to be computed at every time instant n. These computations can be further alleviated by utilizing fixed, time invariant equalization matrices in each data block as,

$$\mathbf{F}_{TI}^{H} = \left[\sigma_w^2 \mathbf{I}_N + \mathbf{H}(\mathbf{I}_{t(N_1+N_2+L)} - \mathbf{C}_{TI}^{fb}(\mathbf{C}_{TI}^{bb})^{-1}\mathbf{C}_{TI}^{fbH})\mathbf{H}^H\right]^{-1}\mathbf{s} \tag{42}$$

$$\mathbf{B}_{TI}^{H} = -(\mathbf{C}_{TI}^{bb})^{-1}\left(\mathbf{H}\mathbf{C}_{TI}^{fb}\right)^{H}\mathbf{F}_{TI}^{H} \tag{43}$$

$$\mathbf{d}_n = E\{\mathbf{x}_n\} - \mathbf{F}_{TI}\mathbf{H}E\{\mathbf{X}_n\} - \mathbf{B}_{TI}E\{\mathbf{X}_n^d\} \tag{44}$$

$$\hat{\mathbf{x}}_n = \mathbf{F}_{TI}\mathbf{Z}_n + \mathbf{B}_{TI}\mathbf{X}_n^d + \mathbf{d}_n \tag{45}$$

where

$$\mathbf{s} = \mathbf{H}[\mathbf{0}_{t\times t(N_2+M-1)}\ \mathbf{I}_t\ \mathbf{0}_{t\times tN_1}]^T$$

$$\mathbf{C}_{TI}^{bb} = \underbrace{\Phi \oplus \Phi \oplus \cdots \oplus \Phi}_{N_3 \text{ times}}$$

$$\mathbf{C}_{TI}^{fb} = \begin{bmatrix} \Psi & 0 & \cdots & 0 \\ 0 & \Psi & \cdots & 0 \\ \vdots & \ddots & \ddots & \vdots \\ 0 & \cdots & 0 & \Psi \\ 0 & \cdots & \cdots & 0 \\ \vdots & \ddots & \ddots & \vdots \\ 0 & \cdots & \cdots & 0 \end{bmatrix},$$

$\Phi = \text{diag}([\phi^1, \phi^2, \ldots, \phi^t])$, $\Psi = \text{diag}([\psi^1, \psi^2, \ldots, \psi^t])$, and $\oplus$ denotes the direct sum of matrices.

5 Convergence Analysis

Turbo equalization, as well as any algorithm using the turbo principle, relies on the information exchange between the equalizer and the decoder. In the case of successful convergence, the information becomes more reliable as the iterations proceed, but such a generic statement of the iterative process provides little information

on the requirements of successful convergence and the more detailed characteristics of the iterative process. A more rigorous approach to analyze the convergence properties of turbo equalizer is provided by extrinsic information transfer (EXIT) charts.

The mutual information $\mathcal{I}$ between the coded bits $\mathcal{C} \in \{\pm 1\}$ and the LLR λ, assuming that the samples are equiprobable is given by [14]

$$\begin{aligned} \mathcal{I} &= \frac{1}{2} \sum_{\mathcal{C}\in\pm 1} \int_{-\infty}^{\infty} p_{\lambda|c}(\xi|\mathcal{C}). \\ &\quad \log_2 \left(\frac{2p_{\lambda|c}(\xi|\mathcal{C})}{p_{\lambda|c}(\xi|-1) + p_{\lambda|c}(\xi|+1)} \right) \\ &= 1 - \int_{-\infty}^{\infty} p_{\lambda|c}(\xi|+1) \log_2(1+e^{-\xi}) \end{aligned} \tag{46}$$

where $p_{\lambda|c}(\xi|\mathcal{C}) = \text{Prob.}[\lambda = \xi|c = \mathcal{C}]$ is the pdf of the LLR ξ conditioned upon the coded bit $\mathcal{C}$. The last equality results from the consistency condition of the LLR that takes into account the symmetric property of the pdf of log likelihood values as

$$p_{\lambda|c}(\xi|+1) = e^{\xi} p_{\lambda|c}(\xi|-1). \tag{47}$$

Thus, mutual information for the equalizer and decoder units can be computed using (46), for which the values of $p_{\lambda|c} = \text{Prob.}[\lambda = \xi|c = \mathcal{C}]$ are obtained by histograms of the *a priori* and extrinsic LLRs.

While calculating the mutual information of the equalizer output is relatively easy for a single transmitter and antenna case, for multiple antennas analyzing the EXIT characteristic becomes more complex since a certain transmitter's mutual information transfer function also depends on the *a priori* of the decoders from other streams. In this case, since each MI depends on feedback MI from both its own decoder and the other streams decoder, the EXIT characteristic is expressed by planes. When the number of streams increases more, the EXIT chart is multidimensional

which is impossible to visualize. However, the convergence analysis can be accommodated by projecting the EXIT functions onto two dimensional planes constructed by the equalizer output MI and decoders output MI.

In this section, we analyze the performance of the proposed receiver, using the tool of extrinsic information transfer chart and study EXIT charts of Turbo equalizers for BPSK, QPSK, 8PSK and 16QAM modulations with different SNR values. In our simulations, we have considered a frequency selective rayleigh channel with 5 taps. The estimator filter parameters are $N_1 = 9, N_2 = 5, N_3 = N_2 + M - 1$. The transmitted binary bits are encoded by a rate $R = 1/2$ convolutional code with generator polynomial in octal notation $G = [7, 5]$, followed by a size 10560 random interleaver. Figures 3-6 illustrate the three dimensional EXIT chart for each constellation. From these figures, we observe that the proposed MIMO-SDFE algorithm converges faster than the approximate MIMO-LE in all cases.

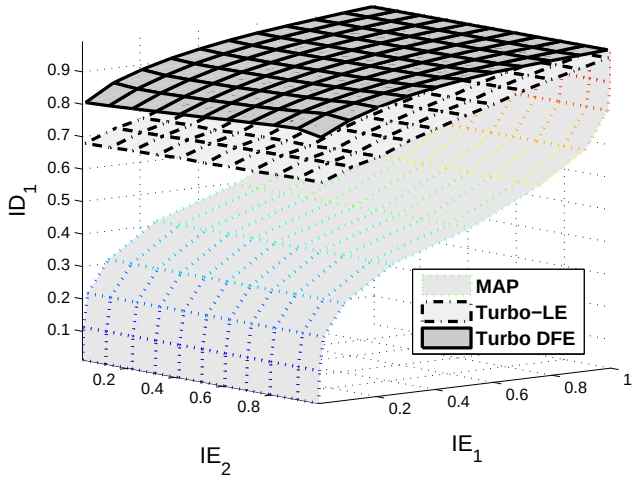

Figure 3. EXIT chart for BPSK constellation (26 dB).

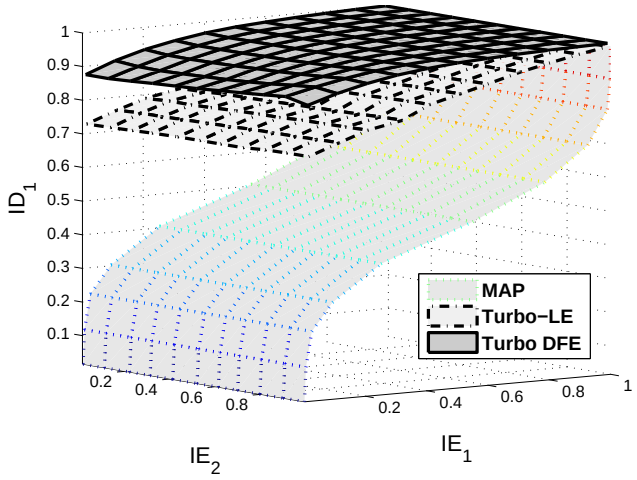

Figure 4. EXIT chart for QPSK constellation (28 dB).

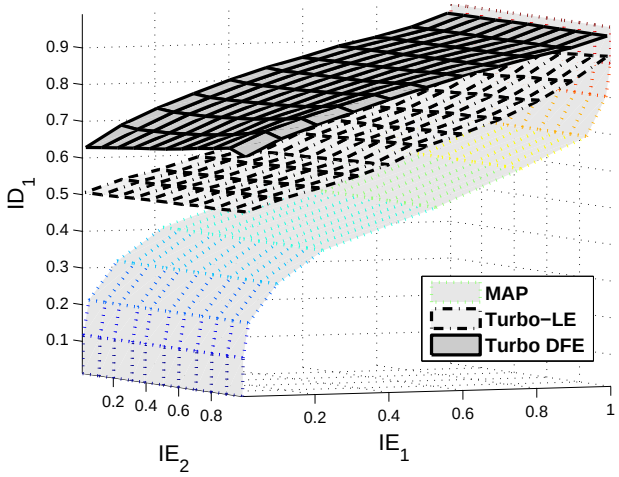

Figure 5. EXIT chart for 8PSK constellation (30dB).

Figure 7 shows the projected exit chart for the 16QAM constellation. Note that due to the multidimensional structure of the equalizer function outputs, here we have only displayed the lower and upper bounds. The lower bound is calculated by

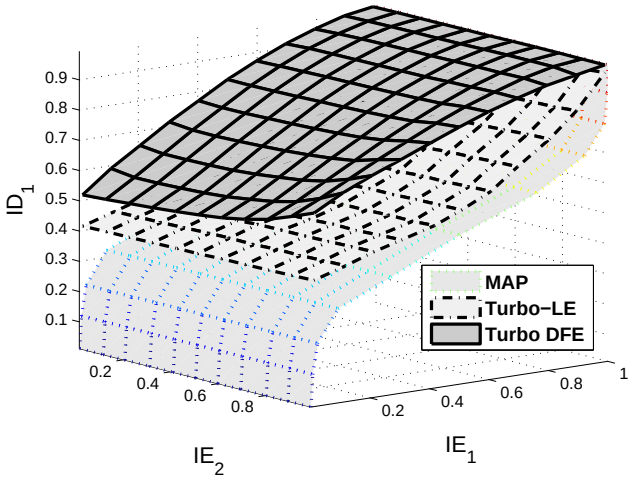

Figure 6. EXIT chart for 16QAM constellation (35dB).

setting the decoder MI of the other transmitter at 0 and the upper bound by setting the MI of the other transmitter at 1.

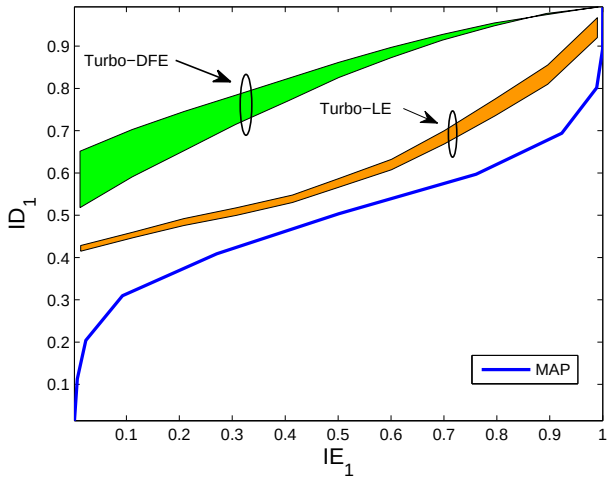

Figure 7. Projected EXIT chart for 16QAM constellation (35 dB).

To better analyze the convergence properties of the proposed algorithm, in the squeal we use the average EXIT charts instead of the EXIT chart contours.

Figure 8 shows the average projected EXIT chart for BPSK constellation. As it can be seen, while the slope of the proposed scheme is almost the same as Approximate-MMSE-LE, it increases substantially as IE_i is increased. In other words, with a larger IE_i input, the MIMO SDFE filter approaches the matched filter with a faster rate, compared to Approximate MMSE LE.

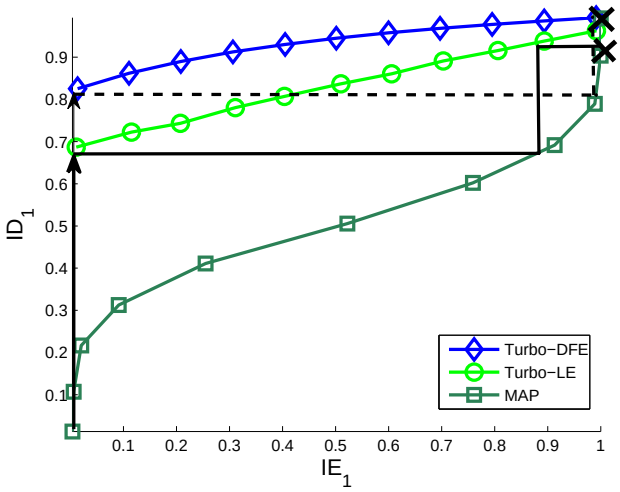

Figure 8. Average Projected EXIT chart for BPSK constellation (26 dB).

Figure 9 depicts the average projected EXIT charts for QPSK modulation. It can be easily seen from the trajectory trace that the convergence rate, which is determined by the width of the tunnel between the transfer curves of the equalizer and the decoder, of the proposed SDFE is faster than Approximate-MMSE-LE. In particular, we have observed that the proposed SDFE algorithm can reach $IE_o = 0.81$ after three iterations while Approximate MMSE LE only gets $IE_o = 0.68$. As the

input gets larger, the proposed SDFE algorithm starts to outperform the approximate MMSE LE.

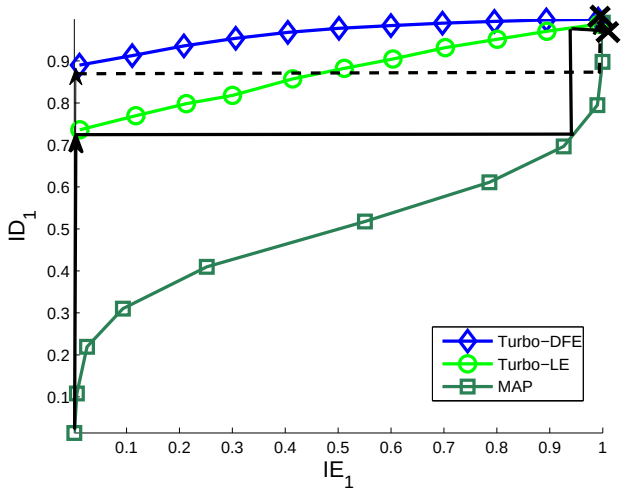

Figure 9. Average Projected EXIT chart for QPSK constellation (28 dB).

For 8PSK case in Figure 10, as it can be seen, in small and medium IE_i input region, the proposed SDFE has a wider tunnel than Approximate-MMSE-LE, which means the proposed SDFE has a faster convergence rate. The similar convergence property can be seen for 16QAM case in Figure 11.

6 Simulation Results

Simulation results are presented in this section to demonstrate the performance of the proposed turbo MIMO detection scheme. We show the performance of the turbo equalizers in a multiple antenna system which is equipped with 2 transmit and 2 receive antennas. In all cases, the transmitted binary bits are encoded by a rate

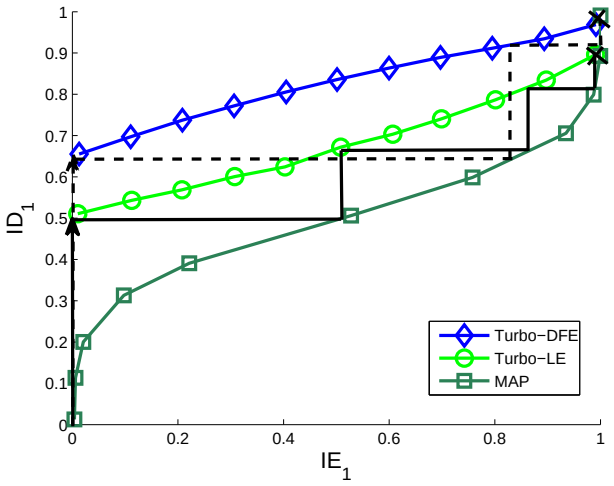

Figure 10. Average Projected EXIT chart for 8PSK constellation (30dB).

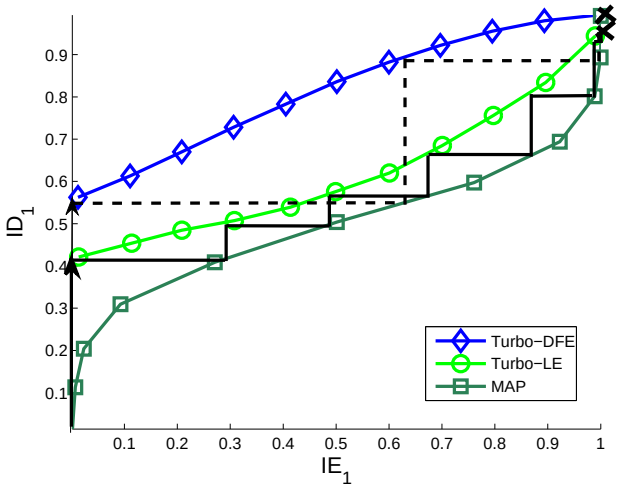

Figure 11. Average Projected EXIT chart for 16QAM constellation (35dB).

$R = 1/2$ convolutional code with generator polynomial in octal notation $G = [7, 5]$, followed by a size 10560 random interleaver. For the ISI channel, we have used a five tap 2×2 channel and the coefficients of the channel are taken from sever ISI SISO

channels introduced in [22]. After normalization, the tap coefficients for each channel are chosen as,

$$\mathbf{h}_1 = \begin{bmatrix} 0.1965 & 0.4233 \\ 0.1818 & 0.8656 \end{bmatrix} \quad \mathbf{h}_2 = \begin{bmatrix} 0.2031 & 0.3603 \\ 0.2208 & 0.8833 \end{bmatrix}$$

$$\mathbf{h}_3 = \begin{bmatrix} 0.2159 & 0.1283 \\ 0.2259 & 0.9412 \end{bmatrix} \quad \mathbf{h}_4 = \begin{bmatrix} 0.2208 & 0 \\ 0.1728 & 0.9599 \end{bmatrix}$$

$$\mathbf{h}_5 = \begin{bmatrix} 0.2169 & 0 \\ 0.2006 & 0.9554 \end{bmatrix}$$

where $\mathbf{h}_k$ is defined in (5).

The filter parameter for Approximate MMSE-LE [1] is set to ($N_1 = 9$, $N_2 = 5$) and for the proposed SDFE to ($N_1 = 9$, $N_2 = 5$, $N_3 = N_2 + M - 1$). LOG-MAP algorithm is employed for channel decoder and we have used the low complexity implementation of MIMO SDFE for all simulations.

As it can be seen from the BER curves in Figure 12-15, the performance gain of the proposed algorithm is significant for higher constellations. Specifically, we observe an improvement of over 10dB for the fourth iteration of the proposed algorithm compared to approximate MMSE-LE at BER level of 10^{-3} for 8PSK modulation. The BER improvement is even higher for the 16QAM case. The performance improvement with higher constellations can be justified in estimated soft symbols having more information compared to lower constellations.

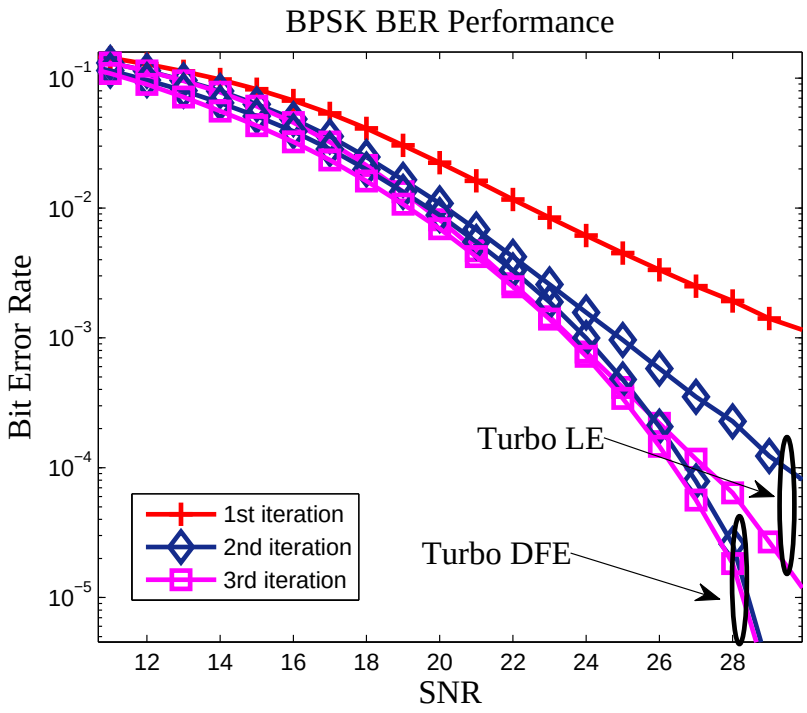

Figure 12. BPSK BER performance.

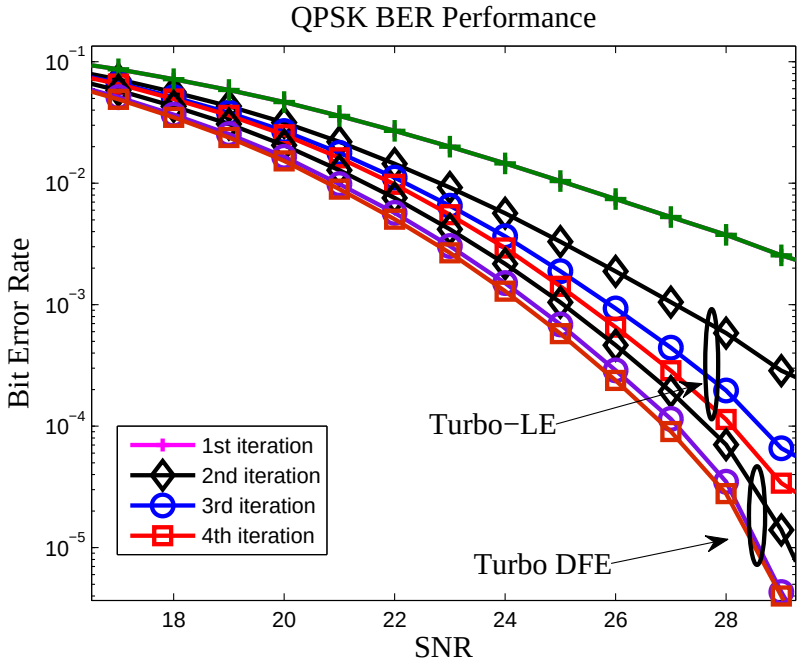

Figure 13. QPSK BER performance.

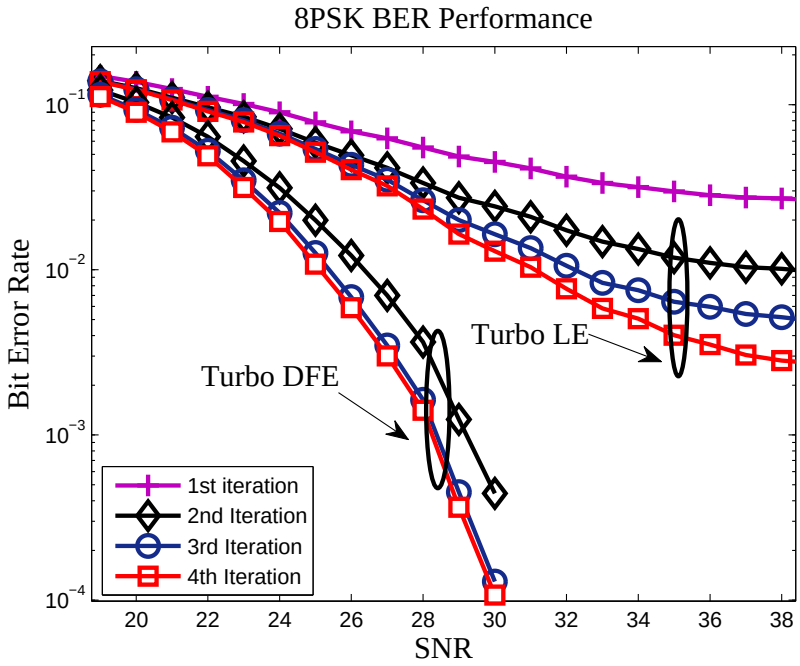

Figure 14. 8PSK BER performance.

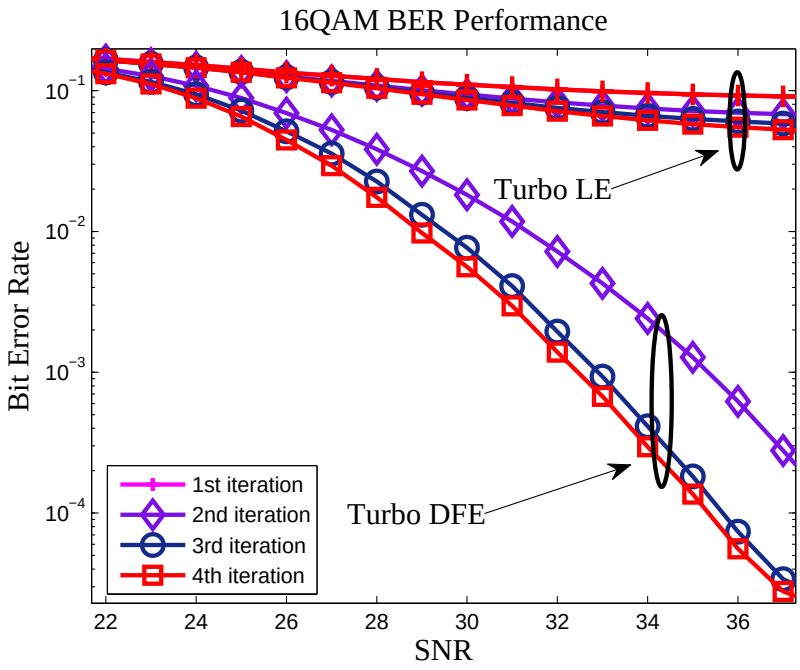

Figure 15. 16QAM BER performance.

7 Conclusion

In this paper, a low-complexity MMSE-based soft-decision feedback turbo equalizer has been proposed for both BPSK and multilevel modulations for multiple antenna systems. The proposed SDFE took into account the reliability of both soft *a priori* information and soft decisions of the data symbols. While for the first iteration, the proposed SDFE is basically a MMSE linear equalizer, the performance of the proposed SDFE scheme improves for subsequent iterations. When both soft *a priori* information and soft decisions become more reliable, the feedforward filter of the proposed SDFE approaches matched filter. Simulation results have shown that the proposed SDFE provides much better performance than the Approximate-MMSE-LE when higher constellations are used for modulation.

8 References

[1] M. T*ü*chler, R. Koetter, and A. C. Singer, "Turbo equalization: Principles and new results," *IEEE Trans. Commun*, vol. 50, pp.754-767, May. 2002.

[2] C. Douillard, C. Berrou, A. Picart, and A. Glavieux, "Iterative correction of intersymbol interference: Turbo equalization," *Eur. Trans. Telecommun.,* vol. 6, pp. 507511, Sept.Oct. 1995.

[3] T. Abe, S. Tomisato, and T. Matsumoto, "A MIMO turbo equalizer for frequency-selective channels with unknown interference," *IEEE Trans. Veh. Technol.*, vol. 52, pp. 476-482, May 2003.

[4] M. T*ü*chler, A. C. Singer, and R. Koetter, "Minimum mean square error equalization using a priori information," in *IEEE Trans. Signal Processing*, vol.50, pp.673-683, Mar. 2002.

[5] J. Wu and Y. R. Zheng, "Low complexity soft-input soft-output block decision feedback equalization," *IEEE J. Select. Areas Commun.*, vol.26, pp.281-289, Feb. 2008.

[6] A. Glavieux, C. Laot and J. Labat, "Turbo equalization over a frequency selective channel," in *Proc. Int. Symp. Turbo Codes, Related Topics*, Brest, France, pp.96-102, Sep. 1997.

[7] Z. Wu and J. Cioffi, "Low complexity iterative decoding with Decision-Aided Equalization for magnetic recording channels," *IEEE J. Select. Areas Commun.*, vol.19, pp.699-708, Apr. 2001.

[8] R. R. Lopes, "Iterative estimation, equalization and decoding," *Ph.D. dissertation, Georgia Inst. Technol.*, Atlanta, GA, 2003.

[9] R. R. Lopes and J. R. Barry, "The soft-feedback equalizer for turbo equalization of highly dispersive channels," *IEEE Trans. Commun*, vol.54, pp.783-788, May. 2006.

[10] H. Lou and C. Xiao, "Soft Decision Feedback Turbo Equalization for Multilevel Modulations," *IEEE Trans. Signal Process.*, vol. 59, pp.186-195, Jan. 2011.

[11] A. Dejonghe and L. Vanderdorpe, "Turbo equalization for multilevel modulation: An efficient low-complexity scheme," in *Proc. IEEE Int. Conf. Commun*, vol.3, pp.1863-1867, Aug. 2002.

[12] P. Vila, I. Fijalkow, C. Laot, D. Leroux, D. Pirez, S. Ronger, and C. Langlais, "Reduced-complexity M-ary decoders for turbo-equalization," in *2nd Int. Symp. Turbo Codes and Related Topics*, Brest, France, Sept.4-7 2000.

[13] Y. Lee and W. R. Wu, "Adaptive channel aided decision feedback equalization for SISO and MIMO systems," *IEEE Proc.Commun.,* vol.153, pp. 657-663, Oct. 2006.

[14] S. Ten Brink, "Convergence behavior of iteratively decoded parallel concatenated codes," *IEEE Trans. Commun.,* vol.49, pp. 1727-1737, Oct. 2001.

[15] N. Al-Dhahir, and J.M. Cioffi, "MMSE decision-feedback equalizers: Finite-length results", *IEEE Trans. Inf. Theory*, vol. 41, pp. 961-975, Jul. 1995.

[16] S. Lee, A. Singer, and N. R. Shanbhag, "Linear turbo equalization analysis via BER transfer and EXIT charts," *IEEE Trans. Signal Process.*, vol. 53, no. 8, pp. 2883-2897, Aug. 2005.

[17] S. Ibi, T. Matsumoto, R. Thoma, S. Sampei, and N. Morinaga, "EXIT chart-aided adaptive coding for multilevel BICM with turbo equalization in frequency-selective MIMO channels," *IEEE Trans. Veh. Technol.*, vol. 56, no. 6, pp. 3757-3769, Nov. 2007.

[18] X. Wang and H. V. Poor, "Iterative (turbo) soft interference cancellation and decoding for coded CDMA," *IEEE Trans. Commun.*, vol. 47, pp. 1046-1061, Jul. 1999.

[19] T. Abe and T. Matsumoto, "Space-time turbo equalization in frequency selective MIMO channels," *IEEE Trans. Veh. Technol.*, vol. 52, pp. 469- 475, May 2003.

[20] G. Bauch and N. Al-Dhahir, "Reduced-complexity space-time turbo equalization for frequency-selective MIMO channels," *IEEE Trans. Wireless Commun.,* vol. 1, pp. 819-828, Oct. 2002.

[21] X. Xiaomei, C. Yougan, Z. Lan and F. Wei, "Comparison of the performance of LDPC codes over different underwater acoustic channels" *12th IEEE International Conference on Communication Technology (ICCT)*, pp. 155-158, Nov 2010.

[22] J. G. Proakis, *Digital Communications*, McGraw-Hill Inc., 2001.

IV. SOFT FEEDBACK TURBO EQUALIZATION FOR UNDERWATER ACOUSTIC COMMUNICATIONS

Amirhossein Rafati, Huang Lou, Yahong Rosa Zheng and Chengshan Xiao

Abstract—In this paper, a low-complexity turbo detection scheme is proposed for single-carrier multiple-input multiple output (MIMO) underwater acoustic (UWA) communications that employs low-density parity-check (LDPC) channel coding. The proposed iterative soft feedback equalization (SFE) algorithm offers a novel approach to combating error propagation by utilizing the past soft decisions to mitigate inter-symbol interference. In addition, its computational complexity grows only linearly with the number of equalizer coefficients, compared to the quadratic complexity of minimum mean square error-based linear turbo equalizer. Performance of the proposed detection scheme is verified through experimental data collected in MACE10. Experimental results show that it provides robust detection and improved Bit Error Rate (BER) for MIMO UWA communications with different modulations schemes.

1 Introduction

Mitigating inter-symbol interference (ISI) is one of the most important challenges in achieving high data rates in underwater acoustic (UWA) communication systems [1]- [2]. To alleviate the fast temporal variations and long multi-path delay spreads of the underwater channels, channel coding has been employed as an indispensable strategy to increase the reliability of decoded symbols. In this regard, LDPC codes have been previously used in UWA systems due to their capacity achieving property which offers considerable coding gain compared to other coding solutions [3]. Besides encoding algorithms, many interesting approaches have also

been proposed for UWA receiver design. Specifically, the advent of turbo equalization technology has enabled powerful receiver designs based on iterative exchanges of soft information between the equalizer and the decoder [4]- [5]. Compared with conventional one-time equalization, turbo equalization has a much more powerful detection capability, attributed to the iterative extrinsic soft information exchanges between a soft-decision equalizer and a soft-decision decoder.

In [5], the turbo linear equalizer (LE) was proposed for long-term UWA communication testing. In [7], the soft-decision-feedback equalizer (DFE) together with the turbo decoder, has been applied to UWA communication. Iterative decoding and turbo detection for orthogonal frequency-division multiplexing (OFDM) UWA systems has also been proposed in [8]. Yet, practical implementation of turbo equalization in an underwater environment still requires a lot of computational complexity due to the extremely long delay spread of the underwater channels [6]- [9].

Recently, a new low-complexity soft feedback inter-symbol interference canceler was proposed in [10] for single-input single-output (SISO) systems employing multilevel constellations. Motivated by [10], we propose a low-complexity, soft feedback equalization (SFE) receiver which is suitable for severe, frequency selective ISI channels in multiple-input multiple-output (MIMO) underwater acoustic communication systems. The proposed SFE algorithm offers a novel approach to combating error propagation by using both anti-causal and causal filters in the equalizer structure. In addition, its computational complexity is considerably smaller compared to the quadratic complexity of minimum mean square error-based linear turbo equalizer with time-varying coefficients [4]. The proposed detection scheme has been tested by undersea trial data collected in the undersea experiment named MACE10 conducted at Buzzards Bay, MA in June 2010.

2 System Model

In UWA communications, front-end preprocessing stages such as synchronization, Doppler shift estimation and compensation , demodulation and waveform resampling is usually required before signal detection can be performed. After preprocessing, the discrete time baseband signal at the mth hydrophone at time instant n is expressed by,

$$z_n^{(m)} = \sum_{k=1}^{t} \sum_{l=0}^{L-1} h_l^{(m,k)} x_{n-l}^k + w_n^{(m)} \tag{1}$$

where x_{n-l}^k is the transmitted symbol at kth transducer at time instant $n-l$ and $h_l^{(m,k)}$ is the lth channel coefficnet between the kth transducer and mth hydrophone. Finally, $w_n^{(m)}$ represents the zero mean additive white Gaussian noise (AWGN) sample on the mth hyrophone. The noise samples $w_n^{(m)}$ are independent and identically distributed (i.i.d.) with the variance of $\sigma^2/2$ for both real and imaginary parts. Based on the block-fading assumption, we can assume that the channel is constant over the block of transmitted symbols. Stacking up all the received symbols on r hydrophones as $\mathbf{z}_n = [z_n^{(1)}, z_n^{(2)}, \ldots, z_n^{(r)}]^T$, we can write,

$$\mathbf{z}_n = \sum_{l=0}^{L-1} \mathbf{h}_l \mathbf{x}_{n-l} + \mathbf{w}_n \tag{2}$$

where

$$\begin{aligned} \mathbf{x}_n &= [x_n^1, x_n^2, \ldots, x_n^t]^T \\ \mathbf{w}_n &= [w_n^1, w_n^2, \ldots, w_n^r]^T \end{aligned} \tag{3}$$

and

$$\mathbf{h}_l = \begin{bmatrix} h_l^{(1,1)} & h_l^{(1,2)} & \cdots & h_l^{(1,t)} \\ h_l^{(2,1)} & h_l^{(2,2)} & \cdots & h_l^{(2,t)} \\ \vdots & \vdots & \ddots & \vdots \\ h_l^{(r,1)} & h_l^{(r,2)} & \cdots & h_l^{(r,t)} \end{bmatrix}. \tag{4}$$

Finally, temporal sampling for N_1 future and N_2 previous received symbols at time instant n to capture the multi-path signals of all the hydrophones for diversity combining yields the following space-time representation of the received signal,

$$\mathbf{Z}_n = \mathbf{H}\mathbf{X}_n + \mathbf{W}_n \tag{5}$$

where $\mathbf{Z}_n$, $\mathbf{H}$, $\mathbf{X}_n$ and $\mathbf{W}_n$ are defined in (6). N_1 and N_2 should be chosen as to include all the received symbols that are correlated with the transmitted symbol at time n. In general, N_1 and N_2 should be chosen according to the channel characteristics and specifically, location of the major channel tap with respect to other taps. In the sequel, several stages of the proposed MIMO UWA detection system are explained in detail.

3 Signalling and Data Structure

We consider a MIMO communication system with t transducers and r hydrophones that employs a digital modulation with constellation size q. Here, the binary information sequence $[b_1\ b_2 \cdots b_{q\times t}]^T$ is first transmitted into t parallel substreams using a serial to parallel converter where each stream is encoded by a low density parity check (LDPC) encoder and followed by an interleaver Π and a constellation mapper and then transmitted through one of the t transmit antennas. Throughout this experiment, we use QPSK, 8PSK and 16-quadrature amplitude modulation

$$\underbrace{\begin{bmatrix} \mathbf{z}_{n-N_2} \\ \vdots \\ \mathbf{z}_n \\ \vdots \\ \mathbf{z}_{n+N_1} \end{bmatrix}}_{\mathbf{Z}_n} = \underbrace{\begin{bmatrix} \mathbf{h}_{L-1} & \cdots & \mathbf{h}_0 & \cdots & \cdots & 0 \\ \vdots & \ddots & \ddots & \ddots & & \vdots \\ & & \ddots & \ddots & \ddots & \vdots \\ 0 & \cdots & & \mathbf{h}_{L-1} & \cdots & \mathbf{h}_0 \end{bmatrix}}_{\mathbf{H}} \underbrace{\begin{bmatrix} \mathbf{x}_{n-N_2-L+1} \\ \vdots \\ \mathbf{x}_n \\ \vdots \\ \mathbf{x}_{n+N_1} \end{bmatrix}}_{\mathbf{X}_n} + \underbrace{\begin{bmatrix} \mathbf{w}_{n-N_2} \\ \vdots \\ \mathbf{w}_n \\ \vdots \\ \mathbf{w}_{n+N_1} \end{bmatrix}}_{\mathbf{W}_n} \tag{6}$$

(16QAM) modulation schemes with constellation sizes being 4, 8 and 16, respectively. Let us denote the block of information to be transmitted by the kth transducer with the binary sequence $\mathbf{b}^k = \begin{bmatrix} b_{(k-1)q+1} & \cdots b_{kq} \end{bmatrix}^T$. After interleaving, the output of the kth interleaver can be stated as $\mathbf{c}^k = \begin{bmatrix} \mathbf{c}_1^k & \mathbf{c}_2^k \cdots \mathbf{c}_{K_c}^k \end{bmatrix}$ where $\mathbf{c}_n^k$ represents $\begin{bmatrix} c_{n,1}^k & c_{n,1}^k \cdots c_{n,q}^k \end{bmatrix}$ with bits $c_{n,j}^k \in \{0, 1\}$. The mapper maps each random vector $\mathbf{c}_n^k$ to a symbol x_n^k from the 2^q-ary constellation set $\mathcal{S} = \{\alpha_1, \alpha_2, \cdots, \alpha_{2^q}\}$, where α_i corresponds to the deterministic bit pattern $\mathbf{s}_i = [s_{i,1} \; s_{i,2} \cdots s_{i,q}]$ with $s_{i,j} \in 0, 1$ in Table 1 which specifies the mapping between the encoded bits and the elements of the constellation.

Table 1. Symbol alphabets.

8PSK:

i	1	2	3	4	5	6	7	8
$s_{i,1}\ s_{i,2}\ s_{i,3}$	000	001	010	011	100	101	110	111
α_i	$e^{(\frac{i9\pi}{8})}$	$e^{(\frac{i11\pi}{8})}$	$e^{(\frac{i15\pi}{8})}$	$e^{(\frac{i13\pi}{8})}$	$e^{(\frac{i7\pi}{8})}$	$e^{(\frac{i5\pi}{8})}$	$e^{(\frac{i\pi}{8})}$	$e^{(\frac{i3\pi}{8})}$

16QAM:

i	1	2	3	4	5	6	7	8
$s_{i,1}\ s_{i,2}\ s_{i,3}\ s_{i,4}$	0000	0001	0010	0011	0100	0101	0110	0111
α_i	$\frac{(-1-i)}{\sqrt{10}}$	$\frac{(-1-3i)}{\sqrt{10}}$	$\frac{(-1+i)}{\sqrt{10}}$	$\frac{(-1+3i)}{\sqrt{10}}$	$\frac{(-3-i)}{\sqrt{10}}$	$\frac{(-3-3i)}{\sqrt{10}}$	$\frac{(-3+i)}{\sqrt{10}}$	$\frac{(-3+3i)}{\sqrt{10}}$
i	9	10	11	12	13	14	15	16
$s_{i,1}\ s_{i,2}\ s_{i,3}\ s_{i,4}$	1000	1001	1010	1011	1100	1101	1110	1111
α_i	$\frac{(1-i)}{\sqrt{10}}$	$\frac{(1-3i)}{\sqrt{10}}$	$\frac{(1+i)}{\sqrt{10}}$	$\frac{(1+3i)}{\sqrt{10}}$	$\frac{(3-i)}{\sqrt{10}}$	$\frac{(3-3i)}{\sqrt{10}}$	$\frac{(3+i)}{\sqrt{10}}$	$\frac{(3+3i)}{\sqrt{10}}$

The data structure is appended with some auxiliary signals and then, the transmission burst is transmitted in the format shown in Figure 1. As it can be seen, the burst begins with a head linear frequency modulation (LFM) chirp signal called (LFMB), followed by three different data payloads containing QPSK, 8PSK and 16QAM modulated symbols. Each data payload starts with an m-sequence of length 511 and is proceeded by 43 data blocks. Then, the same format is repeated with 43 new blocks containing the symbols from the same constellation. Finally, the burst ends with a tail LFM signal called LFME. The chirp LFM signals on the hydrophone side serve multiple purposes such as coarse synchronization, Doppler shift estimation and channel length measurement due to their unique correlation properties. On the other hand, m sequence can be used for evaluating the channel scattering function and estimating the Doppler spread.

4 Proposed Detection Scheme

Figure 2 demonstrates the kth branch of the SFE Turbo receiver at time instant n. Here, $\mathbf{F}_k \in \mathcal{C}^{(N_1+N_2+1)r\times 1}$, $\mathbf{B}_k \in \mathcal{C}^{(N_2+L-1)t\times 1}$ and $\mathbf{P}_k \in \mathcal{C}^{N_1 t\times 1}$ are the filter coefficients for the kth receiver branch. In addition, extrinsic and *a priori* log likelihood ratio (LLR) values for this branch are denoted by $\lambda_{n,j}^{k}$ and $\left(\lambda_{n,j}^{p}\right)^{k}$,

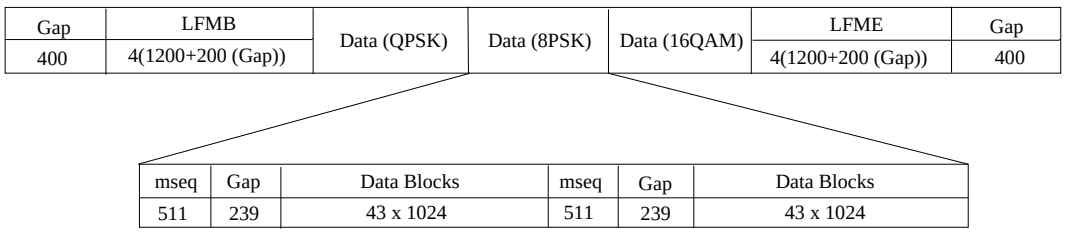

Figure 1. MACE10 data structure.

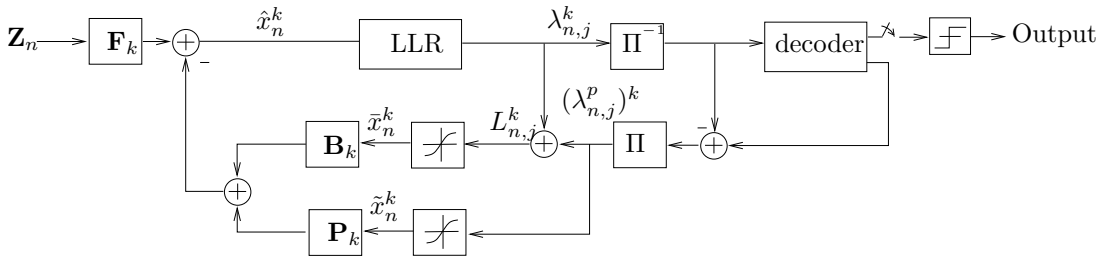

Figure 2. Block diagram of the kth branch of the proposed turbo receiver.

respectively, where $j \in \{1, 2, \cdots, q\}$. The main idea in the proposed SFE algorithm is to utilize both causal and anti-causal filters instead of a general decision feedback filter to mitigate the ISI.

Let us write the output of the SFE equalizer as

$$\hat{x}_n^k = \mathbf{F}_k^H \mathbf{Z}_n - \mathbf{P}_k^H \tilde{\mathbf{x}}_n^k - \mathbf{B}_k^H \bar{\mathbf{x}}_n^k \tag{7}$$

where $\mathbf{Z}_n$ is defined in (6) and,

$$\tilde{\mathbf{x}}_n^k = \left[\tilde{x}_{n+1}^1, \tilde{x}_{n+1}^2, \cdots, \tilde{x}_{n+N_1}^t\right]^T \tag{8}$$

$$\bar{\mathbf{x}}_n^k = \left[\bar{x}_{n-(N_2+L)+1}^1, \bar{x}_{n-(N_2+L)+1}^2, \cdots, \bar{x}_{n-1}^{t-1}, \bar{x}_{n-1}^t\right]^T \tag{9}$$

where N_1 and N_2 determine the length of the filters. Here, instead of trying to cancel all the interference, we pass $\tilde{x}_n^k$ and $\hat{x}_n^k$ through linear filters $\mathbf{B}_k$ and $\mathbf{P}_k$ whose coefficients, along with the equalizer filter coefficient $\mathbf{F}_k$ are computed to minimize the MSE $E\{\left\|\hat{x}_n^k - x_n^k\right\|^2\}$. Hence, proper values for $\mathbf{F}_k$, $\mathbf{P}_k$ and $\mathbf{B}_k$ should be obtained from the following optimization problem

$$\text{MMSE} = \min_{\mathbf{F}_k, \mathbf{B}_k, \mathbf{P}_k} E\left\{\left\|\mathbf{F}_k^H \mathbf{Z}_n - \mathbf{P}_k^H \tilde{\mathbf{x}}_n^k - \mathbf{B}_k^H \bar{\mathbf{x}}_n^k - x_n^k\right\|^2\right\}. \tag{10}$$

In order to solve this problem, we assume that $E\{\tilde{x}_n^i x_m^{j*}\} = E\{\bar{x}_n^i x_m^{j*}\} = E\{\tilde{x}_n^i \bar{x}_m^{j*}\} = 0$, given that if $i = j$, $n \neq m$ and vice versa. These assumptions are justified since $\tilde{x}_n^i$ and $\bar{x}_n^i$ are approximately equal to x_n^i and the transmitted symbols from the same (different) transducers are uncorrelated at different times. Moreover, we adopt the following notations for the remaining nonzero expected values:

$$\phi^k \triangleq E\left\{x_n^k \tilde{x}_n^{k*}\right\}, \qquad \psi^k \triangleq E\left\{x_n^k \bar{x}_n^{k*}\right\} \tag{11}$$

$$\tilde{p}^k \triangleq E\left\{\left|\tilde{x}_n^k\right|^2\right\}, \qquad \bar{p}^k \triangleq E\left\{\left|\bar{x}_n^k\right|^2\right\} \tag{12}$$

where the expectations are taken with respect to time. Using the above assumptions, it can be shown that the optimal values for $\mathbf{F}_k$, $\mathbf{B}_k$ and $\mathbf{P}_k$ that minimize the cost function $E\{\left\|\hat{x}_n^k - x_n^k\right\|^2\}$ are computed as,

$$\mathbf{F}_k = \left(\mathbf{H}\mathbf{H}^T + \sigma^2\mathbf{I} - \mathbf{H}_p\Gamma\mathbf{H}_p^{-1} - \mathbf{H}_b\Lambda\mathbf{H}_b^{-1}\right)^{-1}\mathbf{s}_k \tag{13}$$

$$\mathbf{P}_k = \tilde{\mathbf{P}}^{-1}\Phi^H\mathbf{H}_p^H\mathbf{F}_k \tag{14}$$

$$\mathbf{B}_k = \bar{\mathbf{P}}^{-1}\Psi^H\mathbf{H}_b^H\mathbf{F}_k \tag{15}$$

where

$$\Gamma = \Phi\tilde{\mathbf{P}}^{-1}\Phi^H \qquad \Lambda = \Psi\bar{\mathbf{P}}^{-1}\Psi^H, \tag{16}$$

s_k is the $((N_2 + L - 1)\,t + k)$th column of $\mathbf{H}$, and $\mathbf{H}_b$ and $\mathbf{H}_p$ are the leftmost $(N_2 + L - 1)t$ and rightmost $N_1 t$ columns of $\mathbf{H}$, respectively. In addition,

$$\Phi = \underbrace{\Phi_d \oplus \Phi_d \oplus \cdots \Phi_d}_{N_1 \text{ times}}, \quad \tilde{\mathbf{P}} = \underbrace{\tilde{\mathbf{P}}_d \oplus \tilde{\mathbf{P}}_d \oplus \cdots \tilde{\mathbf{P}}_d}_{N_1 \text{ times}} \tag{17}$$

$$\Psi = \underbrace{\Psi_d \oplus \Psi_d \oplus \cdots \Psi_d}_{N_2 + L - 1 \text{ times}}, \quad \bar{\mathbf{P}} = \underbrace{\bar{\mathbf{P}}_d \oplus \bar{\mathbf{P}}_d \oplus \cdots \bar{\mathbf{P}}_d}_{N_2 + L - 1 \text{ times}} \tag{18}$$

where $\oplus$ denotes the direct sum of matrices and

$$\Phi_d = \text{diag}\left(\phi^1, \phi^2, \ldots, \phi^t\right), \ \tilde{\mathbf{P}}_d = \text{diag}\left(\tilde{p}^1, \tilde{p}^2, \ldots, \tilde{p}^t\right) \tag{19}$$

$$\Psi_d = \text{diag}\left(\psi^1, \psi^2, \ldots, \psi^t\right), \bar{\mathbf{P}}_d = \text{diag}\left(\bar{p}^1, \bar{p}^2, \ldots, \bar{p}^t\right) \tag{20}$$

where $\text{diag}(a_1, \cdots, a_k)$ denotes a diagonal matrix with diagonal entries $a_1, \ldots, a_k$. It should be noted that as the matrices Φ, Ψ, $\tilde{\mathbf{P}}$ and $\bar{\mathbf{P}}$ are all diagonal, Γ and Λ can be computed without any intensive computational complexity.

Exploiting the symmetries, it is straightforward from (11) and (12) that ϕ^k, ψ^k, $\tilde{p}^k$ and $\bar{p}^k$ may be computed by conditioning on $x_n^k = \alpha_i$ where $\alpha_i \in \mathcal{S}$. In other words,

$$\phi^k = \alpha_i E\left\{\tilde{x}_n^{k*} \middle| x_n^k = \alpha_i\right\}, \ \psi^k = \alpha_i E\left\{\bar{x}_n^{k*} \middle| x_n^k = \alpha_i\right\} \tag{21}$$

$$\tilde{p}^k = E\left\{\left|\tilde{x}_n^k\right|^2 \middle| x_n^k = \alpha_i\right\}, \ \bar{p}^k = E\left\{\left|\bar{x}_n^k\right|^2 \middle| x_n^k = \alpha_i\right\}. \tag{22}$$

For MPSK, α_i can be any elements in $\mathcal{S}$, while for QAM, ϕ^k and ψ^k should be re-scaled when $|\alpha_i| \neq 1$. Unfortunately, there are no closed-form solutions for the above expected values. Nevertheless, these functions can be tabulated or computed by simple numerical algorithms. It should also be noted that for numerical computation of the expected values requires a prior knowledge about the probability of $\hat{x}_n^k$. In the sequel, we elaborate a statistical method to generate samples of $\hat{x}_n^k$, which will be later used to estimate the expected values.

Regardless of the structure of the equalizer and without loss of generality, we can express the estimate $\hat{x}_n^k$ of $x_n^k \in S$ as an output of an equivalent AWGN channel as,

$$\hat{x}_n^k = A_k x_n^k + v_n^k \tag{23}$$

where $A_k = \mathbf{F}_k^H \mathbf{s}_k$. Following the same approach in [13], it is straight forward to show that

$$\hat{x}_n^k \sim \mathcal{N}(x_n^k A_k, \sigma_k^2) \qquad \text{where} \quad \sigma_k^2 = A_k(1 - A_k). \tag{24}$$

Let us now define the symbol extrinsic probability as

$$P(\hat{x}_n^k | x_n^k = \alpha_i) = \frac{1}{\sigma^2 \pi} \exp(-\rho_{n,i}^k) \tag{25}$$

$$\rho_{n,i}^k = \frac{\left|\hat{x}_n^k - A_k \alpha_i\right|^2}{\sigma_k^2} \tag{26}$$

where α_i is defined in table 1. The extrinsic LLR $\lambda_{n,j}^k$ of coded bit $c_{n,j}^k$ is the function of $P(\hat{x}_n^k \big| x_n^k = \alpha_i)$:

$$\begin{aligned} \lambda_{n,j}^k &= \log \frac{\sum_{\alpha_i : c_{n,j}^k = 0} P(\hat{x}_n^k | \alpha_i) \prod_{\forall j', j' \neq j} P(c_{n,j'}^k)}{\sum_{\alpha_i : c_{n,j}^k = 1} P(\hat{x}_n^k | \alpha_i) \prod_{\forall j', j' \neq j} P(c_{n,j'})} \\ &= \log \frac{\sum_{\alpha_i : c_{n,j}^k = 0} \exp(-\rho_{n,i}^k + \sum_{\forall j', j' \neq j} \tilde{s}_{i,j} L(c_{n,j'}^k)/2)}{\sum_{\alpha_i : c_{n,j}^k = 1} \exp(-\rho_{n,i}^k + \sum_{\forall j', j' \neq j} \tilde{s}_{i,j} L(c_{n,j'}^k)/2)} \end{aligned} \tag{27}$$

where

$$\tilde{s}_{i,j} = \begin{cases} +1 & \text{if } s_{i,j} = 0 \\ -1 & \text{if } s_{i,j} = 1. \end{cases}$$

For QPSK or QAM modulation, the computational complexity in (27) can be reduced by using minimum-based LLR simplification defined by

$$\log(\exp(-x) + \exp(-y)) \approx -min(x, y) \tag{28}$$

when $|x - y|$ is sufficiently large.

For MPSK ($M > 2$) modulation, the minimum-based LLR simplifications can not be made because several symbols are quite close to each other on the unit

circle. Instead, a geometric approach [14] can be applied to estimate LLR $\lambda_{n,j}$. The approximation is listed in Table 2.

Using (25), (26) and (27), it can be seen that $\lambda_{n,j}^k$ can be computed as a function of $\hat{x}_n^k$ which implies that the pdf of $\lambda_{n,j}^k$ is related to the pdf of $\hat{x}_n^k$. Hence, using (24), and the equations from Table 2, it is easy to generate different samples of $\lambda_{n,j}^k$. Moreover, since

$$\left(\lambda_{n,j}^k\right)^p = \log \frac{P(c_{n,j}^k = 0)}{P(c_{n,j}^k = 1)}, \tag{29}$$

if $c_{n,j}^k = 0$, the distribution of $\left(\lambda_{n,j}^k\right)^p$ can be expressed as $\mathcal{N}(\gamma_p^k, 2\gamma_p^k)$. Now, as $L_{n,j}^k = \lambda_{n,j}^k + \left(\lambda_{n,j}^k\right)^p$, statistical samples of $L_{n,j}^k$ can also be generated using the knowledge ofγ_p^k. Since $\bar{x}_n^k$ is a function of $L_{n,j}^k$, as long as we know the parameters γ_p^k of $\left(\lambda_{n,j}^k\right)^p$ and A_k of $\hat{x}_n^k$, expected values ψ^k and ϕ^k can be calculated through numerical methods.

The ML estimate of γ_p^k can also be estimated using

$$\gamma_p^k = \sqrt{1 + \frac{1}{K_c \times q} \sum_{n=1}^{K_c} \sum_{j=1}^{q} \left| \left(\left(\lambda_{n,j}^k\right)^p \right)^2 \right|} - 1. \tag{30}$$

Table 2. LLR simplifications for different constellations.

QPSK:
- $\lambda_{n,1}^k \approx 2\sqrt{2}\mathrm{Re}\{\hat{x}_n^k\}/\left(1 - A_k\right)$.
- $\lambda_{n,2}^k \approx 2\sqrt{2}\mathrm{Im}\{\hat{x}_n^k\}/\left(1 - A_k\right)$.

8PSK:
- $\lambda_{n,1}^k \approx -4\sin(7\pi/8)\mathrm{Im}\{\hat{x}_n^k\}/\left(1 - A_k\right)$.
- $\lambda_{n,2}^k \approx -4\sin(7\pi/8)\mathrm{Re}\{\hat{x}_n^k\}/\left(1 - A_k\right)$.
- $\lambda_{n,3}^k \approx 1.0824(|\mathrm{Re}\{\hat{x}_n^k\}| - |\mathrm{Im}\{\hat{x}_n^k\}|)/\left(1 - A_k\right)$.

16QAM:
- $\lambda_{n,1}^k \approx -4\mathrm{Re}\{\hat{x}_n^k\}/(\sqrt{10}\left(1 - A_k\right))$.
- $\lambda_{n,2}^k \approx (8A_k - 4\sqrt{10}|\mathrm{Re}\{\hat{x}_n^k\}|)/(10\left(1 - A_k\right))$.
- $\lambda_{n,3}^k \approx -4\mathrm{Im}\{\hat{x}_n^k\}/(\sqrt{10}((1 - A_k))$.
- $\lambda_{n,4}^k \approx (8A_k - 4\sqrt{10}|\mathrm{Im}\{\hat{x}_n^k\}|)/(10\left(1 - A_k\right))$.

In order to determine A_k, we need $\mathbf{F}_k$, while we need A_k to calculate ψ^k and ϕ^k, and thus $\mathbf{F}_k$. This is problematic. To find both A_k and $\mathbf{F}_k$ simultaneously, Lopes *et al.* proposed an iterative procedure for initial A_k and $\mathbf{F}_k$ computation [12]. However, it still involves a lot of computations and induces convergence delay. In our algorithm, MMSE-LE is employed in first turbo iteration to replace this iterative procedure for initial A_k and $\mathbf{F}_k$ computation as in [10].

Finally, the computation of $\bar{x}_n^k$ is given by

$$\bar{x}_n^k = \sum_{\alpha_i \in \mathcal{S}} \alpha_i \Pr\left(\bar{x}_n^k = \alpha_i\right) \tag{31}$$

$$\Pr\left(\bar{x}_n^k = \alpha_i\right) = \prod_{j=1}^{q} \frac{1}{2}\left(1 + \tilde{s}_{i,j} \tanh\left(L_{n,j}^k/2\right)\right). \tag{32}$$

$\tilde{x}_n^k$ can also be computed in a similar fashion.

5 Experimental Results

Multiple-input, multiple-output (MIMO) underwater acoustic experiments were conducted at Buzzards Bay, MA in June 2010. The sampling rate was 39.0625 kilohertz (kHz) and the carrier frequency was 13 kHz. The modulation schemes include QPSK, 8PSK and 16QAM and the information bits were LDPC encoded and then randomly interleaved before symbol modulation. The communication equipment consists of 2 transducers and 12 hydrophones. There were two tows in this experiment; on one tow the transducer array was oriented vertically and on the other, it was horizontal. In this paper, we present the results of tow 2 to illustrate the performance of the proposed MIMO SFE algorithm. As mentioned before, the coarse synchronization and the channel length measurement both can be achieved with the LFM signals. In Figure 3, an example of the LFM correlation signal is demonstrated for a

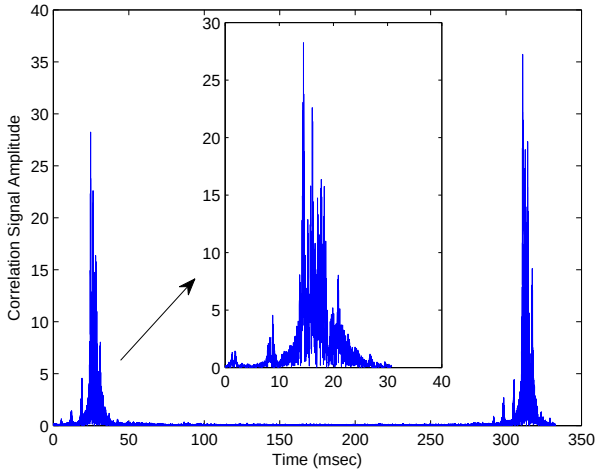

Figure 3. LFM signal correlation.

two-transducer transmission. The coarse synchronization point is found with either of the two ridge peaks. MIMO channel estimation is initially obtained with training symbols, and then updated with newly detected symbols. While for the first iteration, the equalized symbols from the output of the equalizer are used to update the channel for the subsequent sub-blocks, the quality of channel estimation is further improved in the remaining iterations by employing the symbols from the output of the LDPC decoder. Once the synchronization and the channel estimation are obtained, Doppler frequency estimation and the turbo equalization can be performed.

5.1 Doppler Frequency Estimation

For each block, we estimate the Doppler frequency based on the received LFM chirp signal. Figure 4 shows the estimated Doppler frequency for the duration of tow 2. The relative speed was about 11 Hz when the transducer was moving away from the hydrophone array, and about 9 Hz when it was towed back. We see that the estimated doppler frequency changes from negative to positive after 60 minutes,

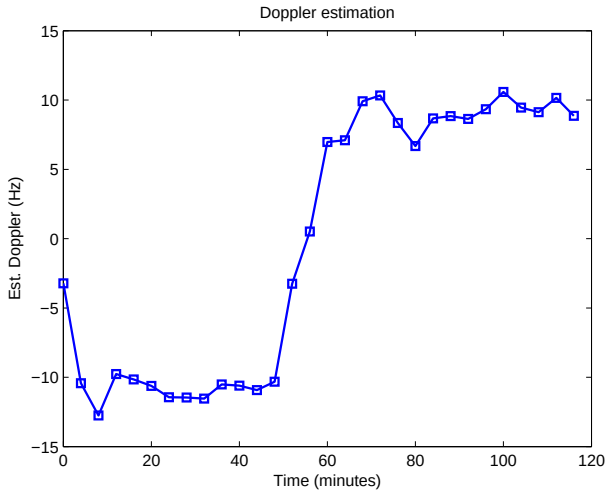

Figure 4. The estimated doppler speed.

indicating that the transducer array began to be towed back from the maximum range at 60th minute.

5.2 BER Results

The experimental results with different modulation schemes are presented next. In our experiment, the estimated channel had 50 taps. In total, 5 Packets, each containing 2×43 symbol blocks for each modulation scheme have been processed. An incurring 12.5% pilot overhead has been adopted for QPSK modulation while 8PSK and 16QAM modulated symbols have been processed with 25 % pilot overhead. In our detection algorithm, we have set $N_1 = N_2 = 60$ and used 20 iterations for the LDPC decoder and 4 iterations for the turbo equalizer. The detection results are listed in Table 3. It is clear that QPSK transmission has the best average BER. This observation is as expected since under the same transmission conditions, using larger constellation size always degrades the BER performance.

Table 3. Detection results for 2×12 MIMO.

Mod. \ N_{iter}		1	2	3	4
Tow 2	QPSK	1.2×10^{-4}	0	0	0
	8PSK	4.3×10^{-3}	3.2×10^{-4}	3.9×10^{-5}	1.2×10^{-5}
	16QAM	5.1×10^{-2}	4.8×10^{-2}	1.4×10^{-2}	5.1×10^{-3}

6 Conclusion

We have demonstrated a time-domain MIMO soft turbo receiver structure for single-carrier underwater acoustic communications.The proposed detection scheme has been tested by undersea trial data collected in the undersea experiment named MACE10 conducted at Buzzards Bay, MA in June 2010. Processing results show that it works effectively with 2×12 QPSK, 8PSK and 16QAM modulation schemes.

7 References

[1] M. Stojanovic, J. Catipovic, and J. Proakis, Phase coherent digital communications for underwater acoustic channels, *IEEE J. Ocean. Eng.,* vol. 19, no. 1, pp. 100-111, Jan. 1994.

[2] T. C. Yang, "Correlation-based decision-feedback equalizer for underwater acoustic communications," *IEEE J. Ocean Eng.,* vol. 30, pp. 865-880, Oct. 2005.

[3] L. Wang, J. Tao, C. Xiao and T. C. Yang, "Low-Complexity Turbo detection for Single-Carrier MIMO Underwater Acoustic Communications," *Wirel. Commun. Mob. Comput.,* accepted for publication, April. 2011.

[4] M. Tuchler, A. C. Singer, and R. Koetter, "Minimum mean squared error equalization using a priori information," *IEEE Trans. Signal Process.,* vol. 50, pp. 673-683, Mar. 2002.

[5] R. Otnes and T. H. Eggen, "Underwater acoustic communications: Long-term test of turbo equalization in shallow water," *IEEE J. Ocean. Eng.,* vol. 33, no. 3, pp. 321-334, Jul. 2008.

[6] E. Sozer, J. Proakis, and F. Blackmon, "Iterative equalization and decoding techniques for shallow wateracoustic channels," in *Proc. MTS/IEEE Int. Oceans Conf.,* vol. 4, Nov. 2001, pp. 2201-2208.

[7] J. Tao, Y. R. Zheng, C. Xiao, T. C. Yang, "Robust MIMO underwater acoustic communications using turbo block decision-feedback equalization," *IEEE J. Ocean. Eng.*, vol. 35, no. 4, pp. 948-960, Oct. 2010.

[8] J. Huang, S. Zhou, and P. Willett, "Nonbinary LDPC coding for multicarrier underwater acoustic communication," *IEEE JSAC Special Issue on Underwater Wireless Communications and Networks, vol.* 26, no. 9, pp. 1684-1696, Dec. 2008.

[9] F. Blackmon, E. Sozer and J. Proakis, "Iterative equalization, decoding, and soft diversity combining for underwater acoustic channels," in *Proc. MTS/IEEE Int. Oceans Conf.,* vol. 4, Oct. 2002, pp. 2425-2428.

[10] H. Lou and C. Xiao, "Soft Feedback ISI Canceller-based Turbo Equalization for Multilevel Modulations, " *IEEE Trans. Commun.*, submitted for considering publication.

[11] A. Rafati, H. Lou and C. Xiao, "Low Complexity Soft-Decision Feedback Turbo Equalization for MIMO Systems with Multilevel Modulations, " *IEEE Trans. Vehicular Technology*, vol.60, No.7, Sept. 2011.

[12] R. R. Lopes and J. R. Barry, "The soft-feedback equalizer for turbo equalization of highly dispersive channels," *IEEE Trans. Commun*, vol.54, no.5, pp.783-788, May. 2006.

[13] A. Dejonghe and L. Vanderdorpe, "Turbo equalization for multilevel modulation: An efficient low-complexity scheme," in *Proc. IEEE Int. Conf. Commun*, vol.3, pp.1863-1867, Aug. 2002.

[14] P. Vila, I. Fijalkow, C. Laot, D. Leroux, D. Pirez, S. Ronger, and C. Langlais, "Reduced-complexity M-ary decoders for turbo-equalization," in *2nd Int. Symp. Turbo Codes and Related Topics*, Brest, France, Sept. 2000.

V. ON THE SOFT-DECISION FEEDBACK TURBO EQUALIZATION FOR UNDERWATER ACOUSTIC COMMUNICATIONS

Amirhossein Rafati, Huang Lou and Chengshan Xiao, *Fellow IEEE*

Abstract—In this paper, A low-complexity turbo detection scheme is proposed for single-carrier multiple-input multiple-output (MIMO) underwater acoustic (UWA) communications that employ low-density parity-check (LDPC) channel coding. The proposed iterative soft-decision feedback equalization (SDFE) algorithm offers a novel approach to combat error propagation by utilizing the past soft decisions to mitigate inter-symbol interference. In addition, its computational complexity grows only linearly with the number of equalizer coefficients, compared to the quadratic complexity of minimum mean square error-based linear turbo equalizer with time-varying coefficients. Performance of the proposed detection scheme is verified using the experimental results for the undersea real-world data collected in ACOMM09 experiments. The results show that the proposed SDFE algorithm provides robust detection for MIMO UWA communications with different modulations and different symbol rates, at different transmission ranges.

1 Introduction

Unlike the development of wireless networks over radio channels, advancement of underwater communication systems has occurred at a much slower pace [1], [2]. However, in the past five to ten years, there has been a tremendous increase in research and development of underwater acoustic (UWA) communication systems due to the rapidly growing needs for wireless underwater communications.

While the largest difficulty encountered in the shallow horizontal UWA communications is mainly considered to be the time-varying multipath propagation phenomena, several other unique characteristics such as the long length of the equivalent discrete-time channel and the Doppler effect of the underwater channel pose considerable challenges for data processing in underwater communication systems. For example, in a typical medium range horizontal UWA channel, the available bandwidth is only tens of kilo Hertz (kHz), the intervocalic interference could span several tens or hundreds of symbol periods, and the normalized carrier frequency offset (CFO) induced by Doppler spread could be on the order of 10^{-4} to 10^{-3}, compared with 10^{-8} to 10^{-6} for radio frequency (RF) channels.

Transmission rates in UWA communications are very limited due to the harsh channel conditions. Nevertheless, with the introduction of multiple-input, multiple-output (MIMO) systems, a fundamental increase in the achievable data rate can be obtained. On the other hand, the signal detection for MIMO systems becomes more challenging due to the spatial interference among concurrent transmission streams. Accordingly, the need for the development of new robust algorithms for UWA communications is crucial.

Many approaches have been proposed for UWA communications in the past three decades. With the advent of turbo equalization [3]- [5] , there has been a wide interest in the application of turbo detection schemes for UWA communications. Compared with conventional one-time equalization, turbo equalization has a much more powerful detection capability, attributed to the iterative extrinsic soft information exchanges between a soft-decision equalizer and a soft-decision decoder.

Turbo equalization for UWA communications has been first proposed in [6], where a joint maximum *a posteriori* probability (MAP) equalizer and channel decoder has been adopted for signal detection. The scheme has been tested by experimental data, with the modulations of binary phase-shift keying (BPSK) and quadrature

phase-shift keying (QPSK) at a rate of 2.5 kilo-symbols per second (ksps). The MAP equalization has a high complexity, even by employing complexity-reduced technologies like per-survivor processing (PSP). Consequently, a low-complexity turbo equalization using decision-feedback equalizer (DFE) has been proposed and tested by a short-range multichannel UWA transmission with a channel bandwidth of 5 kHz [7]. Turbo DFE has also been studied in [8] recently, for short-range, high data rate UWA communications. This design circumvents the channel estimation and adjusts the equalizer taps adaptively using the least mean square (LMS) algorithm.

In [9]- [12], the soft-decision feedback equalizer together with the turbo decoder, has been applied to UWA communication. In [10], turbo equalizer was proposed for long-term UWA communication testing. In [12], turbo detection using block decision-feedback equalization (BDFE) has also been proposed for single-carrier UWA communications. The BDFE leads to a better detection performance compared with the conventional DFE. Iterative decoding and turbo detection for orthogonal frequency-division multiplexing (OFDM) UWA systems has also been proposed in [13] and [14].

Recently, a new low-complexity soft-decision feedback turbo equalization (SDFE) algorithm for multilevel modulations was developed in [15] for single-input, single-output (SISO) systems and later, extended to MIMO systems in [16]. The proposed SDFE algorithm offers a novel approach to combat error propagation .

In this paper, we apply the turbo SDFE algorithm to a MIMO UWA communication system with low-density parity-check (LDPC) channel coding. The proposed detection scheme is tested by extensive undersea trial data collected in medium-range undersea experiment named ACOMM09. The ACOMM09 experiment was launched at the coastline of New Jersey in May 2009, with a transmission rate of 5 kilo symbols per second (ksps) per transducer at a transmission distance of 2-3 km.

Experimental results show that error-free detection can be achieved by our detection algorithm for two-transducer MIMO transmissions with QPSK modulation.

The rest of this paper is organized as follows. In Section II, the system model for a single-carrier MIMO UWA communication is described. The proposed low-complexity turbo detection scheme is presented in Section III, and the experimental results are presented in Section IV. Finally, conclusions are drawn in Section V.

Throughout this paper, upper case boldface letters are used to indicate matrices, lower case boldface letters are used to show vectors, kth row and kth diagonal element of matrix $\mathbf{A}$ are denoted by $\langle \mathbf{A} \rangle_k$ and $[\mathbf{A}]_k$, respectively and $E\{\cdot\}$ denotes the expectation operator.

2 Signalling and Data Structure

We consider a MIMO underwater communication system with t transducer and r hydrophones that employs a digital modulation with constellation size q in Figure 1. Here, the binary information sequence $[b_1\ b_2 \cdots b_{q\times t}]^T$ is first transmitted into t parallel sub-streams using a serial to parallel converter where each stream is encoded by a low density parity check (LDPC) encoder and followed by an interleaver Π and a constellation mapper and then transmitted through one of the t transducers. Throughout this paper, we use QPSK, 8PSK and 16-quadrature amplitude modulation (16QAM) schemes with constellation sizes being 4, 8 and 16, respectively. Let us denote the block of information to be transmitted by the kth transmitter with the binary sequence $\mathbf{b}^k = \left[b_{(k-1)q+1}\ \cdots b_{kq}\right]^T$. After interleaving, the output of the kth interleaver can be stated as $\mathbf{c}^k = \left[\mathbf{c}_1^k\ \ \mathbf{c}_2^k \cdots \mathbf{c}_{K_c}^k\right]$ where $\mathbf{c}_n^k$ represents $\left[c_{n,1}^k\ \ c_{n,1}^k \cdots c_{n,q}^k\right]$ with bits $c_{n,j}^k \in \{0,1\}$.

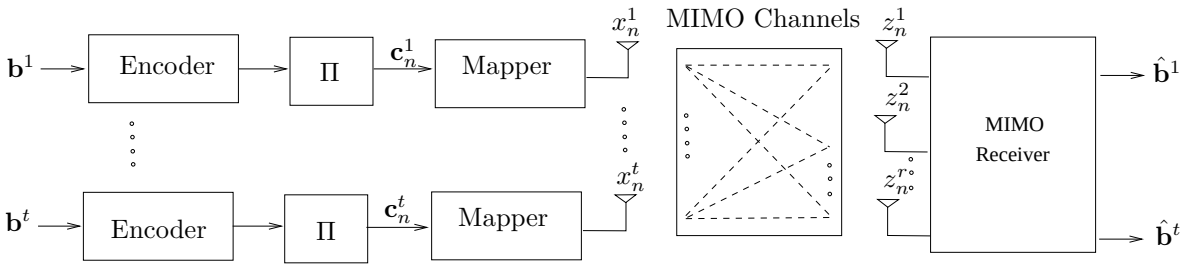

Figure 1. Block diagram of the SDFE transmitter and receiver.

The data structure is appended with some auxiliary signals and then, the transmission burst is transmitted in the format shown in Figure 2. As it can be seen, the burst begins with a head linear frequency modulation (LFM) chirp signal called (LFMB), followed by an m-sequence of length 511, and a data payload of N data blocks, each of which contain N_b data symbols and ends with a tail LFM signal called LFME. Our Experimental values for N and N_b are shown in Table 1. The chirp LFM signals on the receiver side serve multiple purposes such as coarse synchronization, Doppler shift estimation and channel length measurement due to their unique correlation properties. On the other hand, the m sequence can be used for evaluating the channel scattering function and estimating the Doppler spread [17].

Table 1. Data blocks structure.

Number of Blocks (N)	Number of Symbols per Block (N_b)
50	1024
25	2048
2	25600

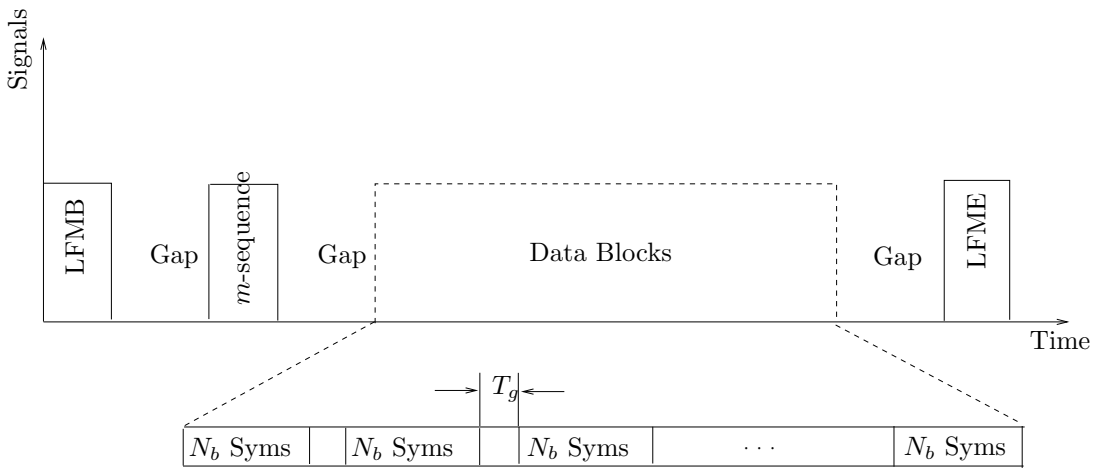

Figure 2. ACOMM09 data structure.

3 Proposed SDFE Detection Scheme

In UWA communications, front-end preprocessing stages such as synchronization, Doppler shift estimation and compensation , demodulation and waveform resampling are usually required before signal detection can be performed [18]. After preprocessing, the discrete time baseband signal at the mth hydrophone at time instant n is expressed by

$$z_n^{(m)} = \sum_{k=1}^{t} \sum_{l=0}^{L-1} h_{n,l}^{(m,k)} x_{n-l}^{k} + w_n^{(m)} \tag{1}$$

where x_{n-l}^{k} is the transmitted symbol at kth transducer at time instant $n-l$ and $h_{n,l}^{(m,k)}$ is the lth channel coefficient between the kth transducer and mth hydrophone at time instant n. Finally, $w_n^{(m)}$ represents the zero mean additive white Gaussian noise (AWGN) sample on the mth hydrophone. The noise samples $w_n^{(m)}$ are independent and identically distributed (i.i.d.) with the variance of $\sigma_w^2/2$ for both real

and imaginary parts. When the time duration of the pilot sequence or previously detected symbol is less than the channel coherence time, the channel coefficients $h_{n,l}^{(m,k)}$ in (1) can be approximated as time invariant, i.e $h_{n,l}^{(m,k)} \approx h_l^{(m,k)}$. Stacking up all the received symbols on r hydrophones as $\mathbf{z}_n = [z_n^{(1)}, z_n^{(2)}, \ldots, z_n^{(r)}]^T$, we can write

$$\mathbf{z}_n = \sum_{l=0}^{L-1} \mathbf{h}_l \mathbf{x}_{n-l} + \mathbf{w}_n \tag{2}$$

where

$$\mathbf{x}_n = [x_n^1, x_n^2, \ldots, x_n^t]^T \tag{3}$$

$$\mathbf{w}_n = [w_n^1, w_n^2, \ldots, w_n^r]^T \tag{4}$$

and

$$\mathbf{h}_l = \begin{bmatrix} h_l^{(1,1)} & h_l^{(1,2)} & \cdots & h_l^{(1,t)} \\ h_l^{(2,1)} & h_l^{(2,2)} & \cdots & h_l^{(2,t)} \\ \vdots & \vdots & \ddots & \vdots \\ h_l^{(r,1)} & h_l^{(r,2)} & \cdots & h_l^{(r,t)} \end{bmatrix}. \tag{5}$$

Finally, temporal sampling for N_1 future and N_2 previous received symbols at time instant n to capture the multi-path signals of all the hydrophones for diversity combining yields the following space-time representation of the received signal,

$$\mathbf{Z}_n = \mathbf{H}\mathbf{X}_n + \mathbf{W}_n \tag{6}$$

where $\mathbf{Z}_n$, $\mathbf{H}$, $\mathbf{X}_n$ and $\mathbf{W}_n$ are defined in (7). The parameters N_1 and N_2 should be chosen as to include all the received symbols that are correlated with the transmitted symbol at time n. In general, N_1 and N_2 should be chosen according to the channel characteristics and specifically, location of the major channel tap with respect to other

$$\underbrace{\begin{bmatrix} \mathbf{z}_{n-N_2} \\ \vdots \\ \mathbf{z}_n \\ \vdots \\ \mathbf{z}_{n+N_1} \end{bmatrix}}_{\mathbf{Z}_n} = \underbrace{\begin{bmatrix} \mathbf{h}_{L-1} & \cdots & \mathbf{h}_0 & \cdots & \cdots & 0 \\ \vdots & \ddots & \ddots & \ddots & & \vdots \\ & & \ddots & \ddots & \ddots & \vdots \\ 0 & \cdots & & \mathbf{h}_{L-1} & \cdots & \mathbf{h}_0 \end{bmatrix}}_{\mathbf{H}} \underbrace{\begin{bmatrix} \mathbf{x}_{n-N_2-L+1} \\ \vdots \\ \mathbf{x}_n \\ \vdots \\ \mathbf{x}_{n+N_1} \end{bmatrix}}_{\mathbf{X}_n} + \underbrace{\begin{bmatrix} \mathbf{w}_{n-N_2} \\ \vdots \\ \mathbf{w}_n \\ \vdots \\ \mathbf{w}_{n+N_1} \end{bmatrix}}_{\mathbf{W}_n} \tag{7}$$

taps. In the sequel, several stages of the proposed MIMO UWA detection system such as channel estimation and MIMO SDFE turbo detection are explained in detail.

3.1 MIMO UWA Channel Estimation

Channel estimation and tracking play a key role in the detection performance. In this paper, we adopt both pilot-aided channel estimation and the decision directed (DD) channel tracking.

The difference between the two methods lies in the reference symbols. In particular, the former approach utilizes the pilot symbols whereas the latter one employs the previously detected symbols for channel estimation. Therefore, we do not differentiate between the channel estimation and the channel tracking in the rest of the paper.

Assuming that the time duration of the pilot sequence is less than the channel coherence time, the approximated system model for channel estimation can be formulated as

$$\begin{aligned} \mathbf{z}^{(m)} &= \sum_{k=1}^{t} \mathbf{P}_k \mathbf{h}^{(m,k)} + \mathbf{w}^{(m)} \\ &= \mathbf{P}\mathbf{h}^{(m)} + \mathbf{w}^{(m)} \end{aligned} \tag{8}$$

where

$$\begin{aligned}
\mathbf{z}^{(m)} &\triangleq \left[z_{L-1}^{(m)}, z_{L}^{(m)}, \cdots z_{N_p-1}^{(m)}\right]^T \in \mathcal{C}^{(N_p-L+1\times 1)} \\
\mathbf{h}^{(m,k)} &\triangleq \left[h_{0}^{(m,k)}, h_{1}^{(m,k)}, \cdots h_{L-1}^{(m,k)}\right]^T \in \mathcal{C}^{L\times 1} \\
\mathbf{w}^{(m)} &\triangleq \left[w_{L-1}^{(m)}, w_{L}^{(m)}, \cdots w_{N_p-1}^{(m)}\right]^T \in \mathcal{C}^{(N_p-L+1\times 1)}.
\end{aligned} \tag{9}$$

In addition, $\mathbf{P} = [\mathbf{P}_1, \mathbf{P}_2, \cdots, \mathbf{P}_t]$ where the matrix $\mathbf{P}_k \in \mathcal{C}^{(N_p-L+1\times L)}$ is the kth pilot matrix obtained with the pilot sequence $\{p_n^k, 0 \leq n \leq\ N_p - 1\}$ transmitted by the kth transducer and defined by

$$\mathbf{P}_k = \begin{bmatrix} p_{L-1}^k & p_{L-2}^k & \cdots & p_0^k \\ p_L^k & p_{L-1}^k & \cdots & p_1^k \\ \vdots & \vdots & \ddots & \vdots \\ p_{N_p-1}^k & p_{N_p-2}^k & \cdots & p_{N_p-L}^k \end{bmatrix}. \tag{10}$$

Based on (8), the linear minimum mean square error (LMMSE) estimation of $\mathbf{h}^{(m)}$ is obtained as

$$\mathbf{h}^{(m)} = \left(\mathbf{P}^H\mathbf{P} + \sigma_w^2\mathbf{I}_{tL}\right)^{-1}\mathbf{P}^H\mathbf{z}^{(m)} \tag{11}$$

The estimation in (11) is performed on each of the hydrophones to obtain the MIMO UWA channel estimation. It should be noted that to guarantee the system equation in (8) is not undetermined, the pilot block size should be chosen as $N_p > (t+1)L-1$ [12].

To ensure reliable detection under harsh UWA channel conditions, a received data symbols should be partitioned into several small blocks, as shown in Figure 3. Here, N_p represents the number of pilot symbols which are inserted after every N_f symbols. In this way, pilot aided channel estimation can be obtained periodically during the detection. The pilot symbol block size N_p should be selected in a way to

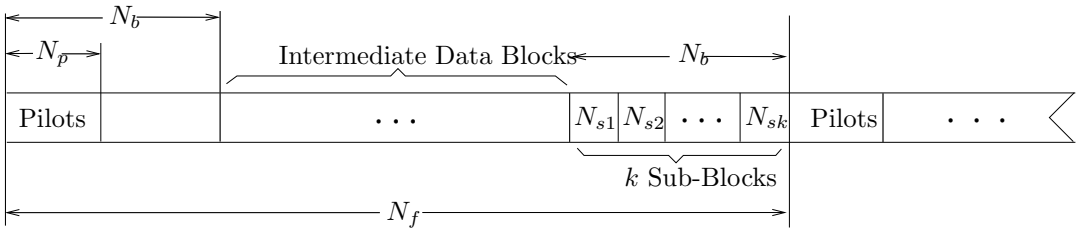

Figure 3. Partition structure of the transmitted data payload.

guarantee a reliable channel estimation while ensuring that the corresponding time duration does not exceed the channel coherence time. In addition, the parameter N_f should be selected in a way to achieve a good tradeoff between the detection performance and the pilot overhead is defined as $\eta = (N_p/N_f) \times 100\%$. It should also be noted that the channel estimation for the intermediate blocks is obtained by decision directed (DD) channel tracking whereby the channel estimated in the previous sub-block is used as the initial state for the channel in the subsequent sub-block. Later on, the channel estimation for the current sub-block will be iteratively improved by a joint channel and data estimation algorithm, as explained in the next section.

3.2 The Proposed SDFE Algorithm

In this section, we propose a new soft decision feedback equalizer (SDFE) algorithm which exploits the *a priori* information on the transmitted symbols, in the form of *a priori* LLR $L_{\text{app}}(c_{n,j}^k)$ and outputs the soft information in the form of the estimate of the *a posteriori* LLR $L_{n,j}^k$. The SDFE will be derived in a general context, in which we assume the availability of channel estimates and *a priori* probabilities.

Figure 4 depicts the structure of the proposed soft decision feedback equalizer. The SDFE consists of a feedforward filter represented by $\mathbf{F}_n \in \mathcal{C}^{r(N_1+N_2+1)\times t}$ and a feedback filter represented by $\mathbf{B}_n \in \mathcal{C}^{r(N3)\times t}$ where $N_3 = N_2 + L - 1$. The feedforward

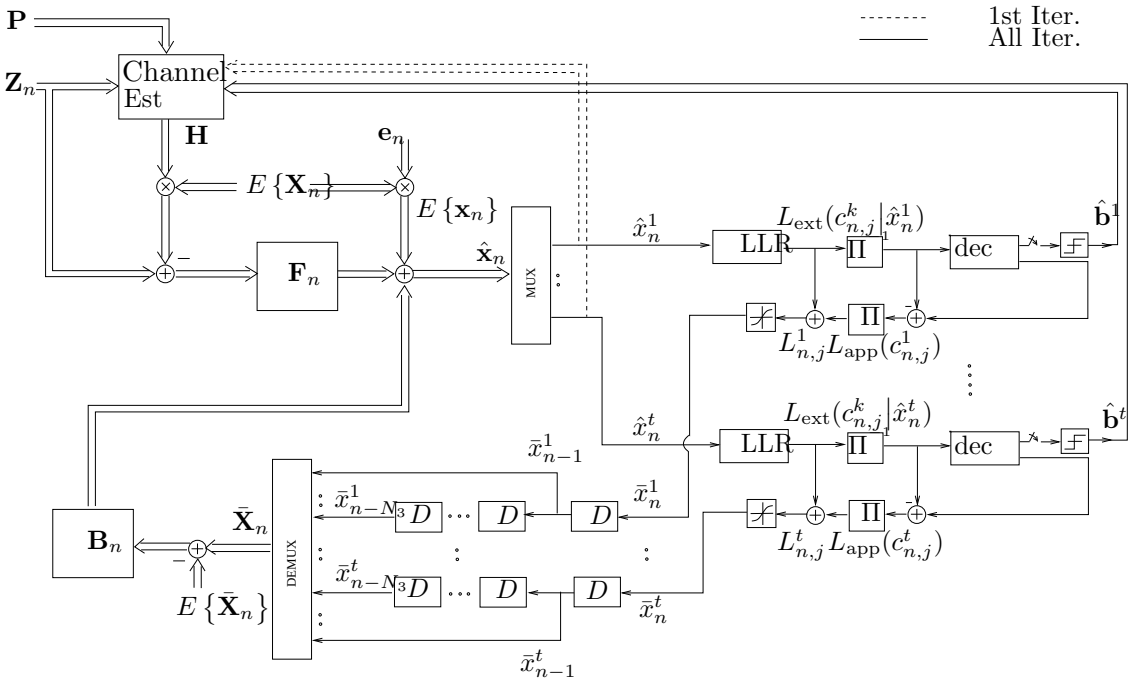

Figure 4. Block diagram of the proposed SDFE receiver.

filter utilizes the future symbols within the current block at time instant n to mitigate the ISI. On the other hand, the ISI due to the past symbols is removed by the feedback filter. At all times, we use the *a priori* information to estimate and cancel the residual ISI. Interference cancelation proceeds as follows. Assume that, at time n, the equalizer seeks to estimate x_n^k. The *a priori* information is used to produce soft estimates $\{\bar{x}_{m\neq n}^k\}$ of the interfering signals $\{x_{m\neq n}^k\}$, according to

$$\bar{x}_m^k = E\left[x_m^k \middle| \left\{L_{\text{app}}(c_{m,j}^k)\right\}_{j=1}^q\right]. \tag{12}$$

If these estimates are correct, their effect on the output of $\mathbf{F}_n$ can be estimated and canceled through linear filtering and subtraction. Specifically, as shown in Figure 4, an interference canceler for each receiver branch feeds the soft decisions through a linear filter $\mathbf{B}_n$, whose response is related to the residual ISI at the output

of $\mathbf{F}_n$. Since the equalizer output will be used to estimate x_n^k, the influence of x_n^k on the equalizer input should not be canceled.

As it can be seen from the figure, the proposed MIMO SDFE receiver iteratively exchanges soft log-likelihood ratio (LLR) information with the LDPC decoders, each corresponding to one transmission stream, through the interleavers (Π)and the deinterleavers $(\Pi)^{-1}$. In the current iteration, the MIMO SDFE performs equalization on the received block and outputs the bit LLRs of the whole packet. The packet LLRs are further demultiplexed onto t branches. On each branch, the extrinsic LLR is obtained by subtracting the *a priori* LLR of the same branch out of output LLR from LDPC decoder in the previous iteration. The extrinsic LLR is then deinterleaved and delivered to the LDPC decoder as its *a priori* input. After the decoding, the LDPC decoder outputs the updated LLR which is further transformed into the extrinsic form, similar to the LLR feedforward process. The extrinsic LLR streams are finally multiplexed and sent to the equalizer to start the next iteration. Detection performance improves over the multiple iterations and the final hard decisions are made once the turbo equalization converges. As the computation of the soft estimated symbols is independent of the equalizer structure, we first derive the equations for the soft estimated symbols, after which we find the optimal values for the feedforward and feedback filters based on the MMSE criterion.

As explained in the previous section, at each block, the channel estimation is performed either by using the N_p pilot symbols within the same block or by employing the decision directed algorithm, whereby by assuming the channel to be time invariant within the current block, the channel estimated in the previous block is used for equalization in the current block, after which, the quality of channel estimation is improved by iterative turbo equalization. In particular, assuming that the receiver is in decision directed (DD) mode, in the first iteration, the symbols from the current sub-block are equalized using the channel from the previous sub-block, assuming that

the channel variations are small within the duration of the current sub-block . As all the sub-blocks need to be processed before the LDPC decoder can decode the transmitted data block, it is not possible to use the output of the decoder to re-estimate the channel at this moment. Consequently, assuming that the bit error rate within the current sub-block is small, for the first iteration, the output of the equalizer is used as an alternative pilot sequence to estimate the channel for the subsequent sub-block. Because the bit error rate of the equalizer is relatively higher than that of the decoder, in the first iteration, channel estimation performance is inferior to the pilot based channel estimation scheme. Yet, with the second iteration onwards, the symbols from the output of the decoder can be used to re-estimate the channel, hence, improving the quality of channel estimation. More details about the iterative channel estimation will be elaborated in Section 4.

The main idea in the proposed SDFE algorithm is to utilize both causal and anti-causal filters instead of a general decision feedback filter to mitigate the ISI. Let us write the output of the SDFE equalizer as

$$\hat{x}_n = (\mathbf{F}_n^k)^H \mathbf{Z}_n + (\mathbf{B}_n^k)^H \overline{\mathbf{X}}_n + d_n^k \tag{13}$$

where $\mathbf{Z}_n$ is defined in (7) and,

$$\overline{\mathbf{X}}_n = \left[\bar{x}^1_{n-(N_2+L)+1}, \bar{x}^2_{n-(N_2+L)+1}, \cdots, \bar{x}^{t-1}_{n-1}, \bar{x}^t_{n-1}\right]^T. \tag{14}$$

Here $\bar{x}_m^k$ is the soft value of x_m^k obtained in previous time instants $m < n$. In addition, $\mathbf{F}_n^k$ and $\mathbf{B}_n^k$ represent the kth columns of matrices $\mathbf{F}_n$ and $\mathbf{B}_n$, respectively, and d_n^k is the kth element of the time varying offset vector $\mathbf{d}_n$. In the sequel, to simplify the notation, we drop the time index from all the equalizer parameters. Moreover, instead of trying to cancel all the interference, we pass $\hat{x}_n^k$ through the linear filter $\mathbf{B}^k$ whose coefficients, along with the equalizer filter coefficients $\mathbf{F}^k$ are computed to

minimize the MSE $E\{\|\hat{x}_n^k - x_n^k\|^2\}$. Hence, proper values for $\mathbf{F}^k$, $\mathbf{B}^k$ and d_n^k should be obtained from the following optimization problem

$$\text{MMSE} = \min_{\mathbf{F}^k, \mathbf{B}^k, d_n^k} E\left\{\left\|(\mathbf{F}^k)^H \mathbf{Z}_n - (\mathbf{B}^k)^H \overline{\mathbf{X}}_n - d_n^k - x_n\right\|^2\right\}. \tag{15}$$

In order to solve this problem, we assume that $E\{\bar{x}_n^i x_m^{j*}\} = 0$, given that if $i = j$, $n \neq m$ and vice versa. These assumptions are justified since $\bar{x}_n^i$ is approximately equal to x_n^i and the transmitted symbols from the same (different) transducers are uncorrelated at different times. Moreover, we adopt the following notations for the remaining nonzero expected values:

$$\bar{p}^k \triangleq E\left\{\left|\bar{x}_n^k\right|^2\right\}, \qquad \psi^k \triangleq E\left\{x_n^k \bar{x}_n^{k*}\right\} \tag{16}$$

where the expectations are taken with respect to time. Using the above assumptions, it can be shown that the optimal values for $\mathbf{F}^k$ and $\mathbf{B}^k$ and d_n^k that minimize the cost function $E\{\|\hat{x}_n^k - x_n^k\|^2\}$ are computed as,

$$\mathbf{F}^k = \left(\mathbf{H}\mathbf{H}^H + \sigma^2 \mathbf{I} - \mathbf{H}_b \Lambda \mathbf{H}_b^{-1}\right)^{-1} \mathbf{s}_k \tag{17}$$

$$\mathbf{B}_k = (\overline{\mathbf{P}})^{-1} \Psi^H \mathbf{H}_b^H \mathbf{F}_k \tag{18}$$

$$d_n^k = E\{x_n^k\} - (\mathbf{F}^k)^H \mathbf{H} E\{\mathbf{X}_n\} - (\mathbf{B}^k)^H E\left\{\overline{\mathbf{X}}_n\right\} \tag{19}$$

where

$$\Lambda = \Psi(\overline{\mathbf{P}})^{-1} \Psi^H \tag{20}$$

$$\Psi = \underbrace{\Psi_d \oplus \Psi_d \oplus \cdots \Psi_d}_{N_2 + L - 1 \text{ times}}, \quad \overline{\mathbf{P}} = \underbrace{\overline{\mathbf{P}}_d \oplus \overline{\mathbf{P}}_d \oplus \cdots \overline{\mathbf{P}}_d}_{N_2 + L - 1 \text{ times}} \tag{21}$$

s_k is the $((N_2+L-1)\,t+k)$th column of $\mathbf{H}$, and $\mathbf{H}_b$ is the leftmost $(N_2+L-1)t$ columns of $\mathbf{H}$. In addition, the $\oplus$ denotes the direct sum of matrices and

$$\Psi_d = \text{diag}\left(\psi^1, \psi^2, \ldots, \psi^t\right), \overline{\mathbf{P}}_d = \text{diag}\left(\bar{p}^1, \bar{p}^2, \ldots, \bar{p}^t\right) \tag{22}$$

where $\text{diag}(a_1, \cdots, a_k)$ denotes a diagonal matrix with diagonal entries $a_1, \ldots, a_k$. It should be noted that as the matrices Ψ and $\bar{\mathbf{P}}$ are all diagonal, Λ can be computed without any intensive computational complexity. Finally, using (13), and the equations (17- 19), it is easy to see that the MMSE estimate $\hat{x}_n^k$ of the symbol x_n^k is found as,

$$\hat{x}_n = (\mathbf{F}^k)^H(\mathbf{Z}_n - \mathbf{H}E\{\mathbf{X}_n\}) + (\mathbf{B}^k)^H\left(\overline{\mathbf{X}}_n - E\left\{\overline{\mathbf{X}}_n\right\}\right). \tag{23}$$

Exploiting the symmetries, it is straightforward from (16) that ψ^k and $\bar{p}^k$ may be computed by conditioning on $x_n^k = \alpha_i$ where $\alpha_i \in \mathcal{S}$. In other words,

$$\bar{p}^k = E\left\{\left|\bar{x}_n^k\right|^2 \left| x_n^k = \alpha_i\right.\right\},\ \psi^k = \alpha_i E\left\{\bar{x}_n^{k*} \middle| x_n^k = \alpha_i\right\}. \tag{24}$$

For MPSK, α_i can be any elements in $\mathcal{S}$, while for QAM, ψ^k should be re-scaled when $|\alpha_i| \neq 1$. Unfortunately, there are no closed-form solutions for the above expected values. Nevertheless, these functions can be tabulated or computed by simple numerical algorithms. It should also be noted that for numerical computation of the expected values requires a prior knowledge about the probability of $\hat{x}_n^k$. In the sequel, we elaborate a statistical method to generate samples of $\hat{x}_n^k$, which will be later used to estimate the expected values.

The equalizer output for the kth branch of the receiver at the time n, $\hat{x}_n^k$ is not a function of $\left\{L_{\text{app}}(c_{n,j}^k)\right\}_{j=1}^q$. Thus, $\hat{x}_n^k$ can only be used to produce extrinsic information.

Regardless of the structure of the equalizer, $\hat{x}_n^k$ can be modeled as an output of an equivalent AWGN channel with input symbol $x_n^k \in S$ as

$$\hat{x}_n^k = A_k x_n^k + v_n^k \tag{25}$$

where $A_k = E\left[\hat{x}_n^k x_n^k\right]$ and v_n^k includes the effect of channel noise and residual ISI. Note that, from this definition, v_n^k is independent of x_n^k. The computation of the extrinsic LLR $L_{\text{ext}}\left(c_{n,j}^k \middle| \hat{x}_n^k\right)$ requires a prior knowledge about the distribution of v_n^k. If v_n^k is approximated by a Gaussian random variable with zero mean and variance σ_k^2, it follows that

$$\hat{x}_n^k \sim \mathcal{N}(x_n^k A_k, \sigma_k^2) \quad \text{where} \quad \sigma_k^2 = A_k(1 - A_k). \tag{26}$$

Using (26), it is straight forward to see that

$$L_{\text{ext}}\left(c_{n,j}^k \middle| \hat{x}_n^k\right) = \frac{2A_k x_n^k}{\sigma_k^2}. \tag{27}$$

The full LLR at the equalizer output is then given by

$$L_{n,j}^k = L_{\text{ext}}\left(c_{n,j}^k \middle| \hat{x}_n^k\right) + L_{\text{app}}\left(c_{n,j}^k\right). \tag{28}$$

Let us now define the symbol extrinsic probability as

$$P(\hat{x}_n^k | x_n^k = \alpha_i) = \frac{1}{\sigma^2 \pi} \exp(-\rho_{n,i}^k) \tag{29}$$

$$\rho_{n,i}^k = \frac{\left|\hat{x}_n^k - A_k \alpha_i\right|^2}{\sigma_k^2} \tag{30}$$

where α_i is defined in Table 2. The extrinsic LLR $L_{\text{ext}}\left(c_{n,j}^k \middle| \hat{x}_n^k\right)$ of coded bit $c_{n,j}^k$ is the function of $P(\hat{x}_n^k | x_n^k = \alpha_i)$:

$$L_{\text{ext}}\left(c_{n,j}^k \middle| \hat{x}_n^k\right) = \log \frac{\sum_{\alpha_i : c_{n,j}^k = 0} P(\hat{x}_n^k | \alpha_i) \prod_{\forall j', j' \neq j} P(c_{n,j'}^k)}{\sum_{\alpha_i : c_{n,j}^k = 1} P(\hat{x}_n^k | \alpha_i) \prod_{\forall j', j' \neq j} P(c_{n,j'})}$$

$$= \log \frac{\sum_{\alpha_i : c_{n,j}^k = 0} \exp(-\rho_{n,i}^k + \sum_{\forall j', j' \neq j} \tilde{s}_{i,j} L_{n,j'}^k / 2)}{\sum_{\alpha_i : c_{n,j}^k = 1} \exp(-\rho_{n,i}^k + \sum_{\forall j', j' \neq j} \tilde{s}_{i,j} L_{n,j'}^k / 2)} \tag{31}$$

where

$$\tilde{s}_{i,j} = \begin{cases} +1 & \text{if } s_{i,j} = 0 \\ -1 & \text{if } s_{i,j} = 1. \end{cases}$$

For QPSK or QAM modulation, the computational complexity in (31) can be reduced by using minimum-based LLR simplification defined by

$$\log(\exp(-x) + \exp(-y)) \approx -min(x, y) \tag{32}$$

when $|x - y|$ is sufficiently large.

For MPSK ($M > 2$) modulation, the minimum-based LLR simplifications can not be made because several symbols are quite close to each other on the unit circle. Instead, a geometric approach [26] can be applied to estimate LLR $\lambda_{n,j}$. The approximation is listed in Table 3.

Using (29), (30) and (31), it can be seen that $L_{\text{ext}}\left(c_{n,j}^k \middle| \hat{x}_n^k\right)$ can be computed as a function of $\hat{x}_n^k$ which implies that the pdf of $L_{\text{ext}}\left(c_{n,j}^k \middle| \hat{x}_n^k\right)$ is related to the pdf of $\hat{x}_n^k$. Hence, using (26), and the equations from Table 3, it is easy to generate different samples of $L_{\text{ext}}\left(c_{n,j}^k \middle| \hat{x}_n^k\right)$. Moreover, since

$$L_{\text{app}}\left(c_{n,j}^k\right) = \log \frac{P(c_{n,j}^k = 0)}{P(c_{n,j}^k = 1)} \tag{33}$$

Table 2. Symbol alphabets.

QPSK:

i	1	2	3	4
$s_{i,1}\ s_{i,2}$	00	01	10	11
α_i	$(+1+i)/\sqrt{2}$	$(+1-i)/\sqrt{2}$	$(-1+i)/\sqrt{2}$	$(-1-i)/\sqrt{2}$

8PSK:

i	1	2	3	4	5	6	7	8
$s_{i,1}\ s_{i,2}\ s_{i,3}$	000	001	010	011	100	101	110	111
α_i	$e^{(\frac{i9\pi}{8})}$	$e^{(\frac{i11\pi}{8})}$	$e^{(\frac{i15\pi}{8})}$	$e^{(\frac{i13\pi}{8})}$	$e^{(\frac{i7\pi}{8})}$	$e^{(\frac{i5\pi}{8})}$	$e^{(\frac{i\pi}{8})}$	$e^{(\frac{i3\pi}{8})}$

16QAM:

i	1	2	3	4	5	6	7	8
$s_{i,1}\ s_{i,2}\ s_{i,3}\ s_{i,4}$	0000	0001	0010	0011	0100	0101	0110	0111
α_i	$\frac{(-1-i)}{\sqrt{10}}$	$\frac{(-1-3i)}{\sqrt{10}}$	$\frac{(-1+i)}{\sqrt{10}}$	$\frac{(-1+3i)}{\sqrt{10}}$	$\frac{(-3-i)}{\sqrt{10}}$	$\frac{(-3-3i)}{\sqrt{10}}$	$\frac{(-3+i)}{\sqrt{10}}$	$\frac{(-3+3i)}{\sqrt{10}}$
i	9	10	11	12	13	14	15	16
$s_{i,1}\ s_{i,2}\ s_{i,3}\ s_{i,4}$	1000	1001	1010	1011	1100	1101	1110	1111
α_i	$\frac{(1-i)}{\sqrt{10}}$	$\frac{(1-3i)}{\sqrt{10}}$	$\frac{(1+i)}{\sqrt{10}}$	$\frac{(1+3i)}{\sqrt{10}}$	$\frac{(3-i)}{\sqrt{10}}$	$\frac{(3-3i)}{\sqrt{10}}$	$\frac{(3+i)}{\sqrt{10}}$	$\frac{(3+3i)}{\sqrt{10}}$

Table 3. LLR simplifications for different constellations.

QPSK:
- $\lambda_{n,1}^k \approx 2\sqrt{2}\mathrm{Re}\{\hat{x}_n^k\}/(1-A_k)$.
- $\lambda_{n,2}^k \approx 2\sqrt{2}\mathrm{Im}\{\hat{x}_n^k\}/(1-A_k)$.

8PSK:
- $\lambda_{n,1}^k \approx -4\sin(7\pi/8)\mathrm{Im}\{\hat{x}_n^k\}/(1-A_k)$.
- $\lambda_{n,2}^k \approx -4\sin(7\pi/8)\mathrm{Re}\{\hat{x}_n^k\}/(1-A_k)$.
- $\lambda_{n,3}^k \approx 1.0824(|\mathrm{Re}\{\hat{x}_n^k\}| - |\mathrm{Im}\{\hat{x}_n^k\}|)/(1-A_k)$.

16QAM:
- $\lambda_{n,1}^k \approx -4\mathrm{Re}\{\hat{x}_n^k\}/(\sqrt{10}(1-A_k))$.
- $\lambda_{n,2}^k \approx (8A_k - 4\sqrt{10}|\mathrm{Re}\{\hat{x}_n^k\}|)/(10(1-A_k))$.
- $\lambda_{n,3}^k \approx -4\mathrm{Im}\{\hat{x}_n^k\}/(\sqrt{10}((1-A_k))$.
- $\lambda_{n,4}^k \approx (8A_k - 4\sqrt{10}|\mathrm{Im}\{\hat{x}_n^k\}|)/(10(1-A_k))$.

if $c_{n,j}^k = 0$, the distribution of $L_{\mathrm{app}}\left(c_{n,j}^k\right)$ can be expressed as $\mathcal{N}(\gamma_p^k, 2\gamma_p^k)$. Now, as $L_{n,j}^k = L_{\mathrm{ext}}\left(c_{n,j}^k \middle| \hat{x}_n^k\right) + L_{\mathrm{app}}\left(c_{n,j}^k\right)$, statistical samples of $L_{n,j}^k$ can also be generated using the knowledge of γ_p^k. Since $\bar{x}_n^k$ is a function of $L_{n,j}^k$, as long as we know the parameters γ_p^k of $L_{\mathrm{app}}\left(c_{n,j}^k\right)$ and A_k of $\hat{x}_n^k$, the expected value of ψ^k can be calculated through numerical methods.

The ML estimate of γ_p^k can also be estimated using

$$\gamma_p^k = \sqrt{1 + \frac{1}{K_c \times q} \sum_{n=1}^{K_c} \sum_{j=1}^{q} \left| \left(L_{\text{app}} \left(c_{n,j}^k \right) \right)^2 \right|} - 1. \tag{34}$$

In order to determine A_k, we need $\mathbf{F}_k$, while we need A_k to calculate ψ^k , and thus $\mathbf{F}_k$. This is problematic. To find both A_k and $\mathbf{F}_k$ simultaneously, Lopes *et al.* proposed an iterative procedure for initial A_k and $\mathbf{F}_k$ computation [24]. However, it still involves a lot of computations and induces convergence delay. In our algorithm, MMSE-LE is employed in first turbo iteration to replace this iterative procedure for initial A_k and $\mathbf{F}_k$ computation as in [15].

Finally, the computation of $\bar{x}_n^k$ is given by

$$\bar{x}_n^k = \sum_{\alpha_i \in \mathcal{S}} \alpha_i \Pr\left(\bar{x}_n^k = \alpha_i \right) \tag{35}$$

$$\Pr\left(\bar{x}_n^k = \alpha_i \right) = \prod_{j=1}^{q} \frac{1}{2} \left(1 + \tilde{s}_{i,j} \tanh\left(L_{n,j}^k / 2 \right) \right). \tag{36}$$

4 Experimental Results

The proposed MIMO-SDFE detector has been tested by real-world data collected in the experiment named ACOMM09, which was launched at the coastline of New Jersey in May 2009. The symbol period and carrier frequency in this experiment were chosen as 0.2 ms and 17 kHz, respectively. Three different modulation schemes, namely, QPSK, 8PSK and 16QAM were employed for symbol transition. The transmit filter was a square-root raised cosine filter with roll-off factor of $\beta = 0.2$. The

transmit equipment was a four-transducer array, for which the number of active transducers was flexibly configured to implement different MIMO transmission during the experiment. In the receiving end, two hydrophone arrays named ACDS2 and ACDS3 each consisting of eight elements were used and the distances between ACDS2 and ACDS3 to the transmit equipment were 2 km and 3 km, respectively. In the sequel, several stages of the receiver such as the synchronization channel estimation, equalization and phase correction are explained in detail, after which, numerical results for the BER of different experiments are presented.

4.1 Synchronization

Detecting the exact starting point of the received data stream is an important problem in studying underwater communication systems. In this section, we illustrate the use of correlation of chirp signals in finding the rough starting point of the data stream and moreover, propose a new algorithm, based on the wavelet transform denoising to refine the original estimation for the starting point of the received blocks.

Figure 5 demonstrates a received burst at the first array hydrophone, containing 50 blocks of 16QAM symbols with 1024 symbols in each block. Since the data are not calibrated, an arbitrary unit has been adopted for the signal amplitude. The waveforms contain signals received simultaneously from two transducers before the down-sampling stage. From the figure, the interferences from the two transducers are observed in the received signal.

The transmitted block consists of two linear frequency modulation (LFM) sequences named LFMB and LFME, and one m-sequence. The LFM sequences serve multiple purposes like packet coarse synchronization, Doppler shift estimation, and channel length measurement. The m-sequence can be used to evaluate the channel scattering function. The data payload consists of multiple blocks separated by padded

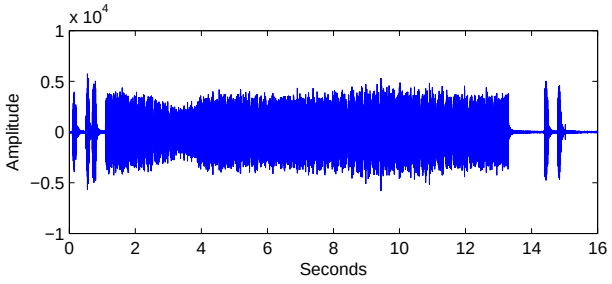

Figure 5. Received passband signal (2Tx),one burst.

zeros. The zero-padding length has been chosen as $N_g = 200$ symbols to avoid inter-block interference under highly-dispersive UWA channels. In Figure 6, an example of the normalized correlation between the received signal and the local LFMB signal is demonstrated where each peak indicates the coarse synchronization point. To measure the length of the practical channel, right correlation ridge is zoomed-in, after which, it is found that most of the correlation energy is concentrated inside a time window of 12 msec.

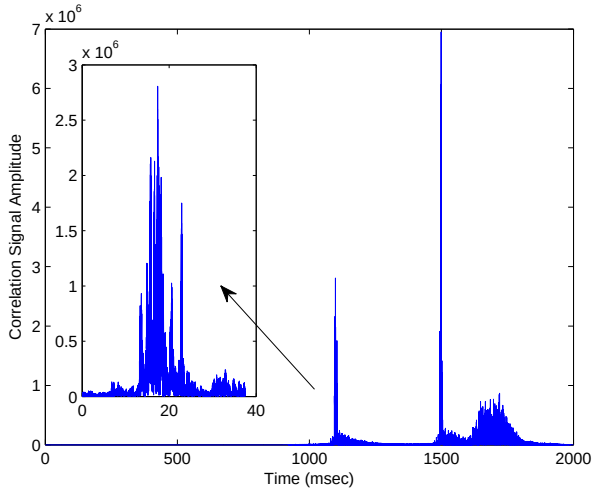

Figure 6. Correlation between the received signal and the local LFMB signal.

While this method is good for finding the starting point of the data in scenarios where the highest peak of the channel impulse response is at the beginning, it fails to provide an accurate starting point for cases where the intermediate taps of the channel have a higher peak. This synchronization problem can further spread itself into other problems such as improper equalization and phase rotation. Therefore, finding the exact synchronization point is of substantial importance.

An intuitive way to resolve this issue is to use a sliding window centered around the estimated starting point and observing the amplitude of the received signal at the center point as the window slides back. In this case, if at any point, the signal amplitude drops below a chosen threshold, that point can be selected as the starting point of the data stream. The threshold can be chosen based on the amplitude of the received signal. Yet, this method is very sensitive to the amplitude of the additive ambient noise, and therefore, in most cases, it cannot provide a robust solution to the synchronization problem.

In order to resolve this issue and fine tune the coarse synchronization point found by the correlation method, first, as shown in Figure 7, we apply a wavelet transform on the received signal to remove the noisy components of the signal. As it can be seen from the figure, by employing the wavelet transform based de-noising, the variations of the received signal due to the ambient noise are filtered out. After the application of wavelet transform, we can employ the threshold based synchronization algorithm on the received signal. Throughout our experiments, we used the threshold $v_{th} = 200$ to fine tune the starting point of the received data packets. This value was chosen based on studying the amplitude of the received signal for a single packet and proved to be useful for processing subsequent data packets.

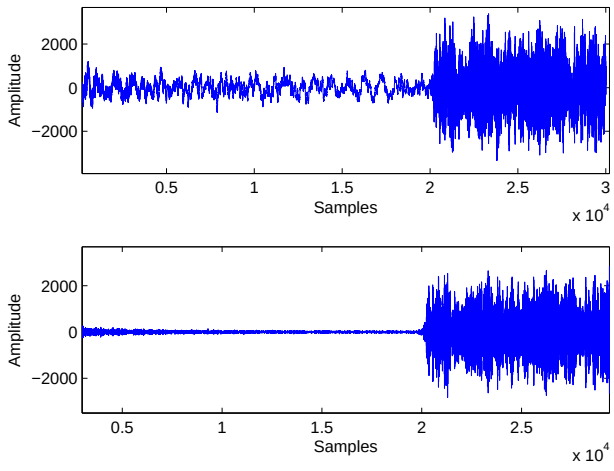

Figure 7. Application of wavelet transform for synchronization.

4.2 Channel Estimation

An example of the estimated UWA channels between the transmit array and the receive array ACDS3 for the duration of 20 blocks is illustrated in Figure 8. From the figure, channel amplitude variations along different blocks are easily observed. Moreover, the channel length is almost 12 ms, which corresponds to the time span from Figure 6 where the correlation of the LFMB signals are more concentrated. Hence, channel length is approximately $L \approx 60$ taps in terms of the symbol period $T_s = 0.2$ ms.

The process of iterative channel estimation for two different sub-channels have been shown in Figures 9 and 10 where T and H denote transducer and hydrophone, respectively. Clearly, it can be seen that the impulse response of the sub-channels are sparse, and nonhomogeneous. Consequently, it can be expected that the characteristics of the UWA channel make the channel equalization difficult. Here, we have used

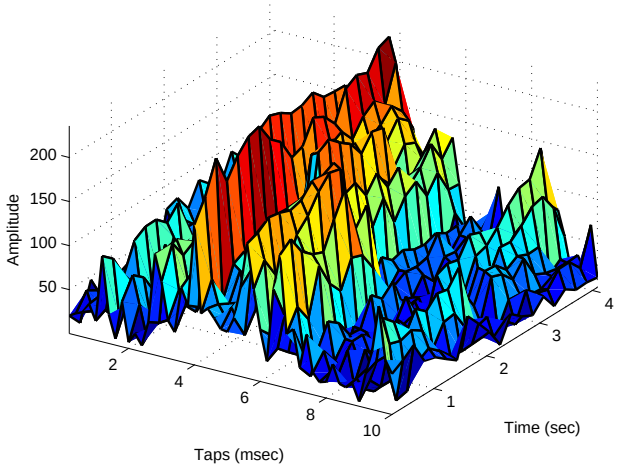

Figure 8. Amplitude of the time varying channel for the duration of 20 blocks.

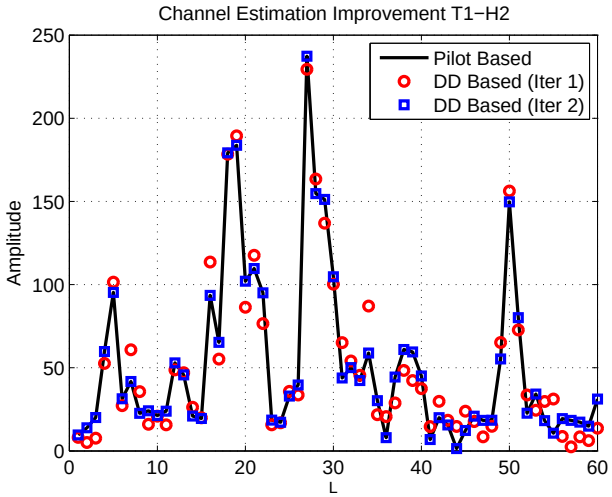

Figure 9. Demonstration of channel estimation improvement for sub-channel T1-H2.

$N_p = 512$ and $N_f = 10240$ as the parameters of our channel estimation algorithm. In other words, we estimate the channel for the first 512 symbols of the received block using pilots and the channel for remaining 20 blocks is estimated by the DD based channel estimation algorithm, after which, another 512 symbols are used as pilots

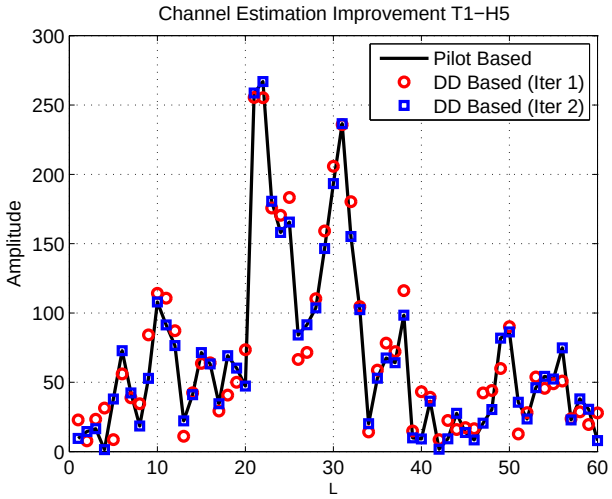

Figure 10. Demonstration of channel estimation improvement for sub-channel T1-H5.

for the 21st block. The choice of these parameters yields a pilot overhead of 2.5% for the QPSK packets. The channel estimation shown in the figures is performed on the 10th block of the received data stream for QPSK modulation. Here, the solid line shows the results of the channel estimation based on the assumption that pilots were available for the 10th block. On the other hand, the circle and square markers illustrate the DD based channel estimation algorithm results for the first and second iteration, respectively. As explained earlier, in the first iteration we already know the coefficients of the channel from the previous sub-block. Hence, assuming that the channel variations are small compared to the sub-block length, the same channel is used to equalize the symbols for the current channel. After the first iteration is over, the final decoded symbols would be available at the output of the LDPC decoder. Naturally, we expect these symbols to have less errors compared to the symbols from the output of the equalizer. Hence, in the subsequent iteration(s) we use the symbols from the output of the decoder to re-estimate the sub-channel for the current block. As it can be seen from the figures, although the channel estimated from the first

iteration does not match the channel estimated from the pilots, the quality of the channel estimation is significantly improved in the second iteration. This strategy proves useful in reducing the pilot overhead and increasing the spectral efficiency.

4.3 Phase Correction

We know from the nature of ocean waters that the instantaneous Doppler spreads changes gradually from time to time, rather than changing arbitrarily. Therefore, the rotating phase $\angle\alpha$ is also changing gradually with time. We treat $\angle\alpha$ to be a constant for a small number of N_s consecutive symbols and adjust the phase compensation for every group of N_s symbols. Let ϕ_k denote the estimated phase for the pth group of $\{\angle\alpha_{(p-1)N_s+1}, \angle\alpha_{(p-1)N_s+2}, \cdots, \angle\alpha_{(p-1)N_s+N_s}\}$, with $p = 1, 2, \cdots, N_g$ where N_g is the total number of groups. Let ϕ_0 denote the initial phase, $\Delta\phi_p$ the phase difference $\phi_k - \phi_{k-1}$.

Our group-wise phase estimation and compensation algorithm is presented in several steps: Initially, we designate the first N_{ts} symbols in each transmitted block data as the training symbols for phase reference and determine the initial phase ϕ_0, after which we compensate the phase of the p-th group data by $e^{-j\psi_{p-1}}$. The aforementioned procedure is continued until $p = N_g$. In our experiments, we have considered N_{ts} to be 100, and N_s and N_g to be 512 and 2. Scatter plots of the 16QAM symbols before and after phase correction are illustrated in Figures 11 and 12, respectively.

4.4 Equalization and Decoding

With the estimated channel knowledge, turbo equalization can be performed. Figure 13 shows the estimated symbols at the output of the DFE and the soft-decision symbols at the output of the LDPC decoder over multiple iterations for 16QAM constellations.

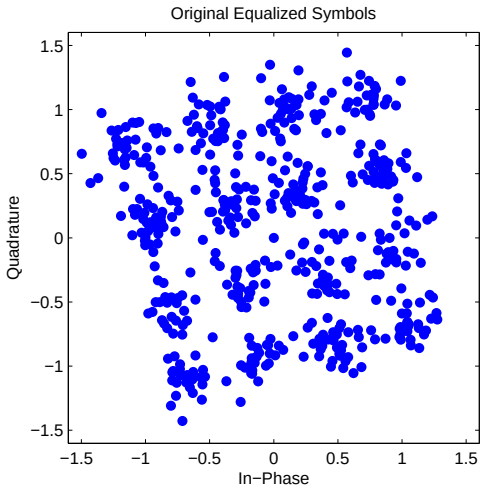

Figure 11. Scatter plot of the original equalized symbols for 16QAM Constellation.

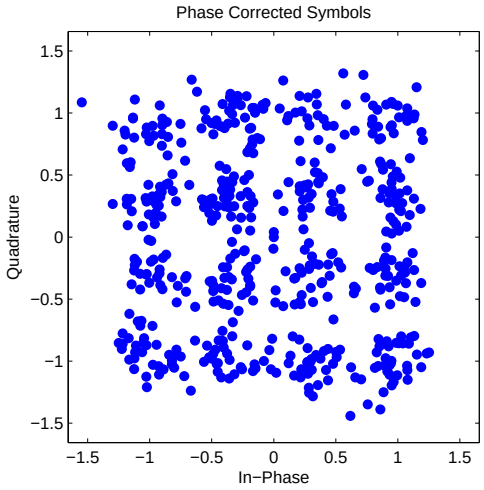

Figure 12. Scatter plot of the 16QAM symbols after phase correction.

From the figure, it can be seen that the system performance improves considerably by each iteration. Moreover, in any given iteration, LDPC decoder provides

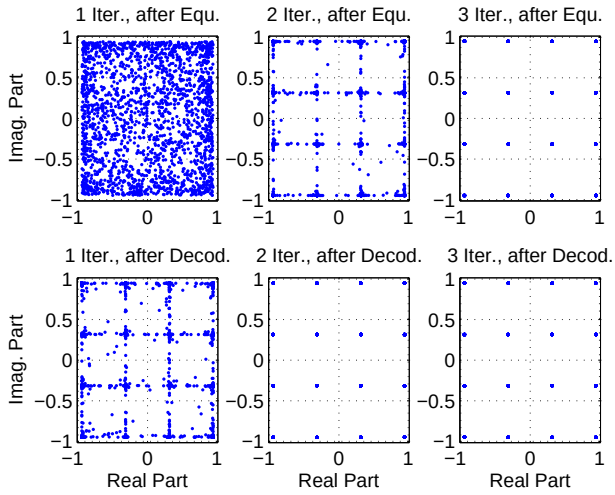

Figure 13. Demonstration of turbo equalization with 16QAM constellation.

better symbol estimation than the equalizer due to the extra information gleaned during the decoding process.

4.5 BER Results

Forty packets have been detected for each of the three modulations, for both ACDS2 and ACDS3. The parameter N_{det} in Tables 4-6 denotes the number of detection iteration. For all tables, the BER results corresponding to different detection iteration number have been provided for comparison. We make the following observation for the results. For a fixed number of LDPC decoding iterations, the system performance improves with the number of decoding iterations, N_{det}. As it can be seen, bit error rates of up to 10^{-4} can be achieved by combined Turbo soft decision feedback equalization and LDPC decoding.

Table 4. BER for 2×8 MIMO in ACOMM09 experiment ($N_b = 1024$).

Mod. \ N_{det}		1	2	3	4
ACDS2	QPSK	2.7×10^{-4}	0	0	0
	8PSK	2.3×10^{-3}	4.2×10^{-4}	4.5×10^{-5}	0
	16QAM	2.9×10^{-3}	5.1×10^{-4}	4.2×10^{-4}	3.1×10^{-4}
ACDS3	QPSK	1.2×10^{-4}	3.2×10^{-6}	0	0
	8PSK	1.8×10^{-3}	3.9×10^{-4}	7.0×10^{-5}	2.1×10^{-6}
	16QAM	1.9×10^{-3}	4.7×10^{-4}	2.9×10^{-4}	1.1×10^{-4}

Table 5. BER for 2×8 MIMO in ACOMM09 experiment ($N_b = 2048$).

Mod. \ N_{det}		1	2	3	4
ACDS2	QPSK	4.7×10^{-4}	3.2×10^{-4}	0	0
	8PSK	6.3×10^{-3}	3.1×10^{-3}	2.5×10^{-3}	7.5×10^{-4}
	16QAM	8.9×10^{-3}	6.1×10^{-3}	5.2×10^{-3}	9.7×10^{-4}
ACDS3	QPSK	3.2×10^{-4}	2.6×10^{-4}	0	0
	8PSK	4.8×10^{-3}	3.9×10^{-3}	3.1×10^{-3}	4.2×10^{-4}
	16QAM	5.6×10^{-3}	4.6×10^{-3}	3.5×10^{-3}	5.1×10^{-4}

Table 6. BER for 2×8 MIMO in ACOMM09 experiment ($N_b = 25600$).

Mod. \ N_{det}		1	2	3	4
ACDS2	QPSK	9.1×10^{-4}	5.5×10^{-4}	4.2×10^{-4}	0
	8PSK	6.5×10^{-3}	5.7×10^{-3}	5.1×10^{-3}	9.8×10^{-4}
	16QAM	9.2×10^{-3}	7.8×10^{-3}	7.2×10^{-3}	6.5×10^{-3}
ACDS3	QPSK	6.3×10^{-3}	4.2×10^{-3}	2.4×10^{-3}	0
	8PSK	5.1×10^{-3}	4.9×10^{-3}	4.5×10^{-3}	6.1×10^{-4}
	16QAM	6.2×10^{-3}	5.4×10^{-3}	5.1×10^{-3}	7.2×10^{-4}

5 Conclusion

A robust detection scheme using turbo block decision-feedback equalization was proposed for single-carrier MIMO UWA communications. It had two major parts: first, the iterative channel estimation provides reliable channel knowledge; second, MIMO SDFE performs iterative detection. The proposed algorithm has been tested by extensive undersea real-world data collected in ACOMM09 experiments. The testing has been performed with different transmission ranges, different modulation schemes, and different MIMO system configurations. The results show that the proposed SDFE algorithm provides robust detection for MIMO UWA communications with different modulations and different symbol rates, at different transmission ranges. Finally, the proposed detection scheme had a reasonable detection complexity suitable for practical applications.

6 Acknowledgement

This work was supported in part by the National Science Foundation under Grants CCF-0915846, and the Office of Naval Research under Grants N00014-09-1-0011 and N00014-10-1-0174.

7 References

[1] M. Stojanovic, "Recent advances in high-speed underwater acoustic communications," *IEEE Journal of Oceanic Engineering*, vol. 121, no. 2, pp. 125136, Apr. 1996.

[2] D. B. Kilfoyle and A. B. Baggeroer, "The state of the art in underwater acoustic telemetry," *IEEE Journal of Oceanic Engineering*, vol. 25, no. 1, pp. 427, Jan. 2000.

[3] C. Douillard, C. Berrou, A. Picart, and A. Glavieux, "Iterative correction of intersymbol interference: Turbo equalization," *Eur. Trans. Telecommun.,* vol. 6, pp. 507511, Sept.-Oct. 1995.

[4] M. T*ü*chler, R. Koetter, and A. C. Singer, "Turbo equalization: Principles and new results," *IEEE Trans. Commun*, vol. 50, pp.754-767, May. 2002.

[5] M. T*ü*chler, A. C. Singer, and R. Koetter, "Minimum mean square error equalization using a priori information," *IEEE Trans. Signal Processing*, vol.50, pp.673-683, Mar. 2002.

[6] E. M. Sozer, J. G. Proakis and F. Blackmon, "Iterative equalization and decoding techniques for shallow water acoustic channels," *OCEANS '01 MTS/IEEE ,* pp.2201-2208 vol.4, 2001.

[7] E. M. Sozer, J. G. Proakis and F. Blackmon, "Iterative equalization, decoding, and soft diversity combining for underwater acoustic channels," *OCEANS '02 MTS/IEEE ,* pp. 2425-2428 vol.4, 29-31 Oct. 2002.

[8] J. W. Choi, R.J. Drost, A.C. Singer and J. Preisig, "Iterative multi-channel equalization and decoding for high frequency underwater acoustic communications," *Sensor Array and Multichannel Signal Processing Workshop,* 2008. SAM 2008. 5th IEEE, pp.127-130, 21-23 July. 2008.

[9] S. Roy, T. M. Duman, V. McDonald, and J. G. Proakis, "High rate communication for underwater acoustic channels using multiple transmitters and space-time coding: receiver structures and experimental results," *IEEE J. Ocean. Eng.*, vol. 32, pp. 663-688, July 2007.

[10] R. Otnes and T. H. Eggen, "Underwater acoustic communications: long-term test of turbo equalization in shallow water," *IEEE J. Ocean Eng.*, vol. 33, no. 3, pp. 321-334, July 2008.

[11] L. Bahl, J. Cocke, F. Jelinek, and J. Raviv, "Optimal decoding of linear codes for minimizing symbol error rate," *IEEE Trans. Inform. Theory*, vol. 20, pp. 284-287, March 1974.

[12] J. Tao, Y. R. Zheng, C. Xiao, T. C. Yang, "Robust MIMO underwater acoustic communications using turbo block decision-feedback equalization," *IEEE J. Ocean. Eng.*, vol. 35, no. 4, pp. 948-960, Oct. 2010.

[13] J. Huang, S. Zhou, and P. Willett, "Nonbinary LDPC coding for multicarrier underwater acoustic communication," *IEEE JSAC Special Issue on Underwater Wireless Communications and Networks, vol.* 26, no. 9, pp. 1684-1696, Dec. 2008.

[14] B. Li, J. Huang, S. Zhou, K. Ball, M. Stojanovic, L. Freitag, and P. Willett, "MIMO-OFDM for high rate underwater acoustic communications," *IEEE J. Ocean. Eng., vol.* 34, pp. 634-644, Oct. 2009.

[15] H. Lou and C. Xiao, "Soft-decision feedback turbo equalization for multilevel modulations, " *IEEE Trans. Signal Processing*, vol.59, pp.186-195, Jan. 2011.

[16] A. Rafati, H. Lou and C. Xiao, "Low-Complexity Soft-Decision Feedback Turbo Equalization for MIMO Systems With Multilevel Modulations," *IEEE Trans. on Vehicular Technology*, vol. 60, no. 7, pp.3218-3227, Sept. 2011.

[17] J. Tao, Y. R. Zheng, C. Xiao, T. C. Yang, and W. B. Yang, "Channel equalization for single carrier MIMO underwater acoustic communications," *EURASIP J. Adv. Signal Process.*, vol. 2010, 2010, DOI: 10.1155/2010/281769, article ID 281769.

[18] B. S. Sharif, J. Neasham, O. R. Hinton, and A. E. Adams, "A computationally efficient Doppler compensation system for underwater acoustic communications," *IEEE J. Ocean. Eng.*, vol. 25, no. 1, pp. 5261, Jan. 2000.

[19] T. Abe, S. Tomisato, and T. Matsumoto, "A MIMO turbo equalizer for frequency-selective channels with unknown interference," *IEEE Trans. Veh. Technol.*, vol. 52, pp. 476-482, May 2003.

[20] J. Wu and Y. R. Zheng, "Low complexity soft-input soft-output block decision feedback equalization," *IEEE J. Select. Areas Commun.*, vol.26, pp.281-289, Feb. 2008.

[21] A. Glavieux, C. Laot and J. Labat, "Turbo equalization over a frequency selective channel," in *Proc. Int. Symp. Turbo Codes, Related Topics*, Brest, France, pp.96-102, Sep. 1997.

[22] Z. Wu and J. Cioffi, "Low complexity iterative decoding with Decision-Aided Equalization for magnetic recording channels," *IEEE J. Select. Areas Commun.*, vol.19, pp.699-708, Apr. 2001.

[23] R. R. Lopes, "Iterative estimation, equalization and decoding," *Ph.D. dissertation, Georgia Inst. Technol.*, Atlanta, GA, 2003.

[24] R. R. Lopes and J. R. Barry, "The soft-feedback equalizer for turbo equalization of highly dispersive channels," *IEEE Trans. Commun*, vol.54, pp.783-788, May. 2006.

[25] A. Dejonghe and L. Vanderdorpe, "Turbo equalization for multilevel modulation: An efficient low-complexity scheme," in *Proc. IEEE Int. Conf. Commun*, vol.3, pp.1863-1867, Aug. 2002.

[26] P. Vila, I. Fijalkow, C. Laot, D. Leroux, D. Pirez, S. Ronger, and C. Langlais, "Reduced-complexity M-ary decoders for turbo-equalization," in *2nd Int. Symp. Turbo Codes and Related Topics*, Brest, France, Sept.4-7 2000.

[27] Y. Lee and W. R. Wu, "Adaptive channel aided decision feedback equalization for SISO and MIMO systems," *IEEE Proc.Commun.,* vol.153, pp. 657-663, Oct. 2006.

[28] S. Ten Brink, "Convergence behavior of iteratively decoded parallel concatenated codes," *IEEE Trans. Commun.,* vol.49, pp. 1727-1737, Oct. 2001.

[29] N. Al-Dhahir, and J. M. Cioffi, "MMSE decision-feedback equalizers: Finite-length results", *IEEE Trans. Inf. Theory*, vol. 41, pp. 961-975, Jul. 1995.

[30] X. Wang and H. V. Poor, "Iterative (turbo) soft interference cancellation and decoding for coded CDMA," *IEEE Trans. Commun.*, vol. 47, pp. 1046-1061, Jul. 1999.

[31] T. Abe and T. Matsumoto, "Space-time turbo equalization in frequency selective MIMO channels," *IEEE Trans. Veh. Technol.*, vol. 52, pp. 469- 475, May 2003.

[32] G. Bauch and N. Al-Dhahir, "Reduced-complexity space-time turbo equalization for frequency-selective MIMO channels," *IEEE Trans. Wireless Commun.,* vol. 1, pp. 819-828, Oct. 2002.

[33] J. G. Proakis, *Digital Communications*, McGraw-Hill Inc., 2001.

SECTION

2 CONCLUSIONS

This dissertation has proposed two new decision feedback equalizer structures suitable for multilevel modulation systems employing turbo equalization. One is soft-decision feedback equalizer (SDFE). The proposed SDFE took into account the reliability of both soft *a priori* information and soft decisions of the data symbols. For the first iteration, the proposed SDFE starts as MMSE linear equalizer. As iterations progress, the proposed SDFE behaves as soft-decision feedback MMSE DFE. When both soft *a priori* information and soft decisions become more reliable, the feedforward filter of the proposed SDFE approaches matched filter. Both EXIT chart analysis and simulation results have shown that the proposed SDFE performs close to the high-complexity Exact-MMSE-LE in BPSK/QPSK modulation. For high level modulations, the proposed SDFE exhibits lower SNR threshold and converges much faster than the high-complexity Exact-MMSE-LE.

The drawback of SDFE is its coefficients couldn't reach matched filter bound and therefore after a large number of iterations (e.g. 10), its performance becomes inferior to that of Exact-MMSE-LE. Therefore, soft feedback ISI canceller (SIC) structure is investigated. For the first iteration, SIC starts as MMSE linear equalzier. In following iterations, it took into account the reliability of both soft *a priori* information and soft decisions of the data symbols as SDFE. Both EXIT chart and BER simulations showed that SIC exhibits lower complexity, lower SNR threshold and much faster convergence than Exact-MMSE-LE for multilevel cases. SIC also outperforms SDFE after a large number of iterations.

The SDFE and SIC structures are also extended from SISO systems to MIMO systems and applied for single-carrier underwater acoustic communications. The proposed detection schemes have been tested by undersea trial data collected in the undersea experiments named ACOMM09, which was launched at the coastline of New Jersey in May 2009 and MACE10, that was conducted at Buzzards Bay, MA in June 2010. The testings have been performed with different modulation schemes. The results show that the proposed algorithm provided robust detection for MIMO UWA communications.

The contributions of my PhD research work are summarized in four journal papers and three conference papers, among which, four journal papers and one conference paper are included in this dissertation.

3 PUBLICATIONS

[1] H. Lou, and C. Xiao, "Soft-decision Feedback Turbo Equalization for Multilevel Modulations," *IEEE Trans. Signal Processing*, vol.59, pp.186-195, Jan. 2011.

[2] H. Lou, and C. Xiao, "Soft Feedback ISI Canceller-based Turbo Equalization for Multilevel modulations," submitted to *IEEE Trans. Communications*, 2011.

[3] A. Rafati, H. Lou, and C. Xiao, "Low-complexity soft-decision feedback turbo equalization for MIMO systems with multilevel modulations," *IEEE Trans. Vehicular Technology*, vol.60, No.7, Sept. 2011.

[4] A. Rafati, H. Lou, and C. Xiao, "Soft-decision Feedback Turbo Equalization for Multiple Antenna Systems with Multilevel Modulations," in *Proc. IEEE WCNC'11*, Mexico, March. 28-31, 2011.

[5] A. Rafati, H. Lou, Y. R. Zheng and C. Xiao, "Soft Feedback Turbo Equalization for Underwater Acoustic Communications," *MTS/IEEE OCEANS*, Kona, Hawaii, Sep. 19-22, 2011. pp.1-5.

[6] A. Rafati, H. Lou and C. Xiao, "On the Soft-Decision Feedback Turbo Equalization for Underwater Acoustic Communications," submitted to *Journal of the Acoustical Society of America*, Oct. 2011.

[7] S. Subedi, H. Lou, F. Ren, M. Wang and Y. R. Zheng, "Validation of the Triply Selective Fading Channel Model Through a MIMO Test Bed and Experimental Results," *IEEE Military Commun. (Milcom'11)*, Baltimore, MD, Nov. 7-10, 2011. pp.1-6.

[8] H. Lou, and P. Lin, "A New Lock Detector for Gardner's Timing Recovery Method," *IEEE Trans. Consumer Electron*, vol.54, No.2, pp.349-352, May. 2008.

[9] H. Lou, and P. Lin, "Hybrid Carrier Recovery, Blind Equalization for High-Order QAM Signal Constellations," *IEEE Trans. Consumer Electron*, vol.54, No.2, pp.333-335, May. 2008.

[10] H. Lou, "Timing Recovery Methods for VSB Receivers," *IEEE Trans. Consumer Electron*, vol.53, No.2, pp.310-312, May. 2007.

VITA

Huang Lou was born in Zhuji, Zhejiang Province, China. He received his B.S. degree in Electrical Engineering from Beijing Normal University, Beijing, China, in 2005, and the M.S. degree in Microelectronics and Solid State Electronics from Beijing University of Technology, Beijing, in 2008. He began his Ph.D. study in January 2009 at the Department of Electrical and Computer Engineering at Missouri University of Science and Technology. His research interests include coding theory and equalization with application to communication systems. He is expected to receive his Ph.D. degree in Electrical Engineering from Missouri University of Science and Technology in May 2012.